

Micro and Nano-Tomography of Biological Tissues

Marco Stampanoni and Kevin Mader

Swiss Light Source, Paul Scherrer Institut
Institute for Biomedical Engineering, University and ETH Zürich

ETH-227-0965-00 L



Contents

■ Imaging beamlines

- Requirements
- Imaging geometries
- Optical components
- Standard detector (performances)
- In-situ experiments

■ Imaging biological samples

- An “extrait” from beamline projects

Imaging beamlines

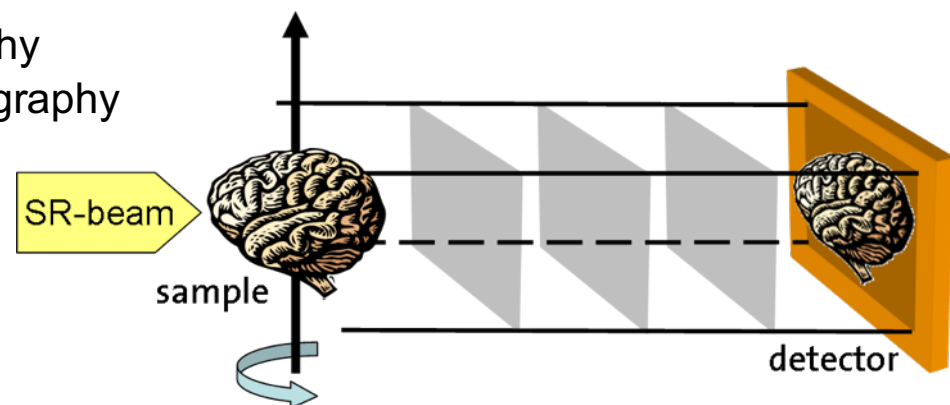
Goal: **Quantitative imaging:** measure a given object quantity as a function of space and time.

- X-rays are well suited but:
 - Not trivial since interaction with matter is not always simple
 - Ad-hoc instrumentation compared to light or electron microscopy
- Strong efforts in the development of:
 - Beamline components (windows, monochromators, mirrors, lenses, mechanics)
 - Detectors
 - Data acquisition protocols, post-processing algorithms, visualization
 - Data quantification

Tomographic (3D) imaging at synchrotrons

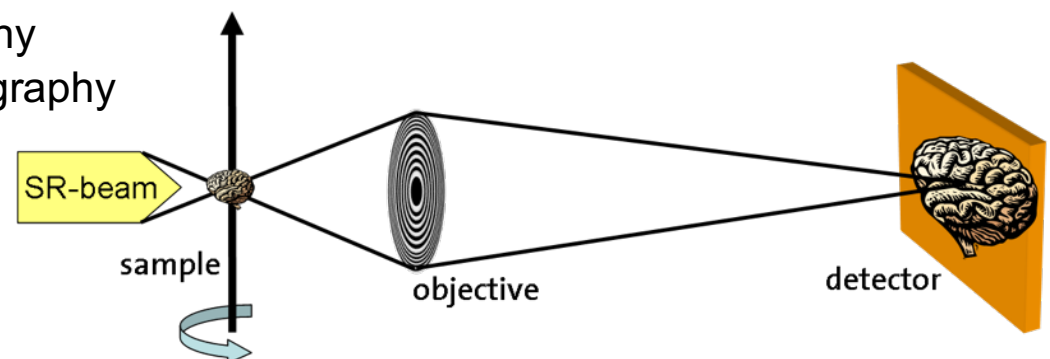
(i) Parallel beam microscopy

- Absorption Radiography / Tomography
- Phase contrast Radiography / Tomography
- Resolution ≥ 1 micron



(ii) TXM: Transmission (full field) microscopy

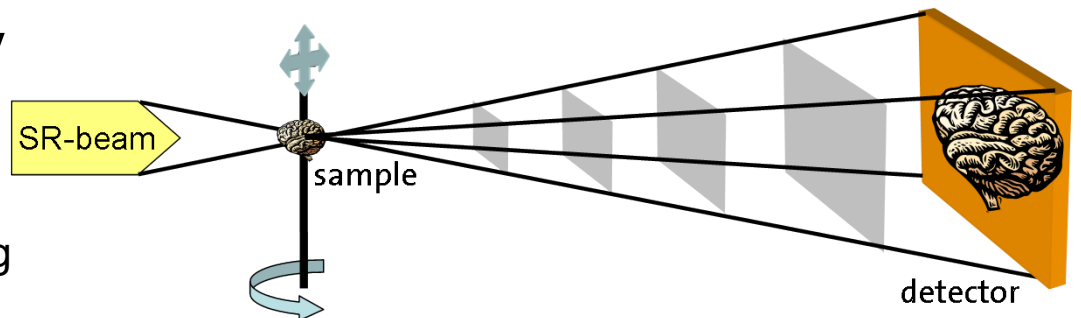
- Absorption Radiography / Tomography
- Phase contrast Radiography / Tomography
- High resolution, down to tens of nm
- Dose inefficient



Tomographic (3D) imaging at synchrotrons

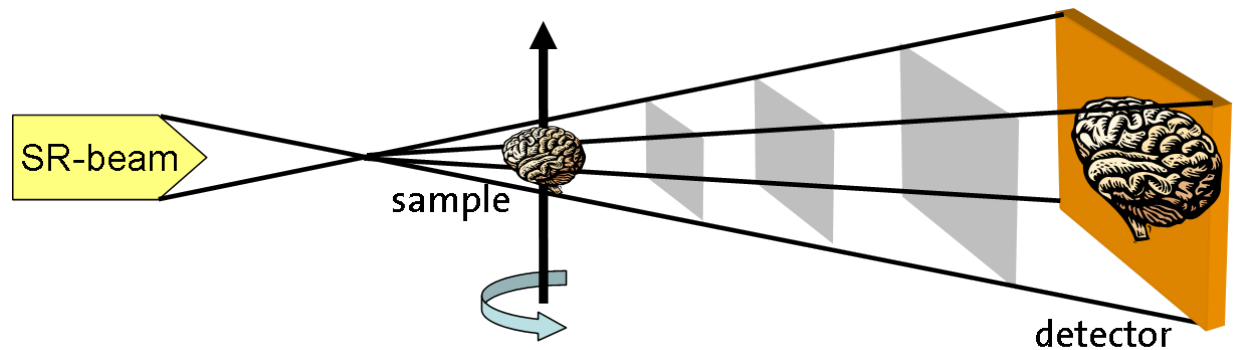
(iii) SXM: Scanning microscopy

- Slow
- Chemical sensitivity / Phase contrast
- Suited for coherent diffraction imaging



(iv) PXM: Projection microscopy

- Phase contrast Radiography / Tomography
- Fast and dose efficient
- High resolution



Key features of an imaging beamline

HIGH

WIDE

- Spatial resolution, field of view
 - **FAST and AUTOMATED**
- Data acquisition
 - **HIGH**
- Sensitivity (absorption / phase contrast)
- Energy range / Sample Flexibility
 - **BROAD**
 - **HIGH**
- Data post-processing
 - **FAST and ONLINE**
- In-situ experiments
 - **MULTIPLE**
- User friendliness
 - **EASY**

The TOMCAT beamline at SLS

- TOMCAT is the acronym for an SLS beamline dedicated to “Tomographic Microscopy and Coherent rAdiology experimenTs”.
- Use TOMCAT as an example of state-of-the-art synchrotron-based hard X-rays imaging beamline
- In particular we will discuss:
 - Source characteristic
 - Front-end
 - Optics
 - Endstation
 - Detector
 - Data acquisition
 - Data visualization
- Ref.: M. Stampanoni et al., *Trends in synchrotron-based tomographic imaging: the SLS experience*, Proc. SPIE Vol. 6318, Developments in X-Ray Tomography V, U. Bonse Editor, Aug. 2006.



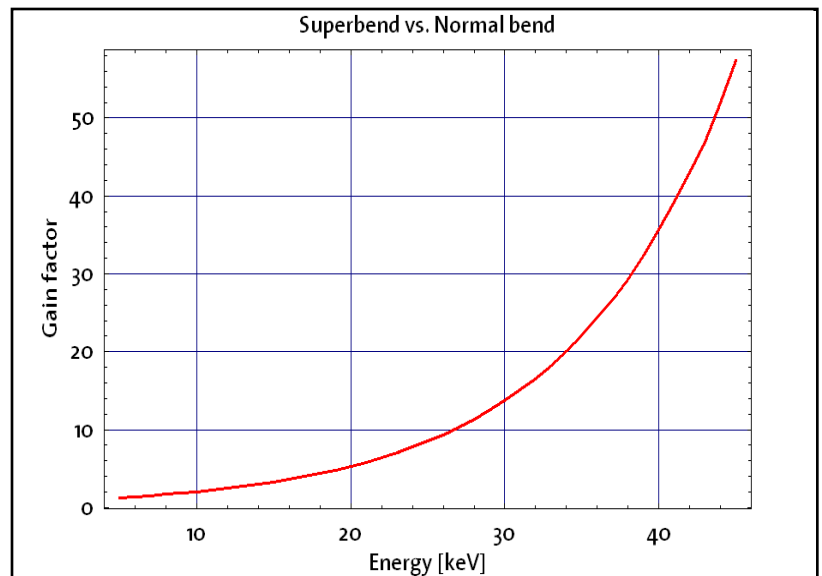
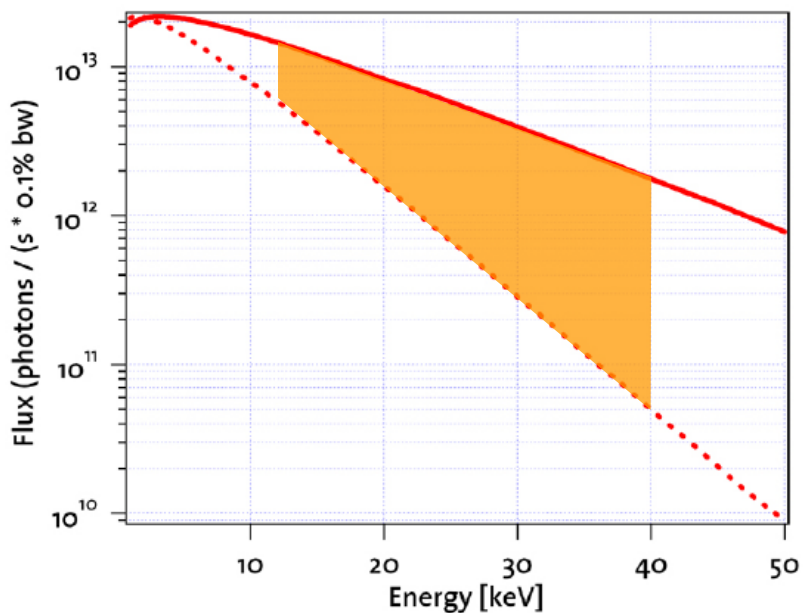
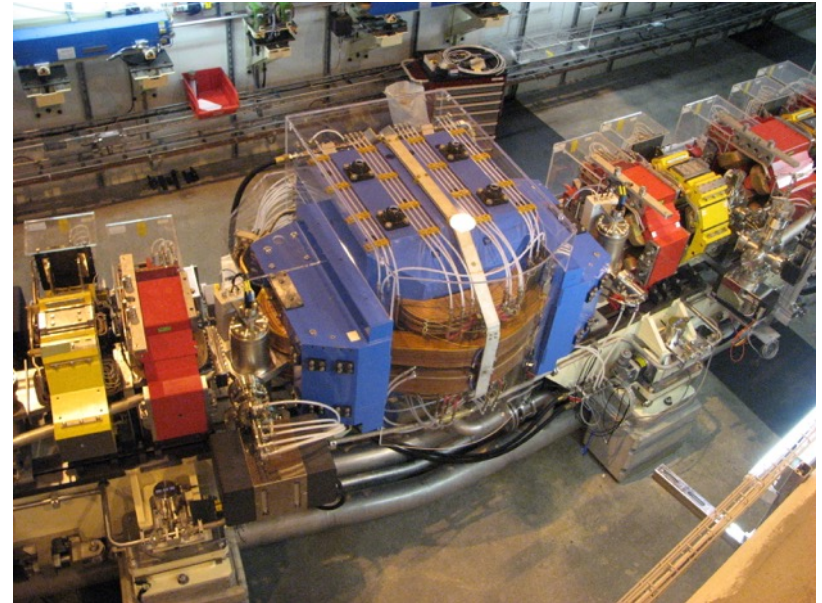
SOURCE: superbend magnet

Machine Parameters

Ring energy	2.4 GeV
Ring current	400 mA

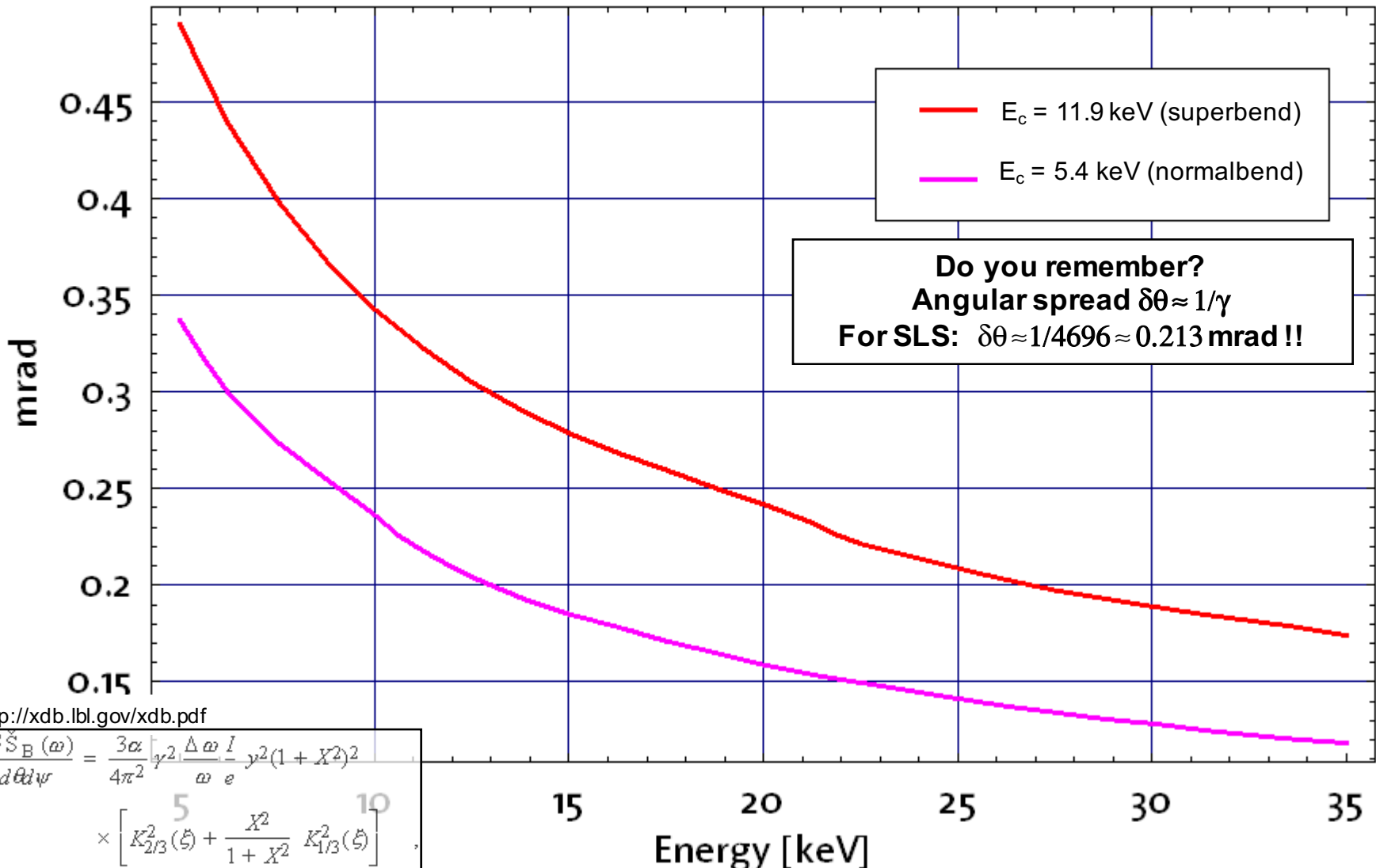
Source parameters

Magnetic field	2.9 T
Critical energy	11.1 keV / 1.12 Å
Electron source size (σ_x, σ_y)	46 μm, 16 μm
Electron source divergence (σ'_x, σ'_y)	109 μrad, 16 μrad
Photon source size (Σ_x, Σ_y)	53 μm, 16 μm
Photon source divergence (Σ'_x, Σ'_y)	2 mrad, 0.6 mrad

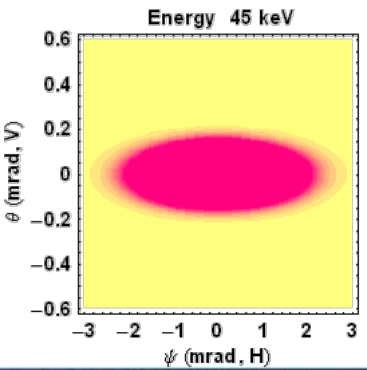
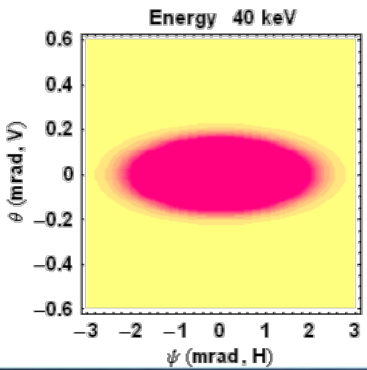
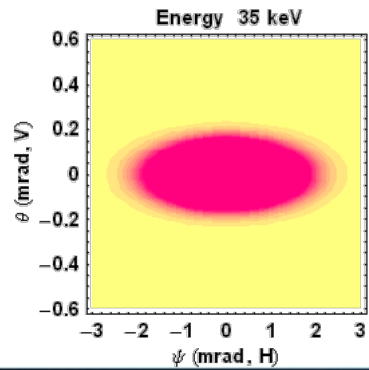
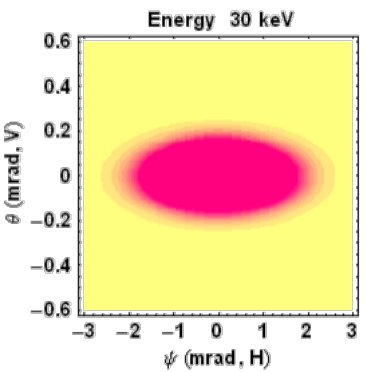
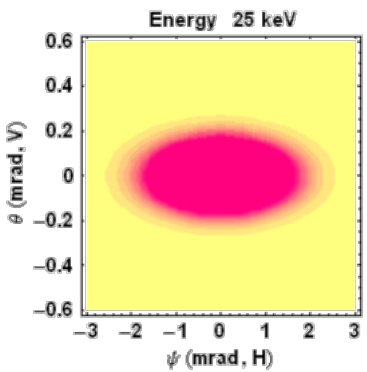
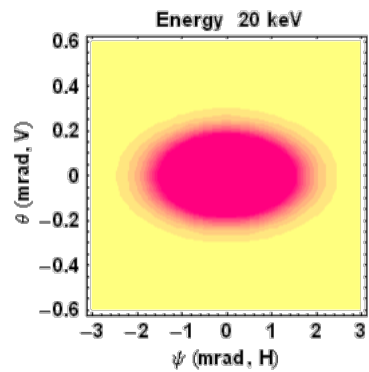
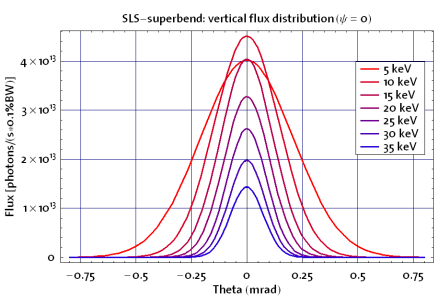
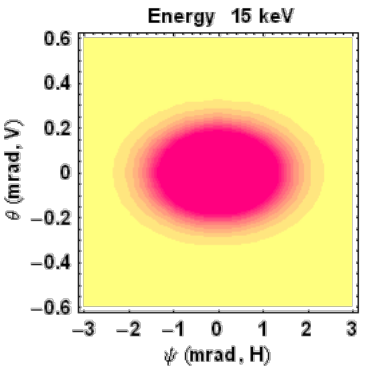
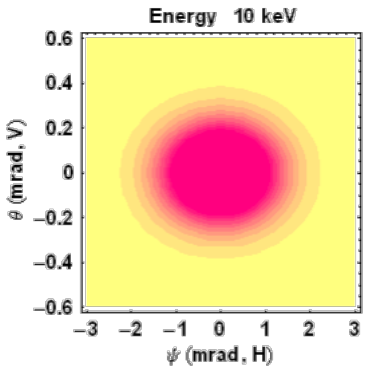
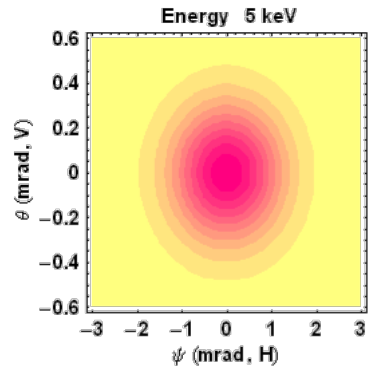


SOURCE: divergence

SLS–bending magnet: vertical angular divergence [FWHM]



SOURCE: energy distribution

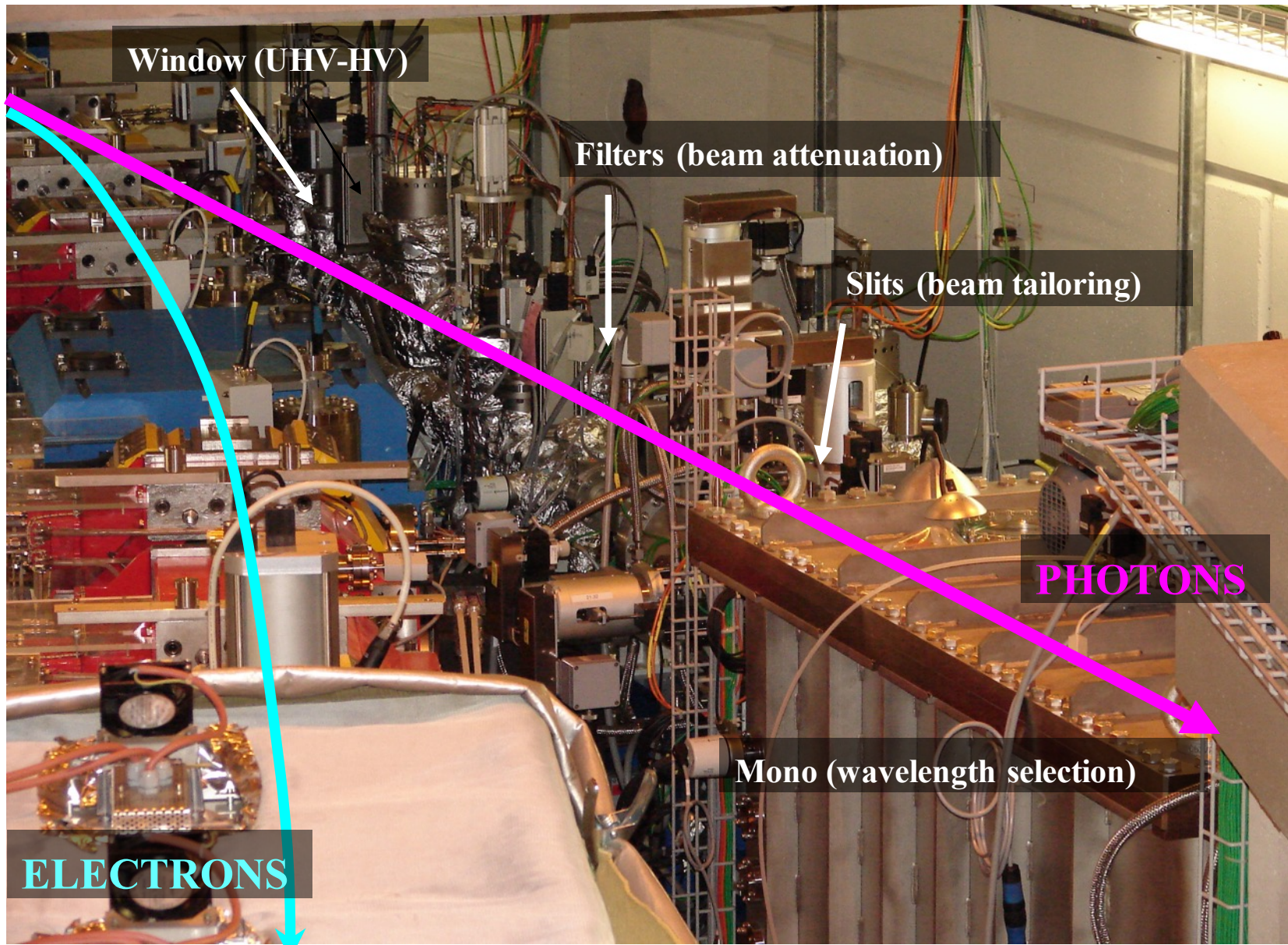


Low energy

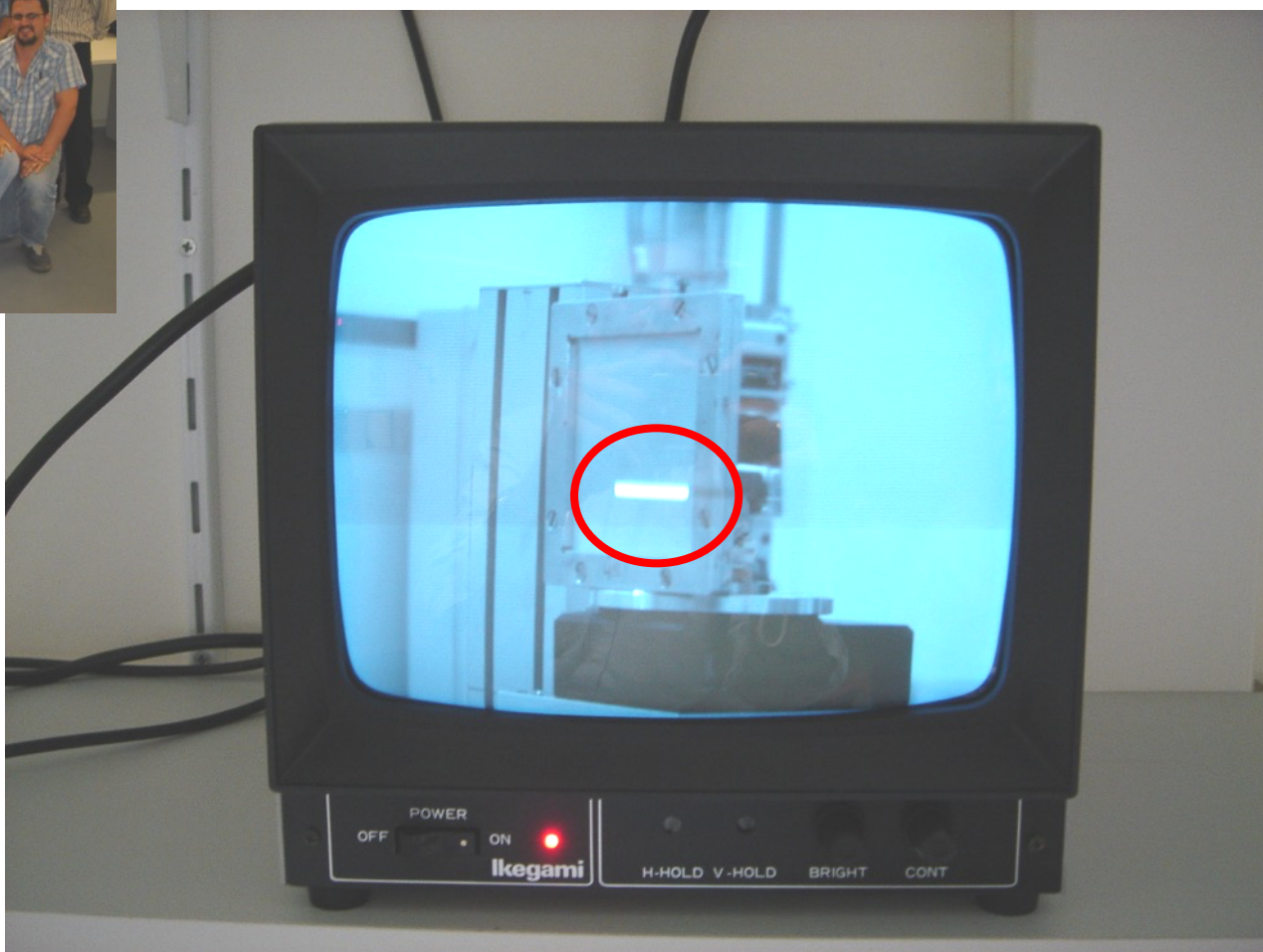


High energy

TOMCAT Front-End

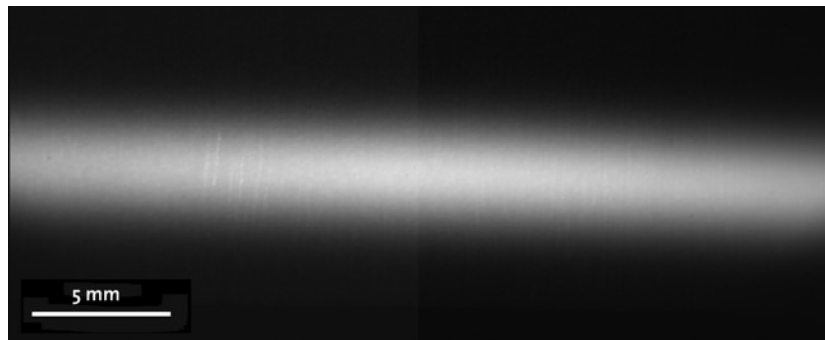


TOMCAT first light !

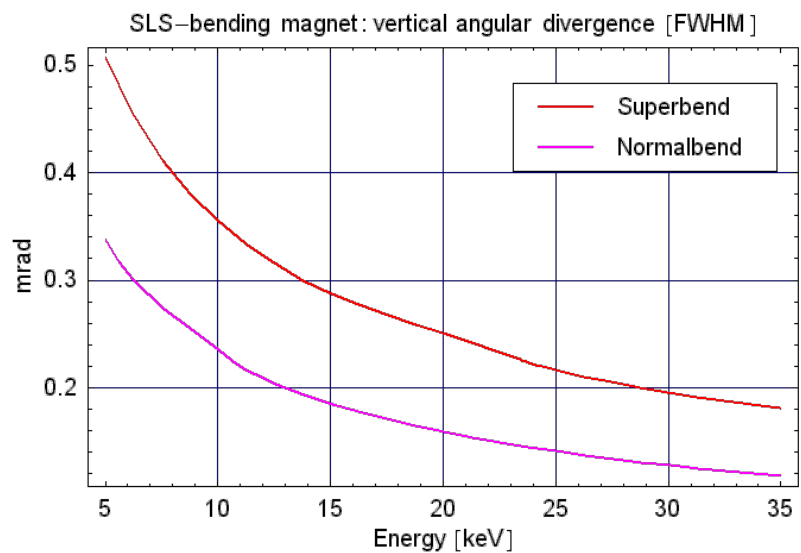
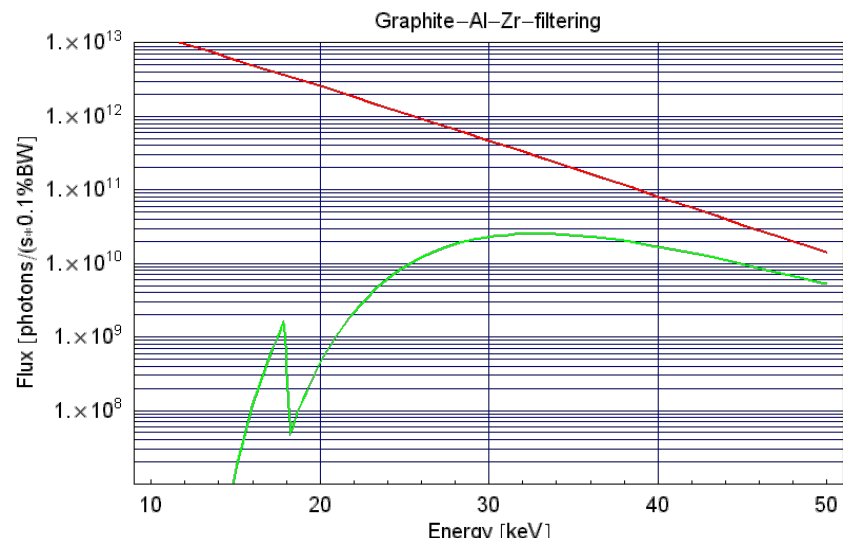
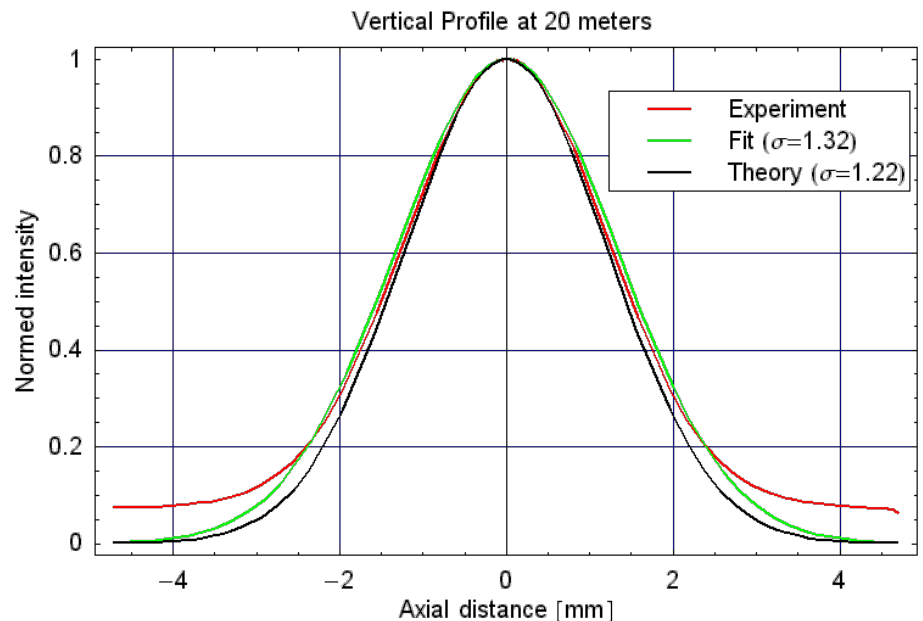


September 20th, 2005

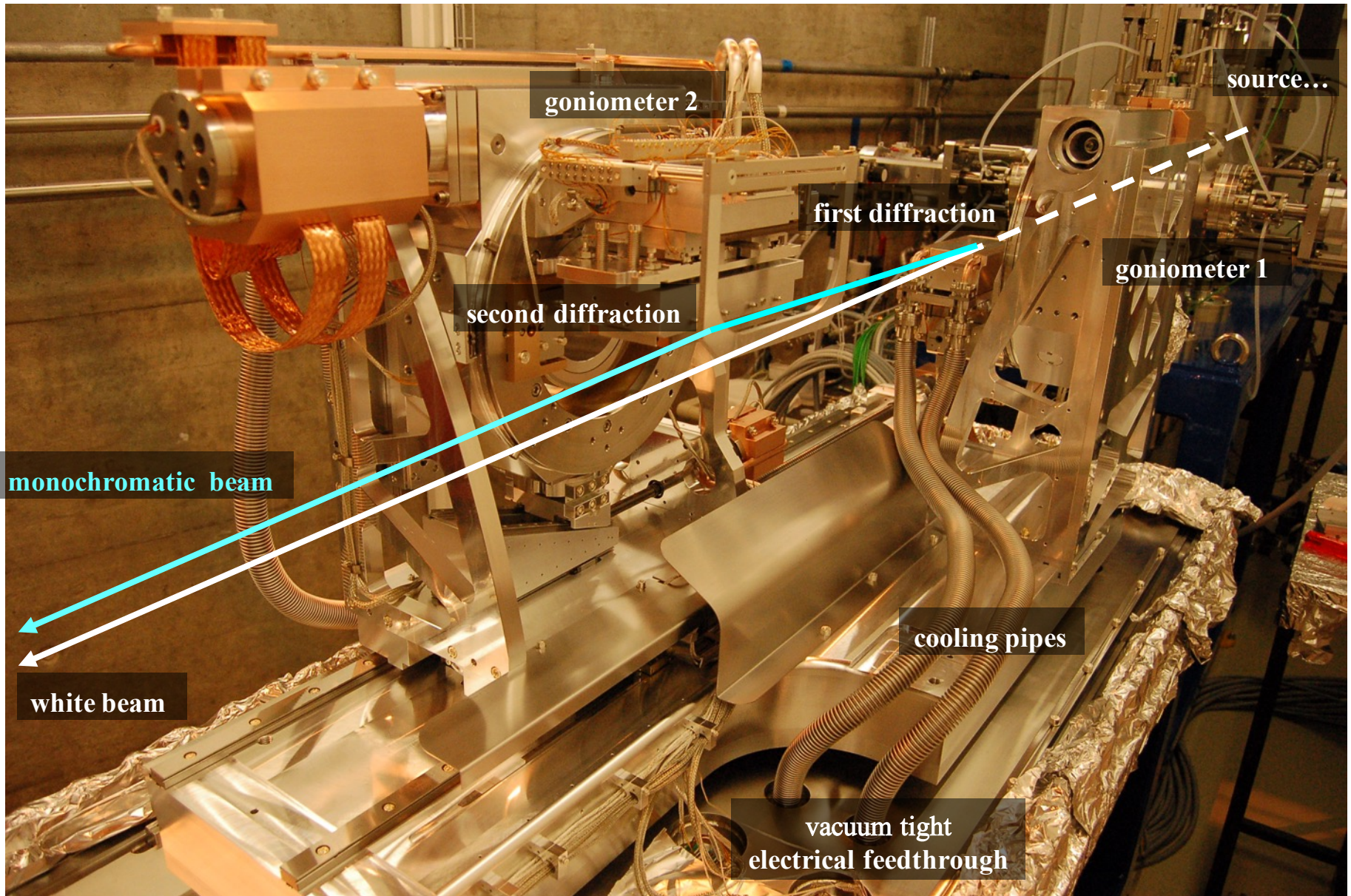
White beam on detector



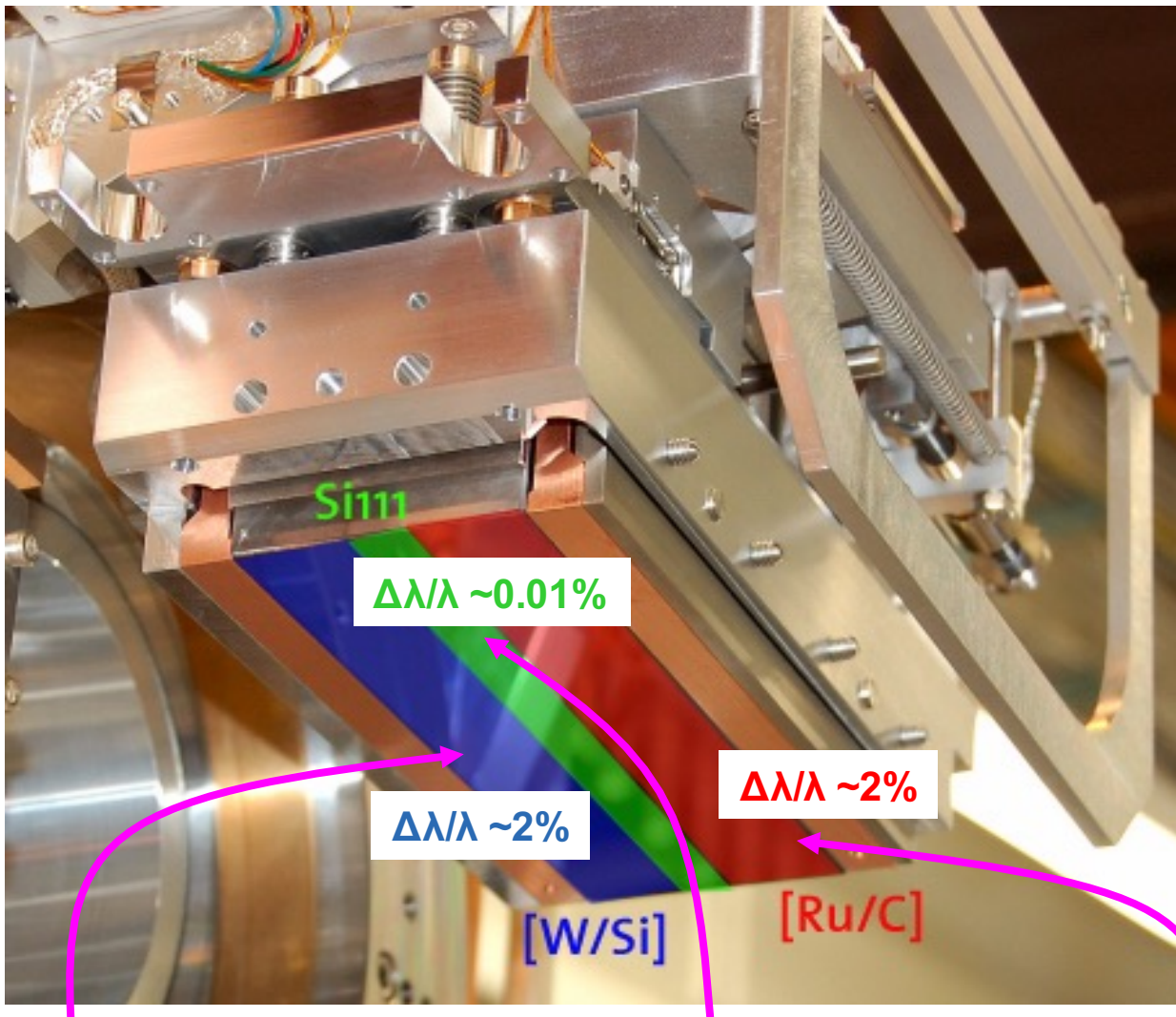
Filter: 5 mm Graphite + 5 mm Al + 75 µm Zr
Exposure: 10 ms



Fixed exit monochromator

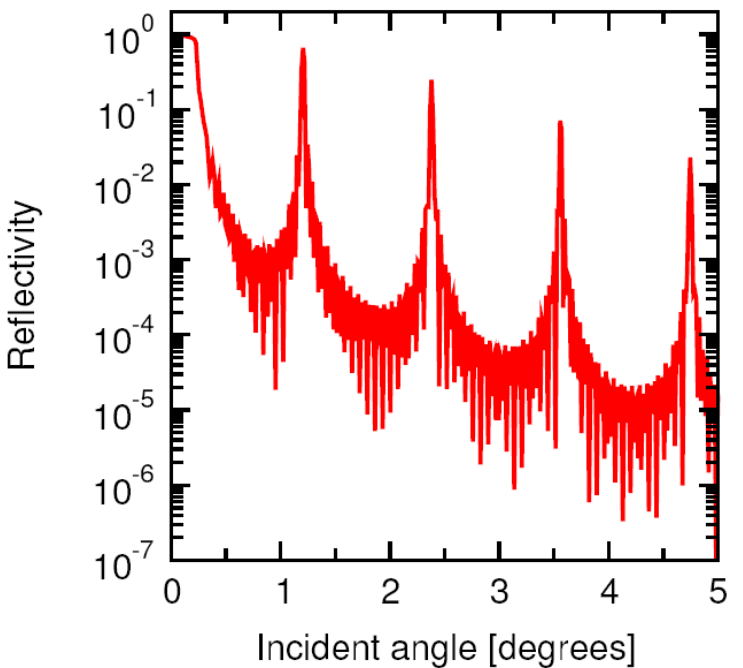
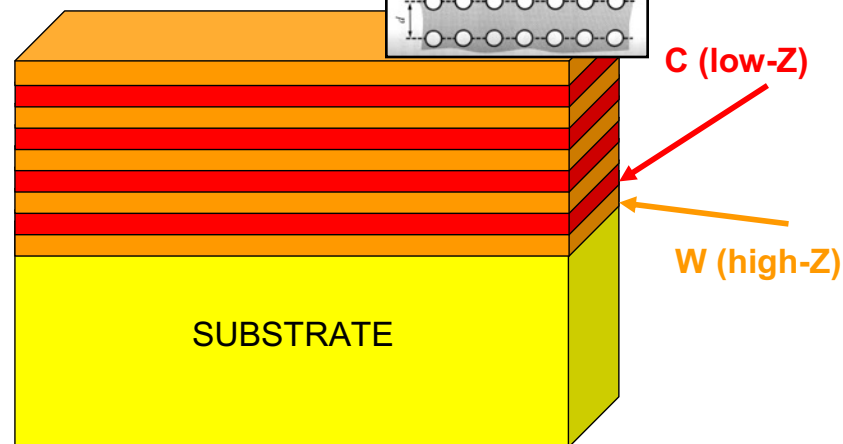


Si111 and multilayers as wavelength selectors

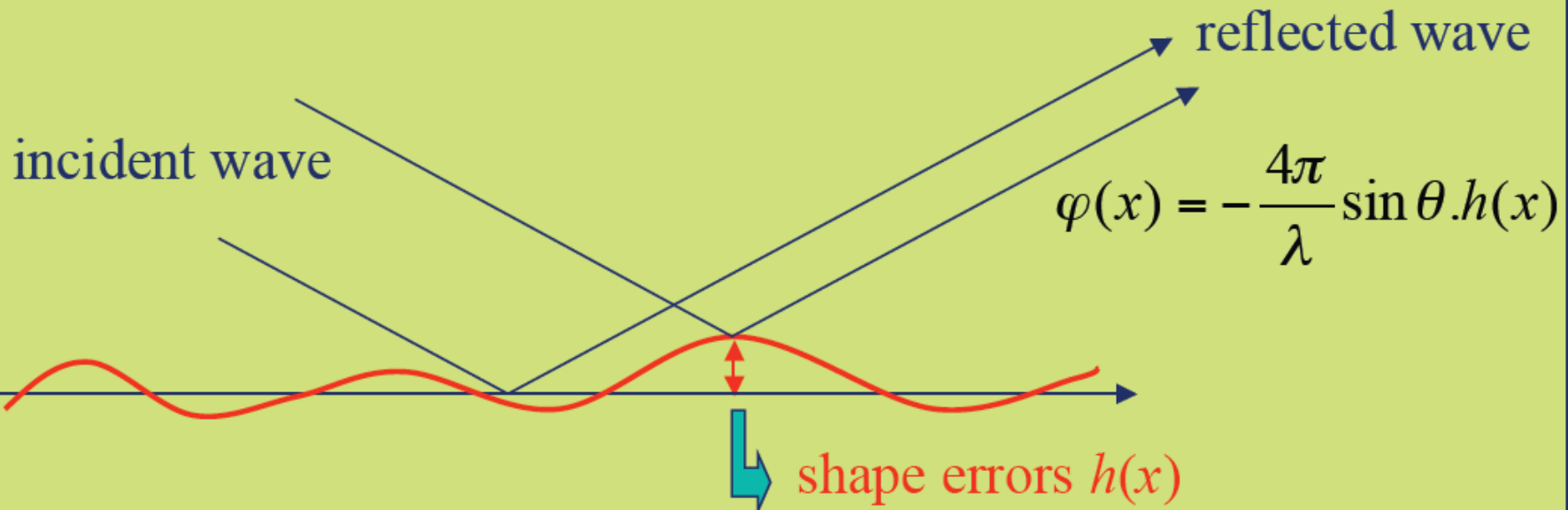


What is a multilayer?

- Multilayers are artificially grown periodic layers of two sorts of material. Each layer normally consists of a thinner sublayer of high-Z material (e.g., tungsten) and a thicker sublayer of a low-Z (i.e., high transmission) material, such as carbon.
- Scattering of the incoming x-rays at the interfaces between the two sublayers results in diffraction maxima occurring in exactly the same manner as in crystals. Multilayers can therefore be thought of as "artificial crystals".
- Because there are relatively few scattering planes (at least compared to the number of scattering planes in a crystal), multilayer monochromators are ideal for beamlines with less stringent requirements regarding the degree of monochromacy, and where photon flux is at a premium
- In fact, the width of the multilayer Bragg peaks is of the order of 0.02° , significantly larger than the natural bandwidth of Si(111), which lies in the region of 0.001° .



Multilayers: quality of the substrate



$$\varphi(x) = -\frac{4\pi}{\lambda} \sin \theta \cdot h(x)$$
$$2d \sin \theta = \lambda$$

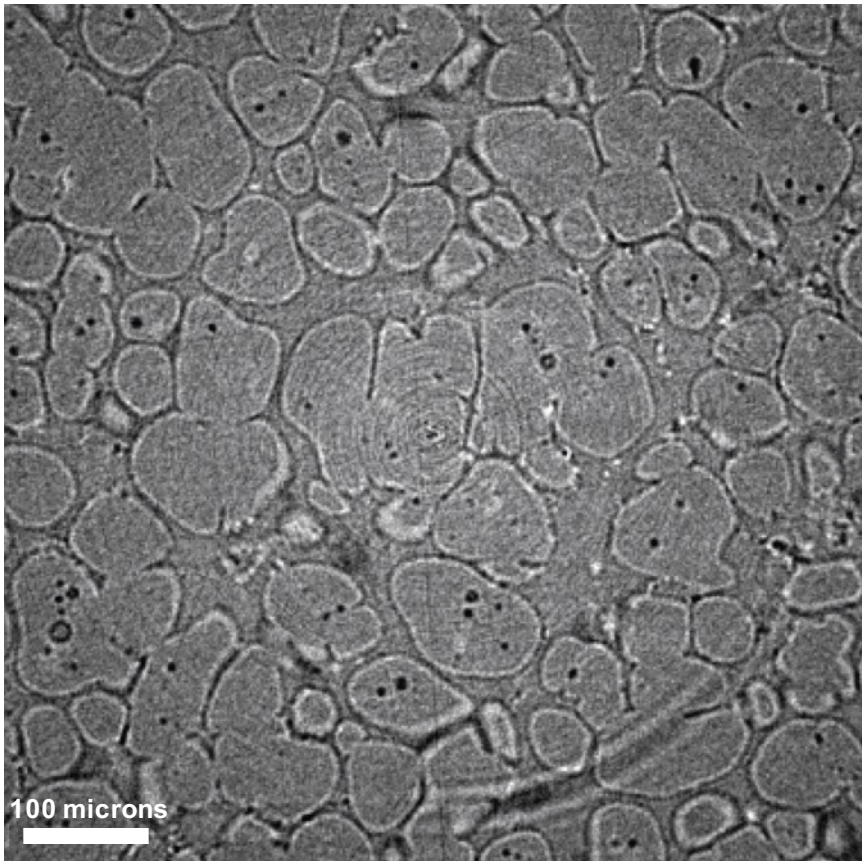
$$\varphi(x) = -2\pi \frac{h(x)}{d}$$

→ **Shape errors** should be much smaller than the **layer period** !

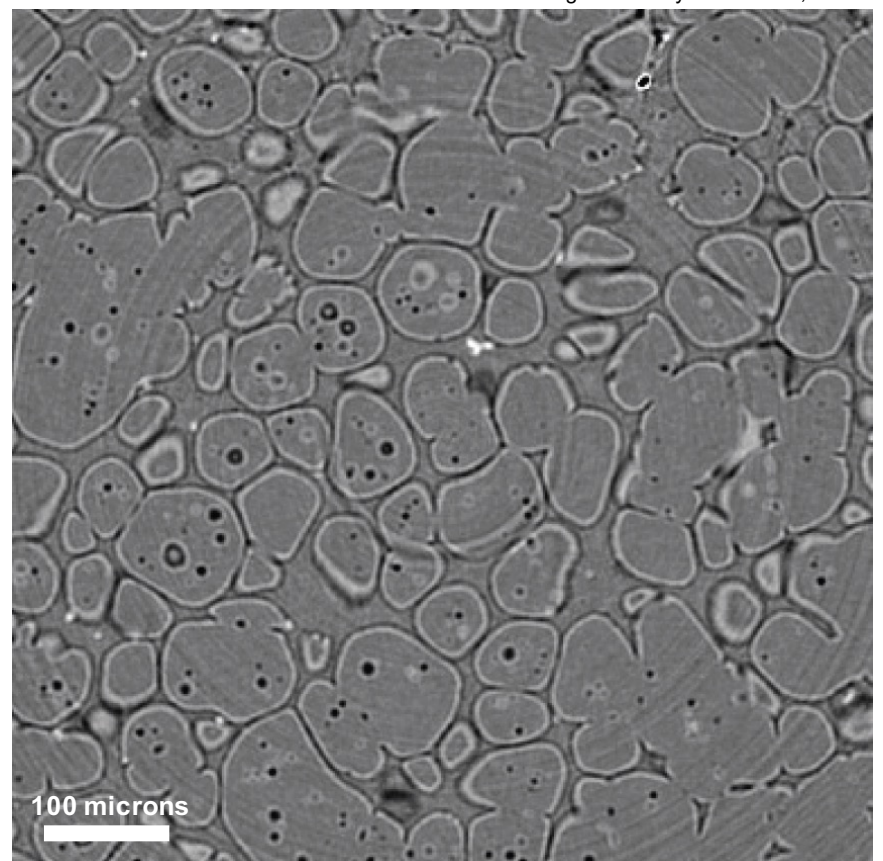
Multilayer vs Crystal monochromators

Al/Al-Si sample, energy 18 keV, pixelsize 2 microns (ID19,ESRF)

Images courtesy P. Cloetens, ESRF

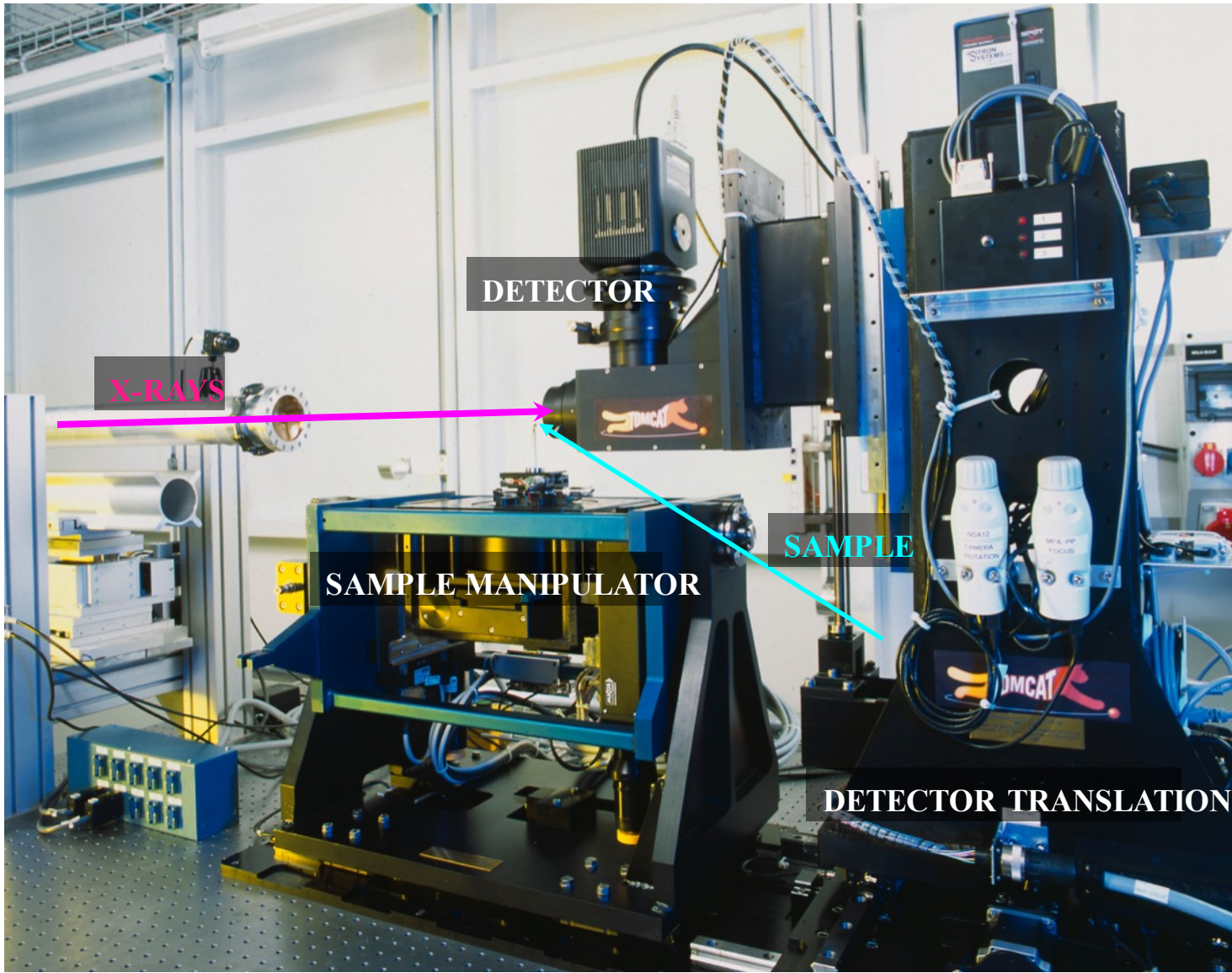


Si111 - 2 hours
 $\Delta\lambda/\lambda \sim 0.01\%$



Multilayer - 9 minutes
 $\Delta\lambda/\lambda \sim 2\%$

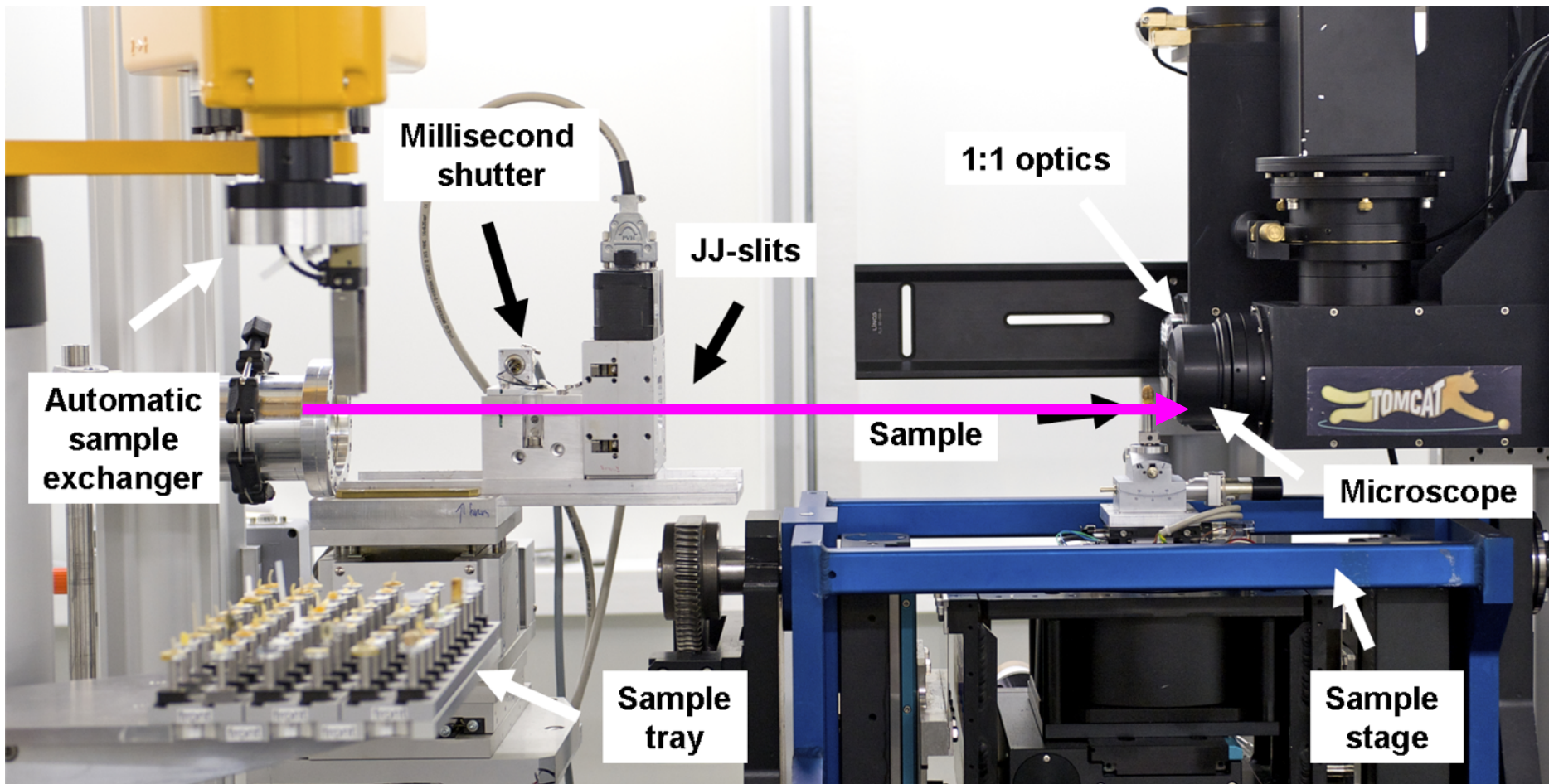
High-resolution endstation



Year 2006

TOMCAT Endstation

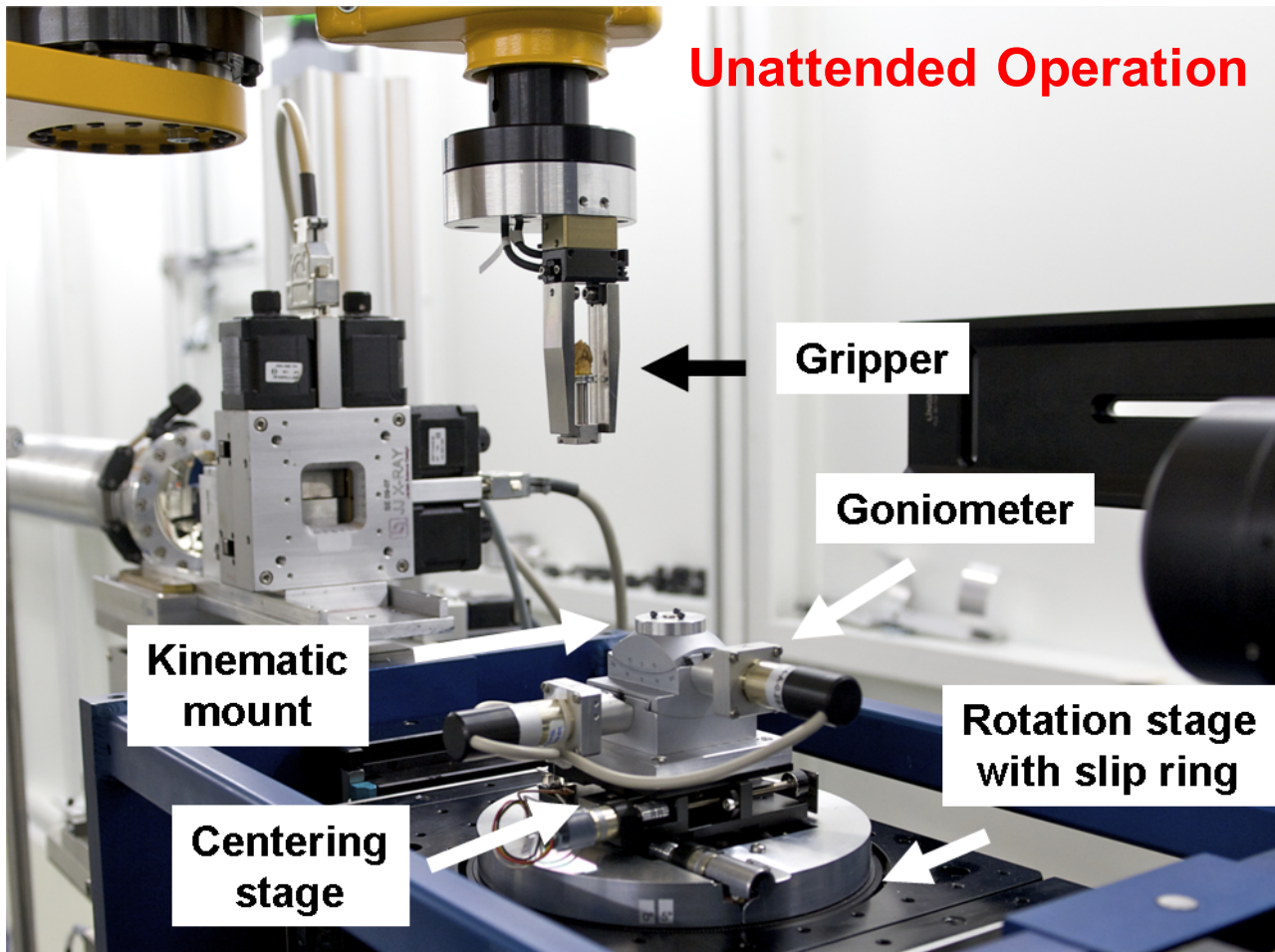
Year 2011



1 micron resolution routinely achieved at 10% contrast

TOMCAT Endstation

Year 2011



60 samples on tray, sequencer and automatic ROI finder

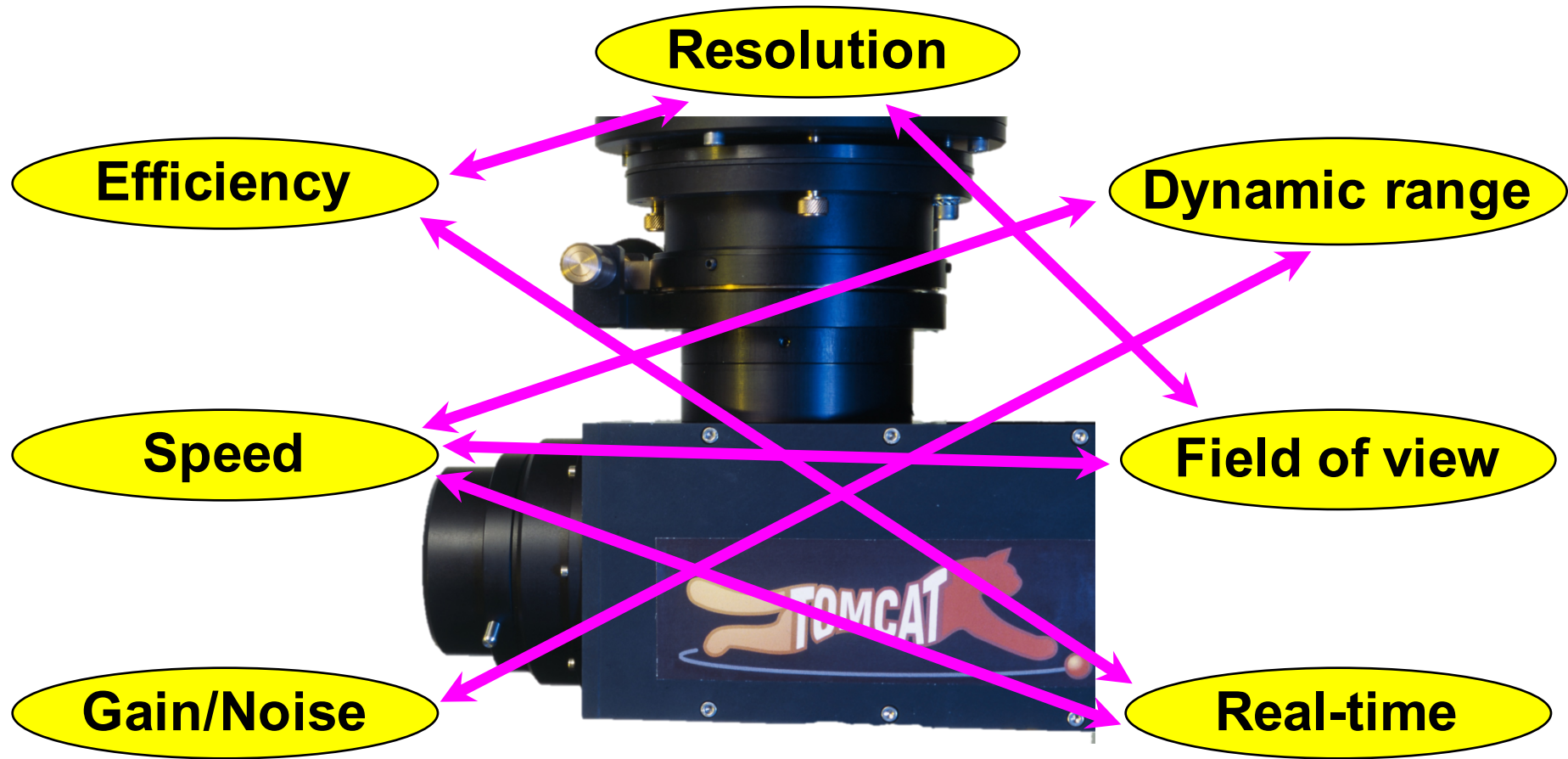
Key features of an imaging beamline

HIGH

WIDE

- 
- Spatial resolution, field of view
 - **FAST and AUTOMATED**
 - Data acquisition
 - Sensitivity (absorption / phase contrast)
 - **HIGH**
 - Energy range / Sample Flexibility
 - **BROAD**
 - **HIGH**
 - Data post-processing
 - **FAST and ONLINE**
 - In-situ experiments
 - **MULTIPLE**
 - User friendliness
 - **EASY**

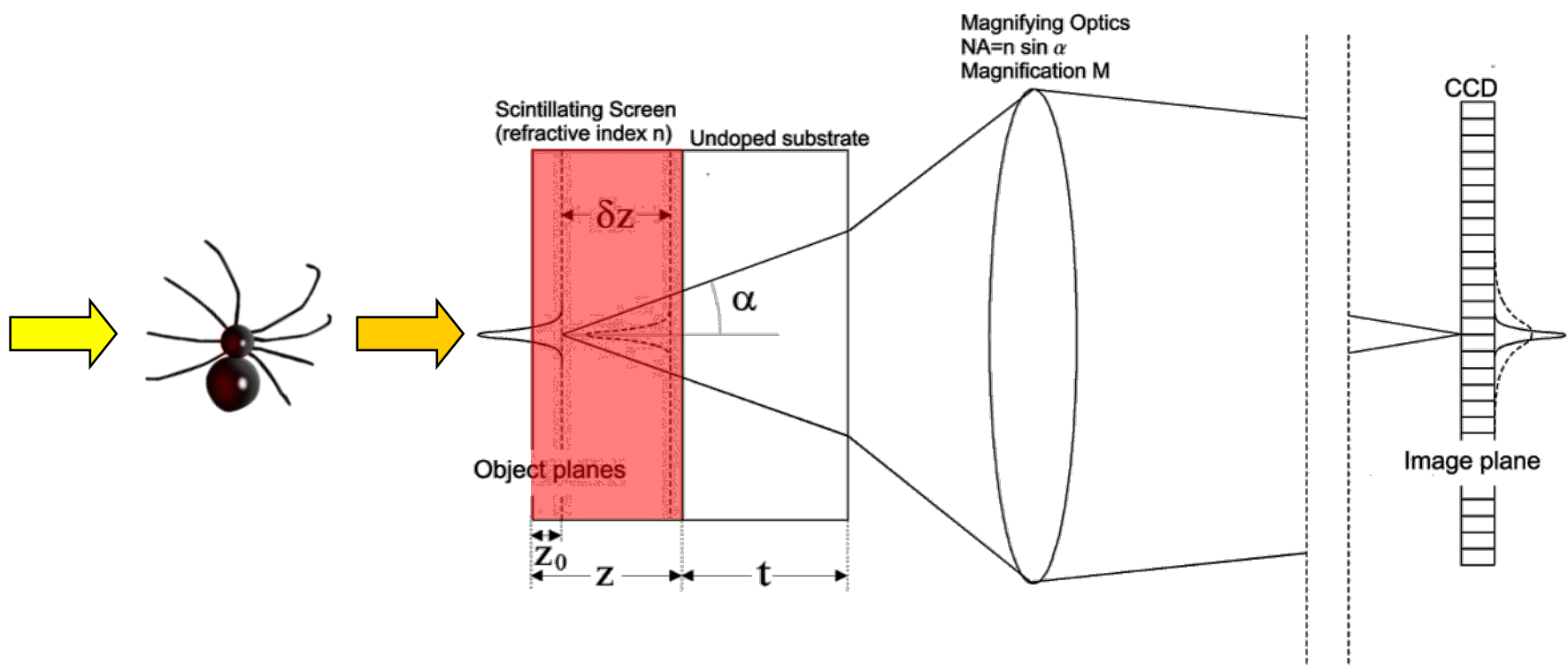
Imaging detector requirements



**Best compromise for resolution < 50 microns:
scintillator screen coupled to CCD/CMOS**

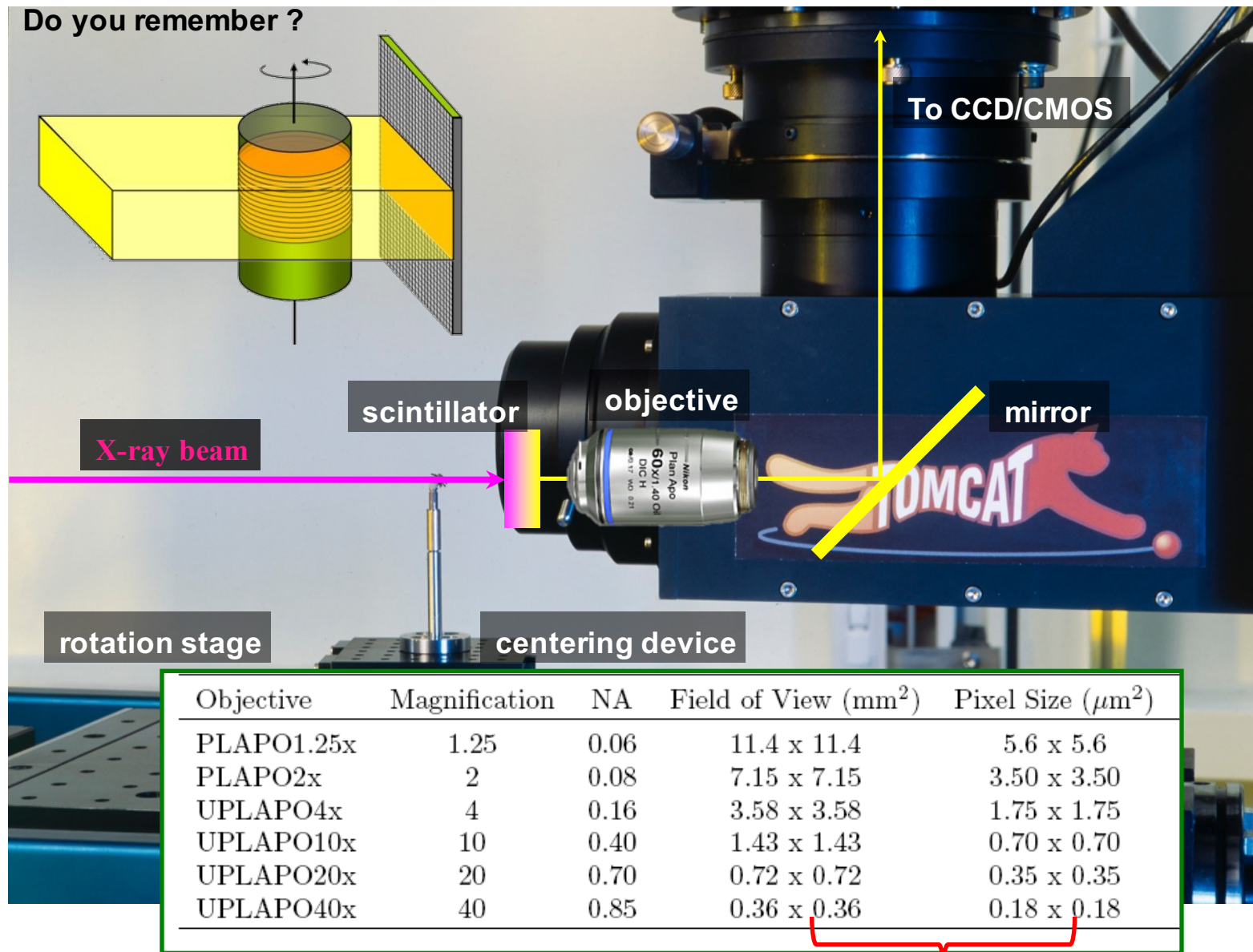
Scintillator-coupled CCD-CMOS detectors

1. X-rays hit scintillating screen
2. Scintillator screen (thin powders) convert X-rays to visible light
3. Visible light is collected by high efficiency lens
4. Lens magnify image onto CCD-CMOS chip



How does this look like?

Do you remember ?



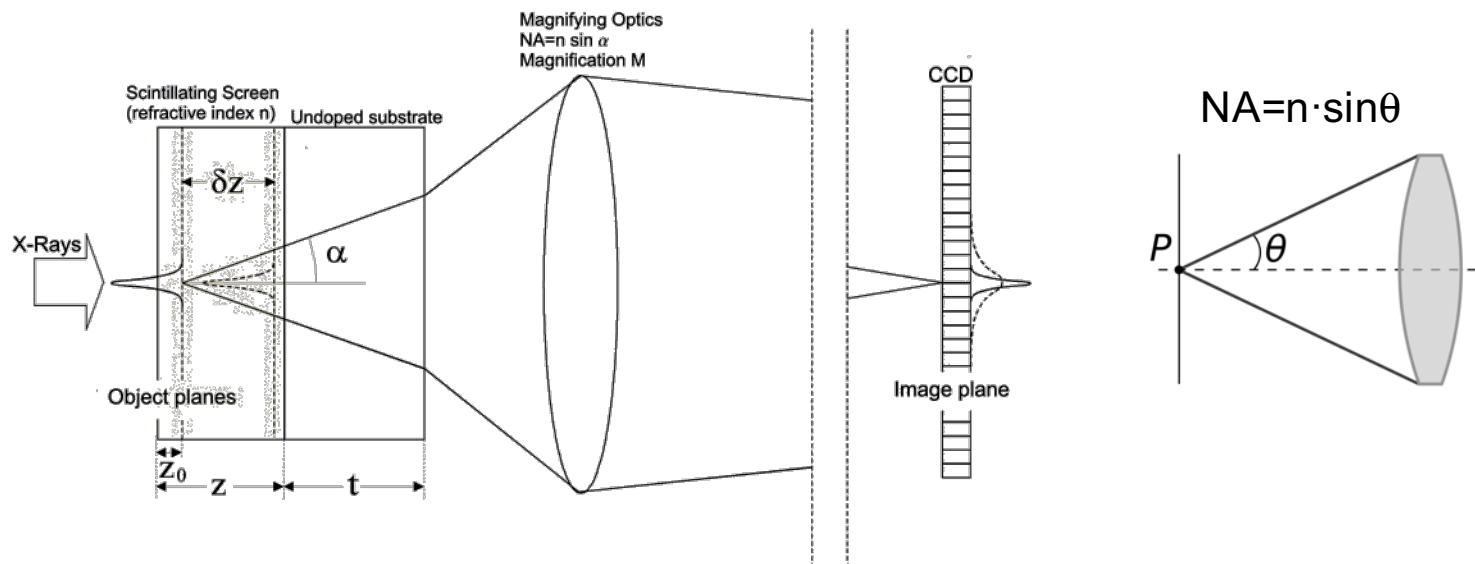
Scintillator requirements

- **High X-ray absorption:** couple high-density, large atomic number and radiation hardness to maximize X-ray stopping power
- **Strong light emission:** high conversion efficiency, emission wavelength well matched to the CCD, low afterglow and linearity
- **Good optical properties:** high transmittance and no scattering
- **Technical aspects:** machinable, non-toxic and mechanical strength

T. Martin, A. Koch, J. Synchrotron Rad. (2006), 13, 180–194

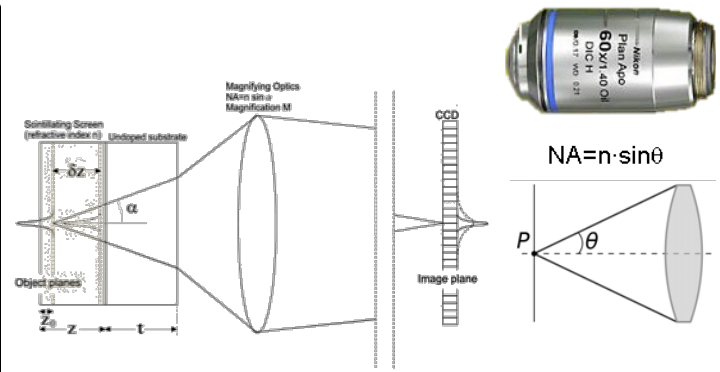
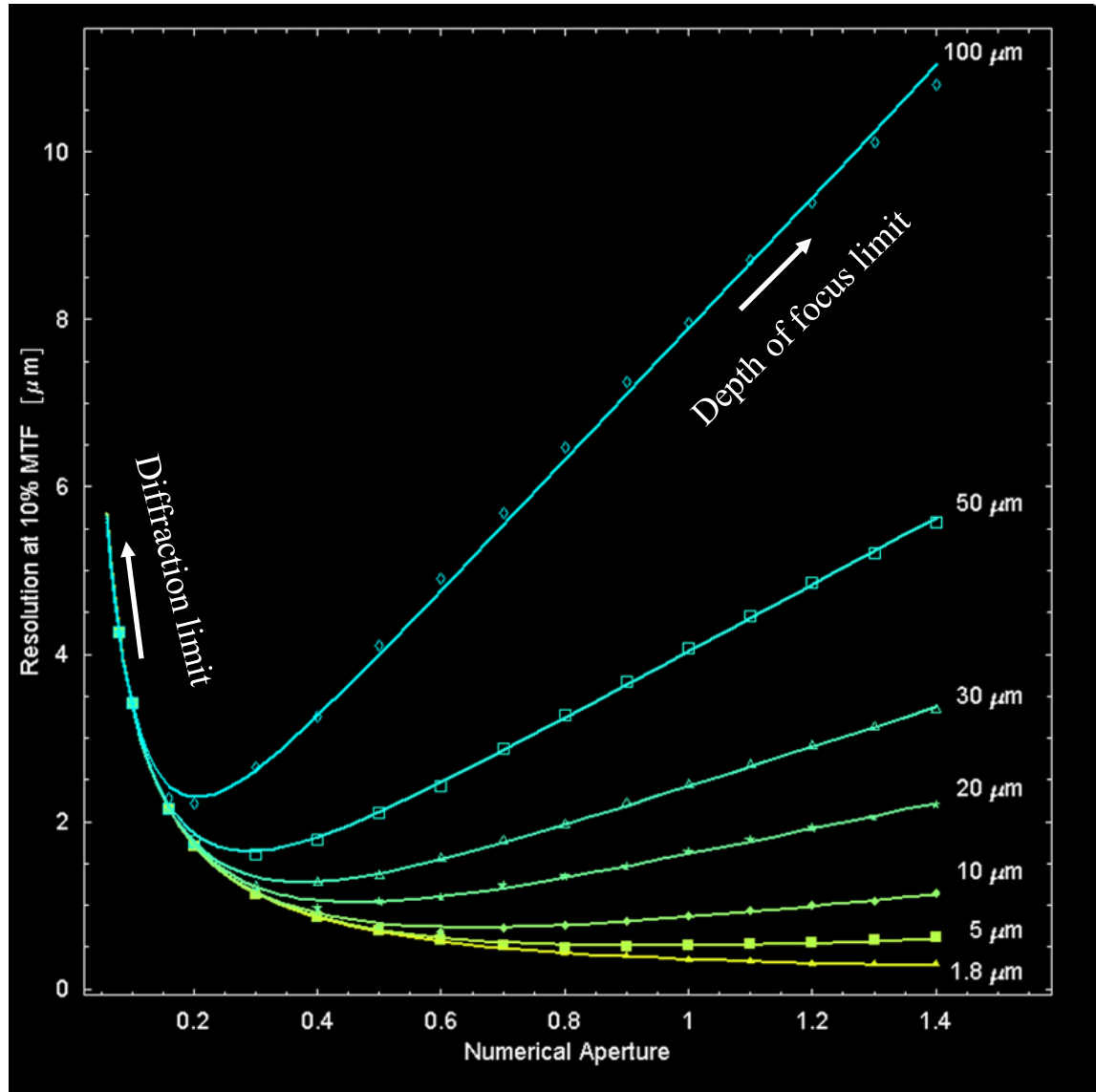
Scintillators	Name	Z_{eff}	ρ (g cm $^{-3}$)	ρZ_{eff}^4 ($\times 10^6$)	$\eta_{x/v}$	Light yield	λ (nm)	n	Cleavage
Gd ₂ O ₂ S:Tb	P43	59.5	7.3	91	13		545		Powder
Y ₃ Al ₅ O ₁₂ :Ce	YAG	32	4.55	5	4.0	40000–50000	550	1.82	None
Bi ₄ Ge ₃ O ₁₂	BGO	75	7.13	225		8200	480	2.15	None
Lu ₃ Al ₅ O ₁₂ :Ce	LAG	61	6.73	93		20000	535	1.85	None
Lu ₃ Al ₅ O ₁₂ :Eu	LAG	61	6.73	93			535	1.85	None
CdWO ₄		63	7.9	124		15000	470	2.2	Yes
Gd ₃ Ga ₅ O ₁₂ :Eu	GGG	52	7.1	80					None
CsI:Tl		54.1	4.52	39	15	65000	540	1.8	None
Lu ₂ O ₃ :Eu		68.8	8.4	180		20000	611	1.8	None
Gd ₂ O ₃ :Eu		61	7.1	98		19000	611	1.88	None
Lu ₂ SiO ₅ :Ce	LSO	65.2	7.4	136		25000	420	1.82	None
Lu ₃ Ga ₅ O ₁₂ :Eu	LGG	58.2	7.4	85					None

Optical coupling: spatial resolution issues



- The object plane z_0 within the scintillator is focused on the CCD camera (image plane)
- Planes in front of and behind the object plane are out of the focus but contribute to the total light emitted in the z thickness of the scintillator projected onto the CCD.
- The image resolution is determined by the defect of focus (δz) of the image distribution outside the object plane.
- Other degradations of the image are due to the diffraction and the spherical aberrations arising from the thickness of the scintillator (z) and the substrate (t).

Implication of optical coupling



Depth of focus $\approx \delta z NA$
 Diffraction $\approx \lambda / NA$
 Spherical aberration $\approx \tau NA^3$

$$R = \sqrt{(p/NA)^2 + (qzNA)^2}$$

Take home message:

- Geom. Pixel Size \neq True Resolution
- Thin scintillator \rightarrow better resolution
- DOF limited at high NA
- Diffraction limit at low NA

Key features of an imaging beamline

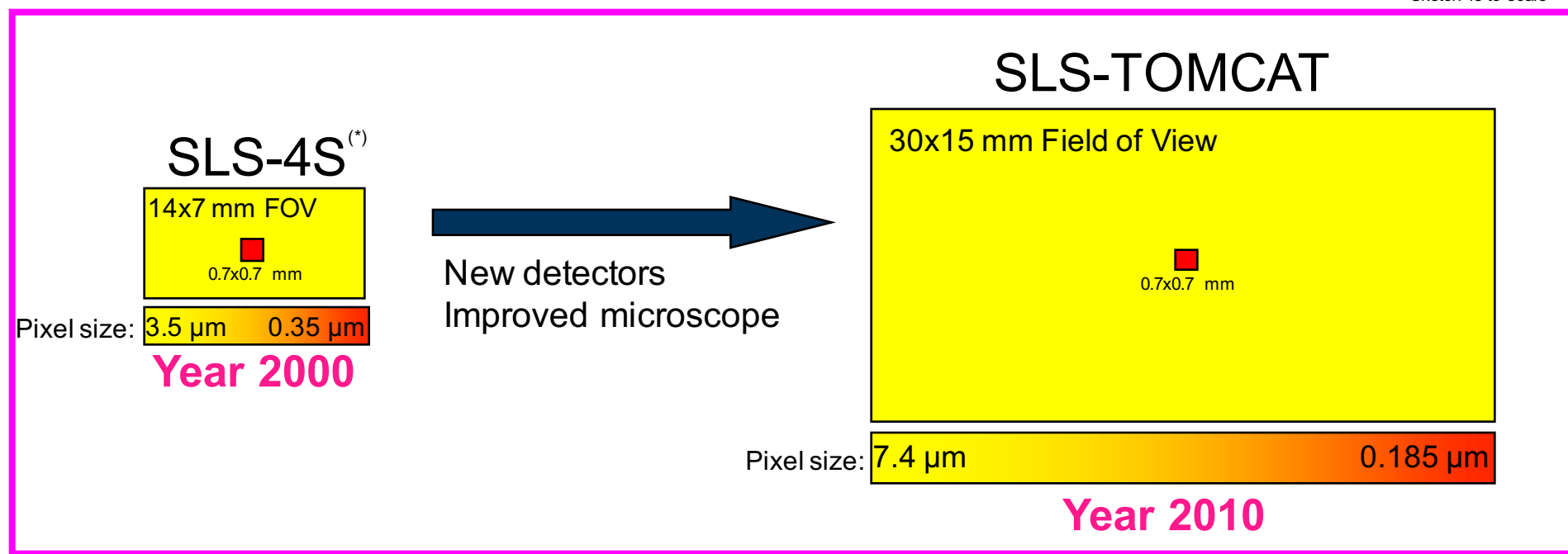
HIGH

WIDE

- Spatial resolution, field of view ←
- **FAST and AUTOMATED**
- Data acquisition
- **HIGH**
- Sensitivity (absorption / phase contrast)
- **BROAD** **HIGH**
- Energy range / Sample Flexibility
- **FAST and ONLINE**
- Data post-processing
- **MULTIPLE**
- In-situ experiments
- **EASY**
- User friendliness

Field of view – Pixel size

Sketch is to scale

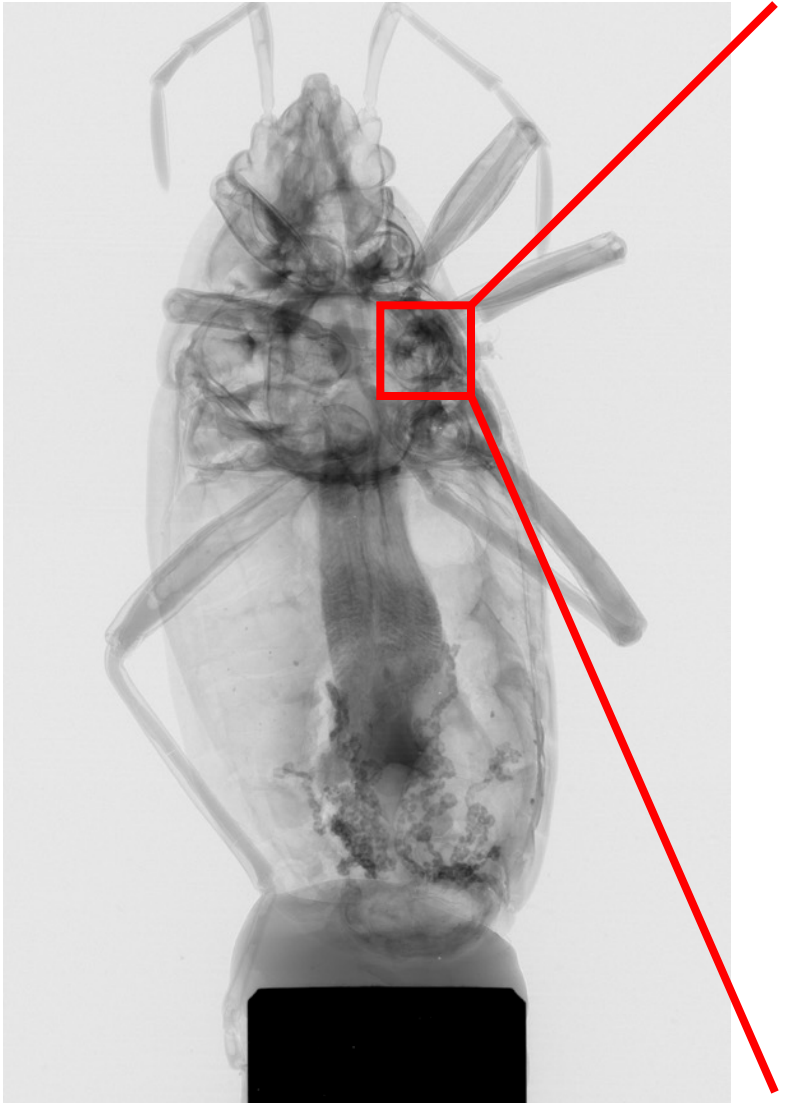


During the last decade an impressive detector development has been observed, leading mainly to smaller and more pixels on a CCD/CMOS device.

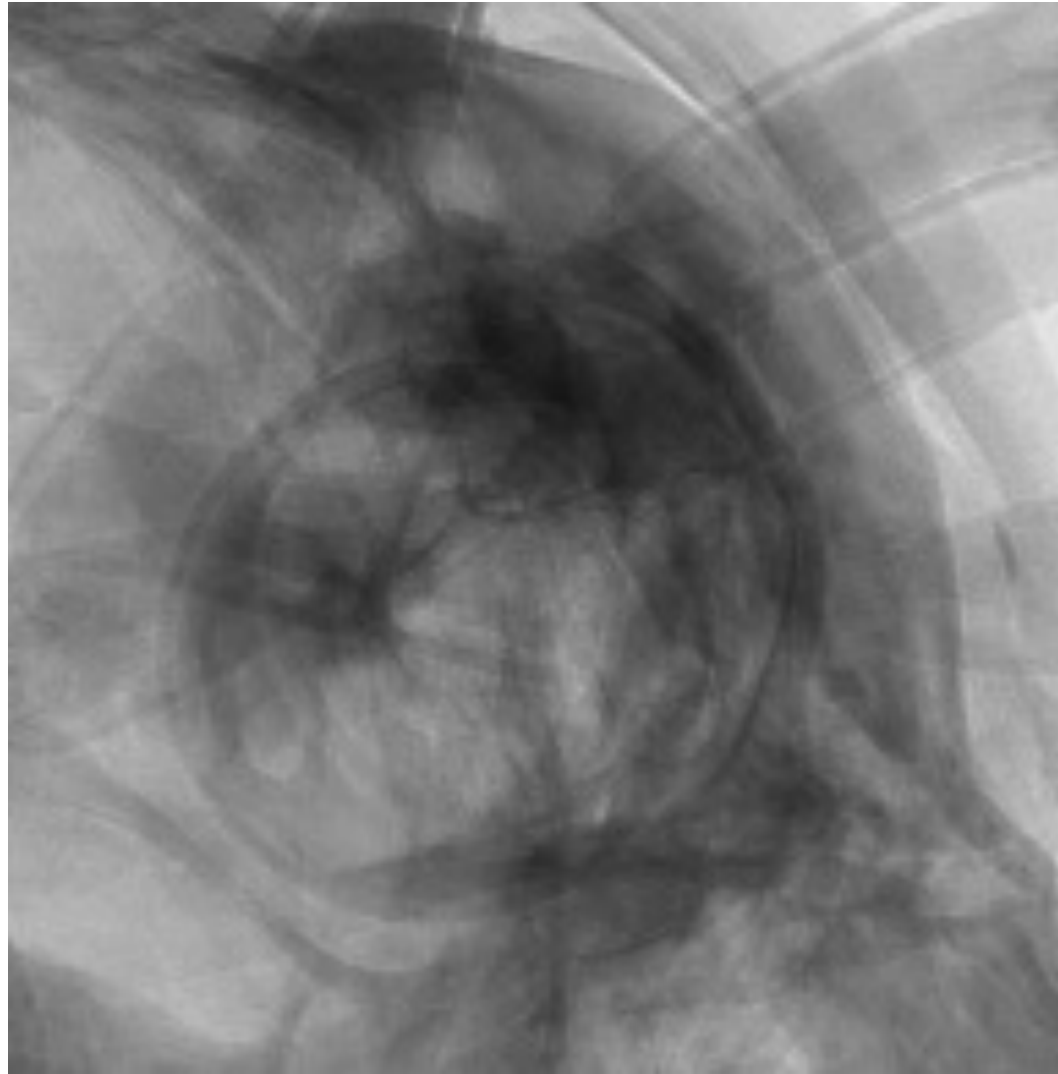
→ Larger area can be covered with a better resolution.

(*) First tomography beamline at SLS, now not used anymore

Pixel size is not the resolution !!



Energy 12.6 keV, Field of view 10x4 mm² Pixel-size 5.6x5.6 μm²

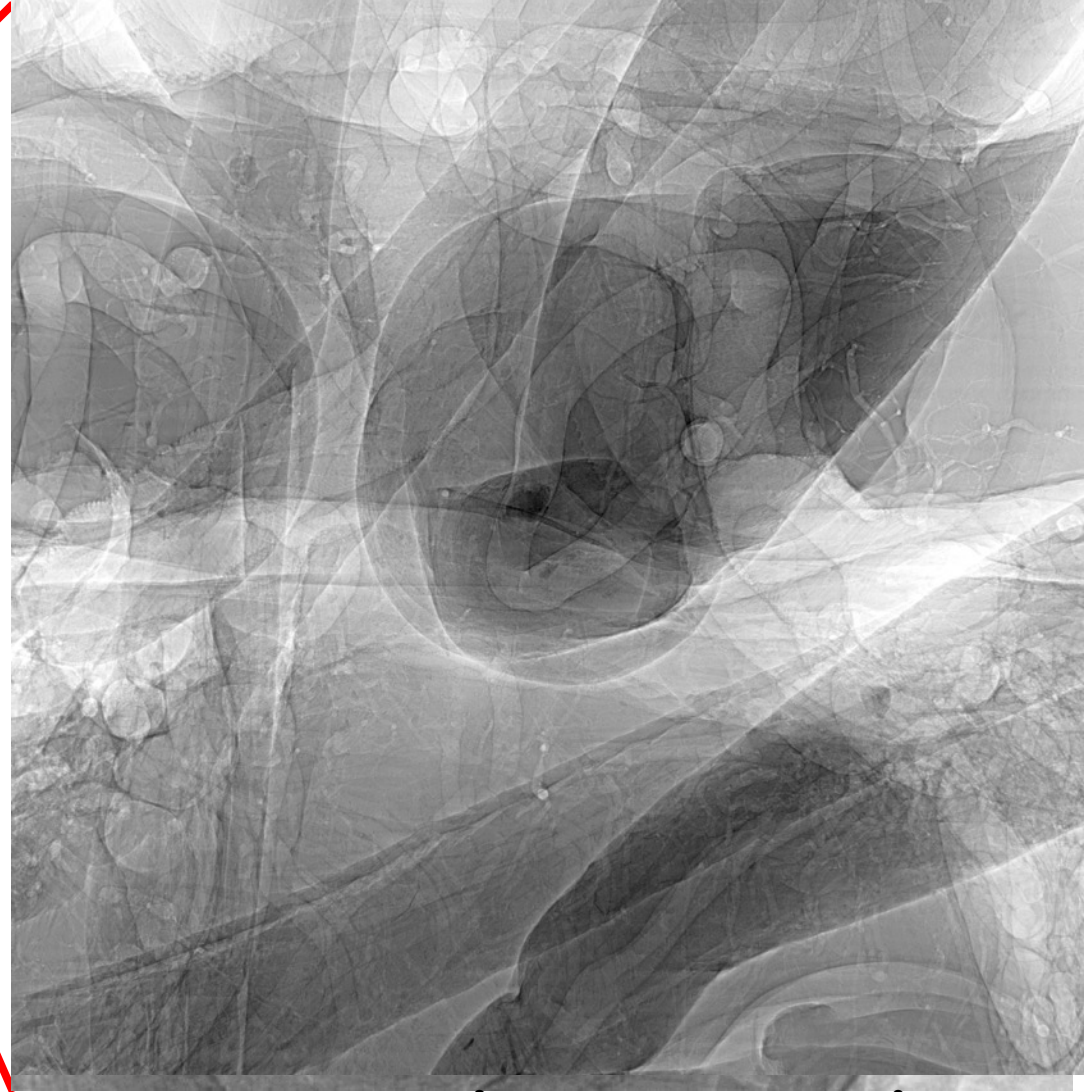


Field of view 10x4 mm² - Pixel-size 5.6x5.6 μm²
Resolution > 11 μm

Pixel size is not the resolution !!



Energy 12.6 keV, Field of view 10x4 mm² Pixel-size 5.6x5.6 μm²



Field of view 1.4x1.4 mm², Pixel-size 0.7x0.7 μm²
Resolution >= 1.5 microns

Pixel size is not the resolution !!

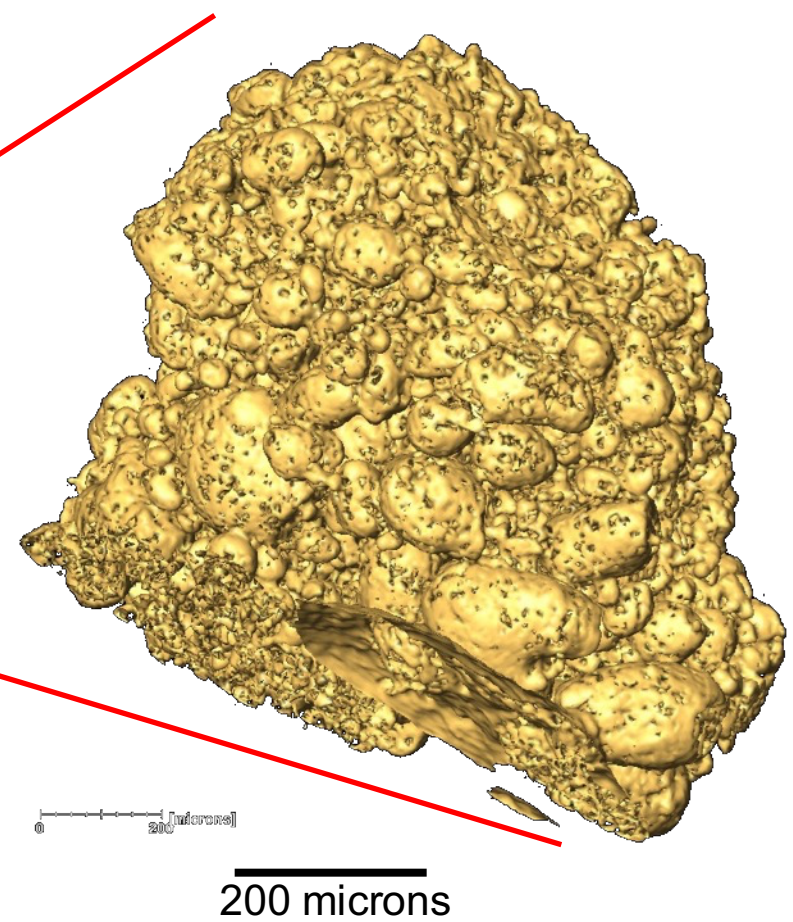


Energy 12.6 keV, Field of view 10x4 mm² Pixel-size 5.6x5.6 μm²

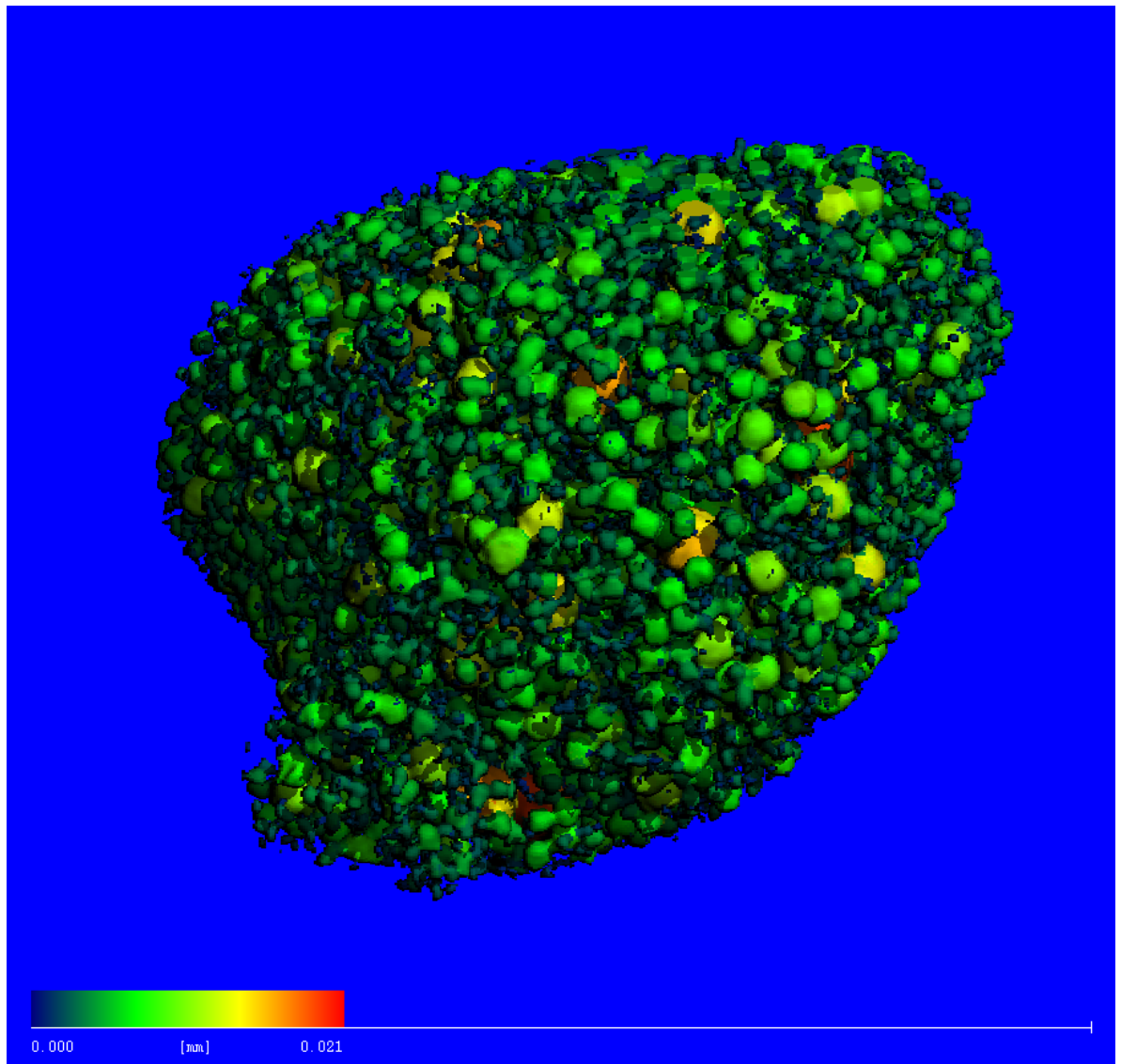
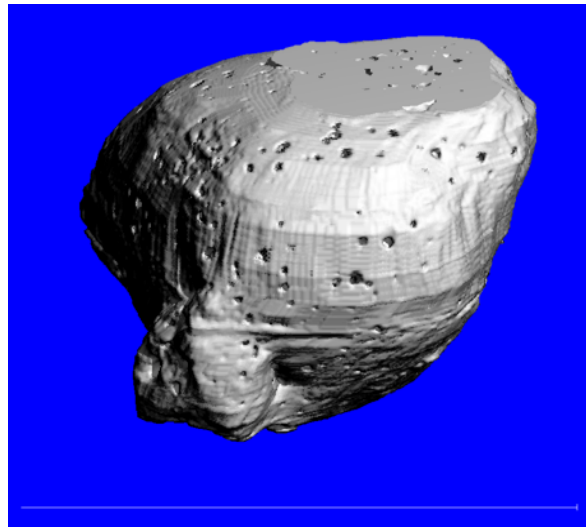
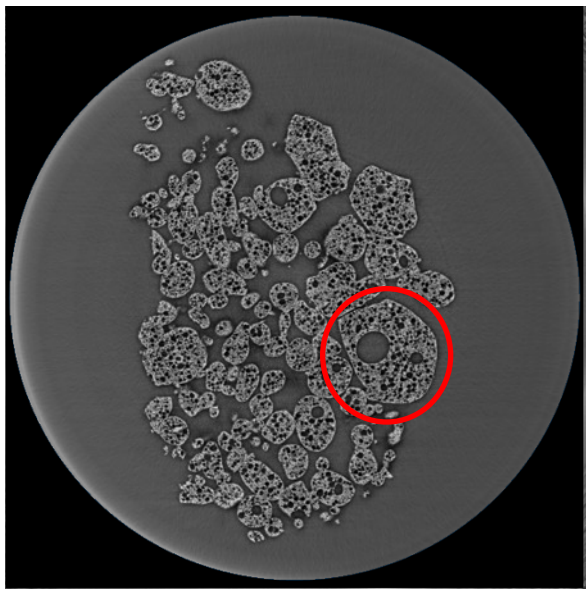


Field of view 1.4x1.4 mm², Pixel-size 0.7x0.7 μm², Resolution >= 1.5 microns **ZOOMED-IN**.

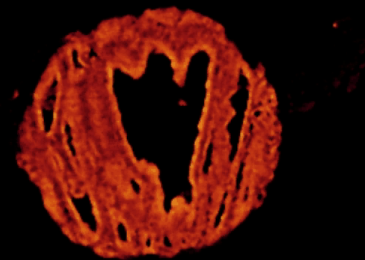
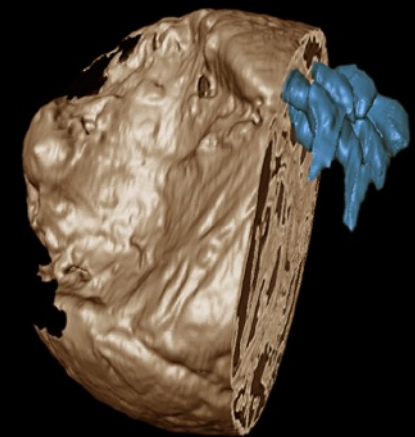
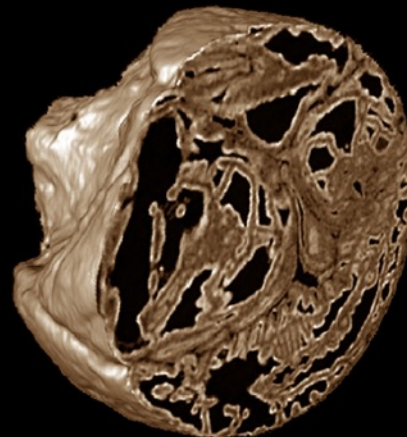
What does 1 micron resolution mean...in practice?



Quantitative analysis: morphology and porosity



SR tomographic microscopy in paleobiology

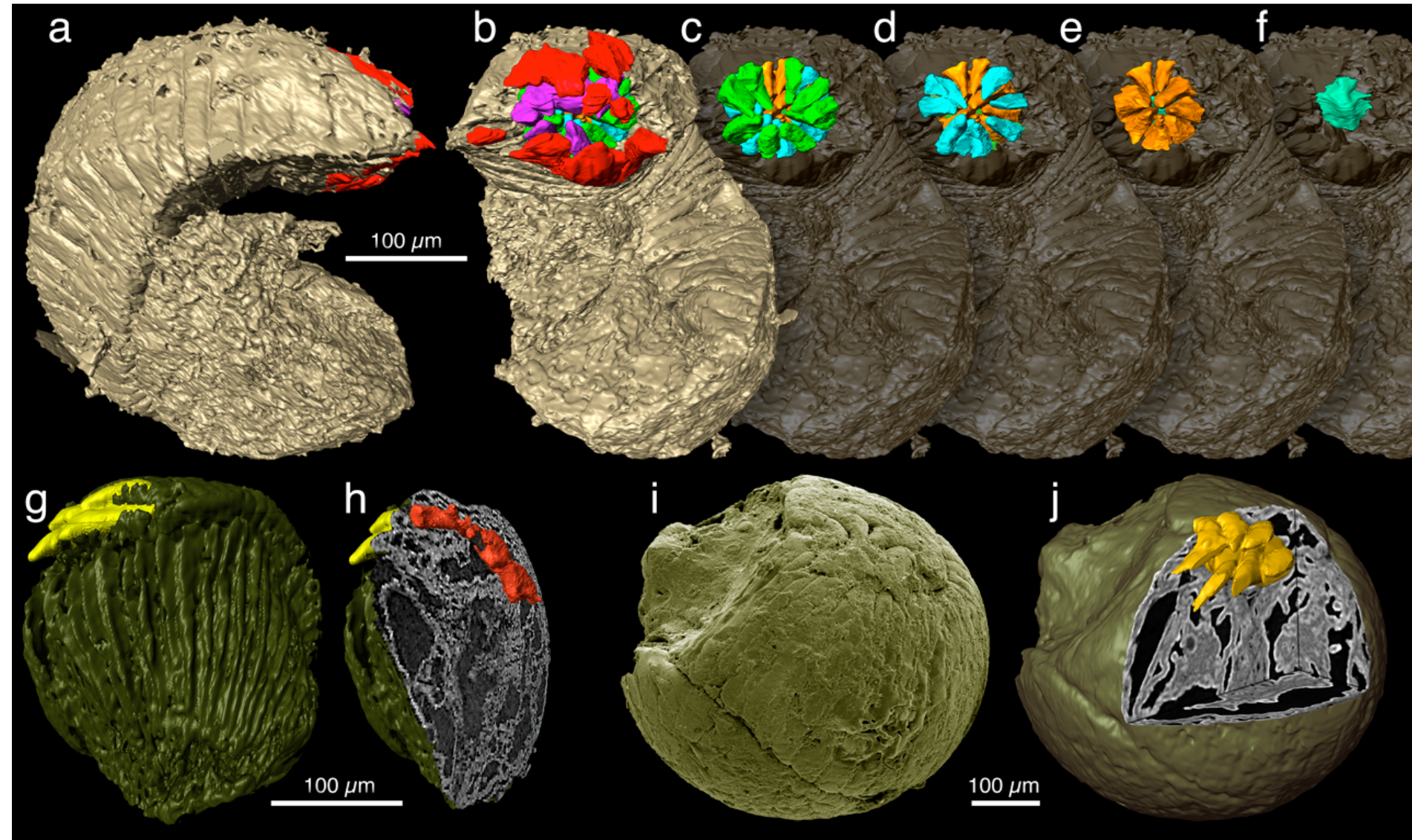


- Unique technology
 - high-resolution
 - 3D quantitative info
- Unique sample (540 My (!))
 - non-destructive testing

Will this help to better understand what triggered the Cambrian explosion, i.e. the animal diversification?

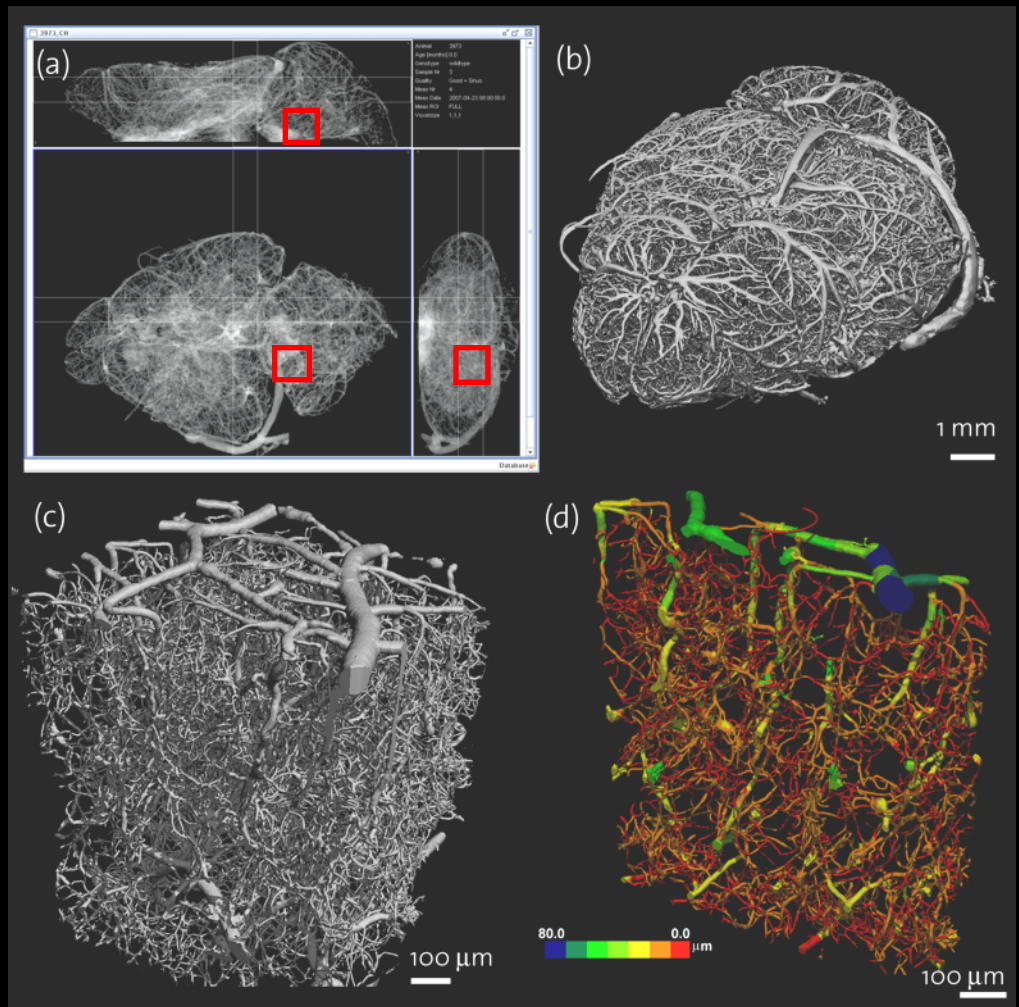
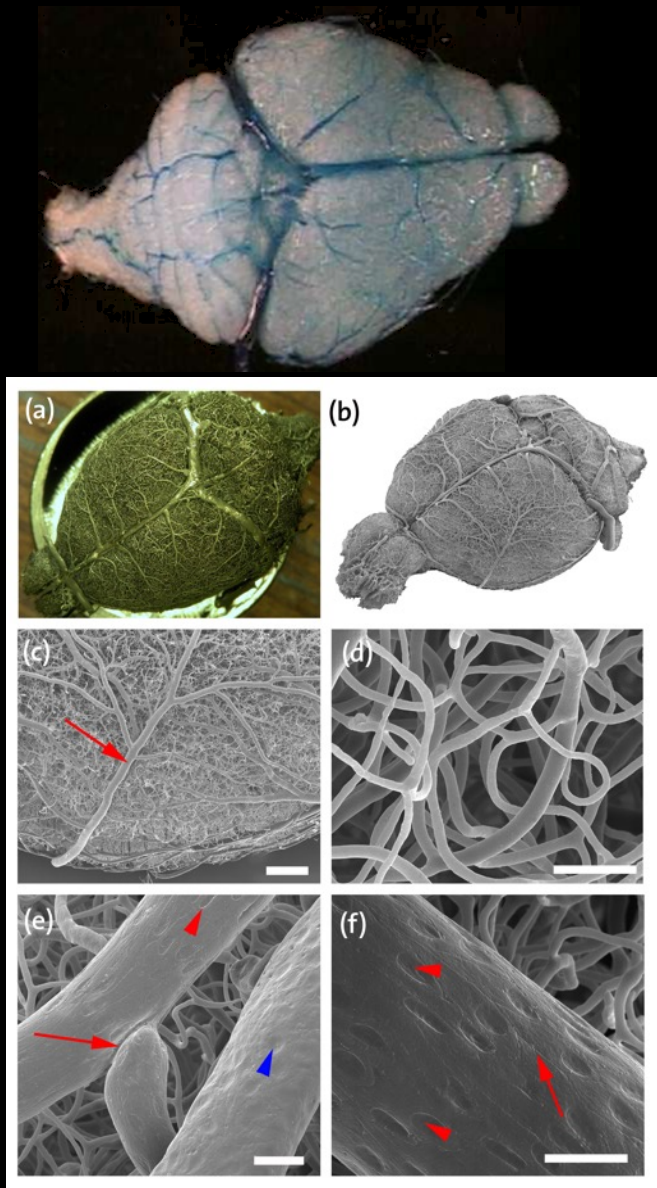
P. Donoghue, M. Stampanoni et al., *Synchrotron X-ray tomographic microscopy of fossil embryos*, NATURE 442, 2006

Complex image analysis and data interpretation



Donoghue et al (2006) Nature 442:680-3

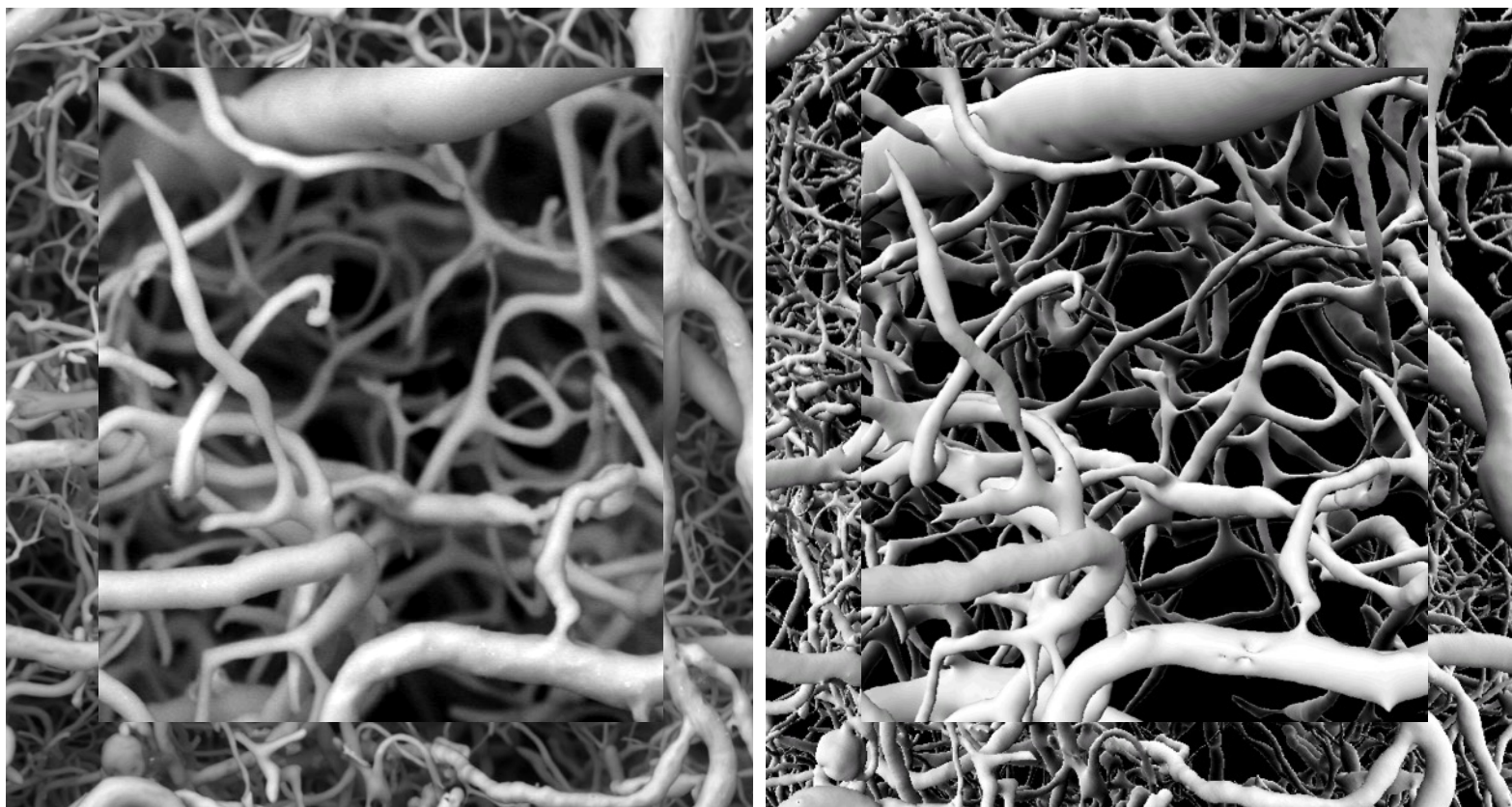
Vascular corrosion casting (PU) combined with SRXTM



S. Heinzer et al., *Hierarchical microimaging for multiscale analysis of large vascular networks*, Neuroimage 32 (2): 626-636, Aug. 15, 2006

M. Stampanoni et al., *Resolving brain microvascular architecture with X-ray tomographic microscopy using vascular corrosion casting*, Advancements in Neurological Research, ISBN: 978-81-308-0225-1, 2008

Validation of SRXTM with SEM



SEM image (2D) of cortical vasculature

SRXTM image (3D) of the same region

S. Heinzer, T .Krucker, M. Stampanoni, R. Abela, E. P. Meyer; A. Schuler, P. Schneider and R. Müller. *Hierarchical microimaging of mouse brain vasculature from cerebral arteries to the capillary network*. Neuroimage, 32 (2), 2006

Modeling the Rat Cerebral Blood Flow

Raw data

- BaSO₄ injection and EPON embedding
- 20 keV, 370 nm pix. siz.

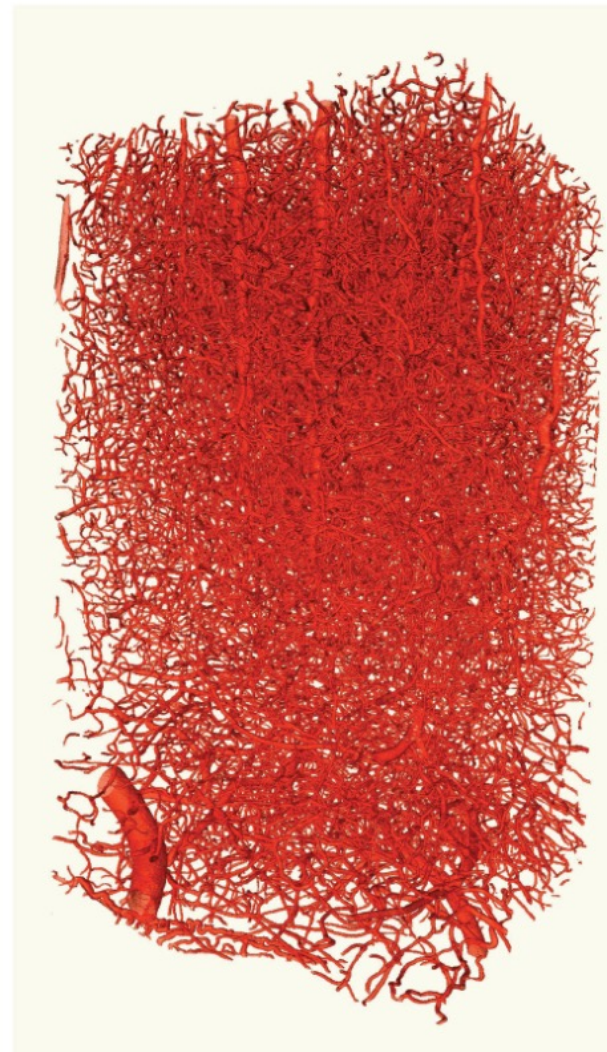
Image processing

- Segmentation
- Midline extraction
- Branching and end points determination

Model construction

- Vessels are represented as cylinders with radius equals the mean radius
- Connectivity analysis for vessel classification
- Topological criteria for artery or veins identification

→ Vascular graph model.



- Pressure difference Δp associated with two different nodes results in blood flow through the vessel connecting them

- Vessel conductance:
$$G = \frac{\rho A^2}{8\pi\mu L}$$

- Mass flow rate:

$$F = G\Delta p$$

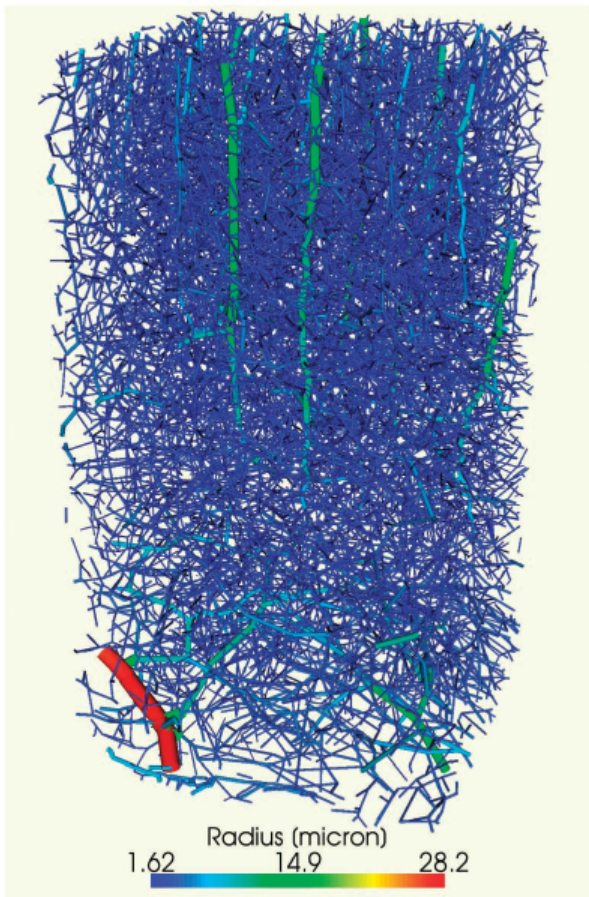
- Continuity equation (net mass flow matches the local accumulation rate, unless node is not a sink or a source):

$$\frac{\partial V_i}{\partial t} + \frac{1}{\rho} \sum_j G_{ij} (p_i - p_j) = \frac{q_i}{\rho}$$

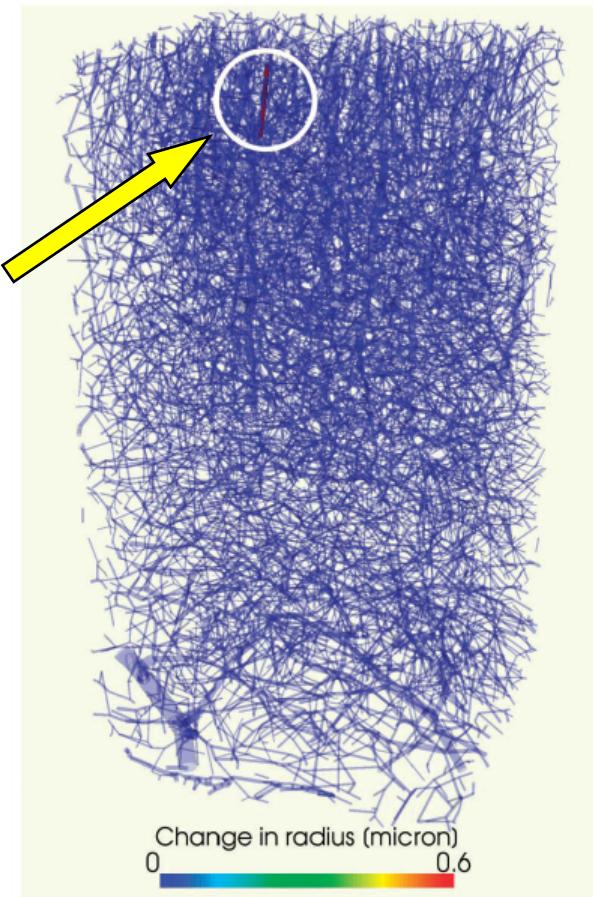
- System of equations is solved numerically.

From Reichold et al., Journal of Cerebral Blood Flow and Metabolism, 29(8), 1429-1443 (2009)

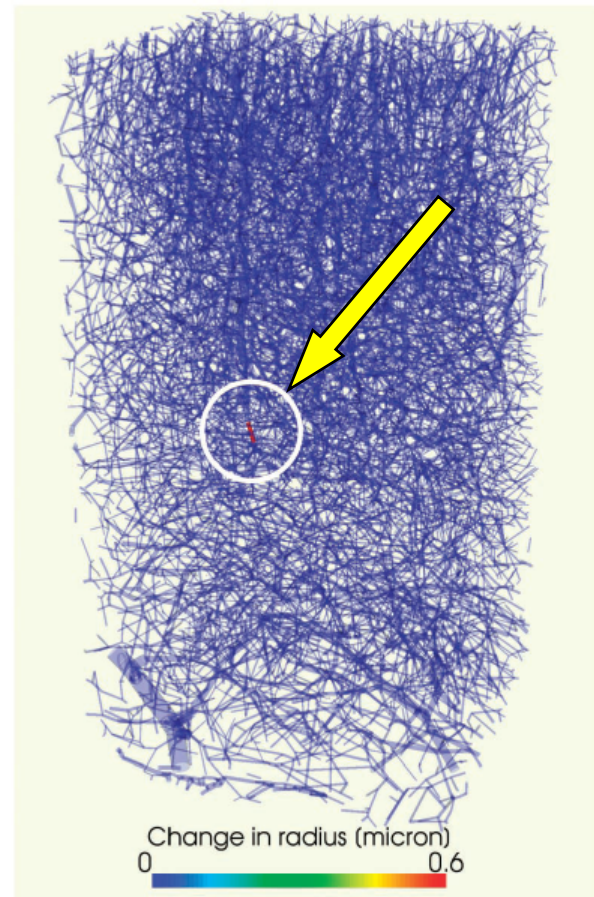
Modeling the Cerebral Blood Flow – Hyperemia



Vascular network



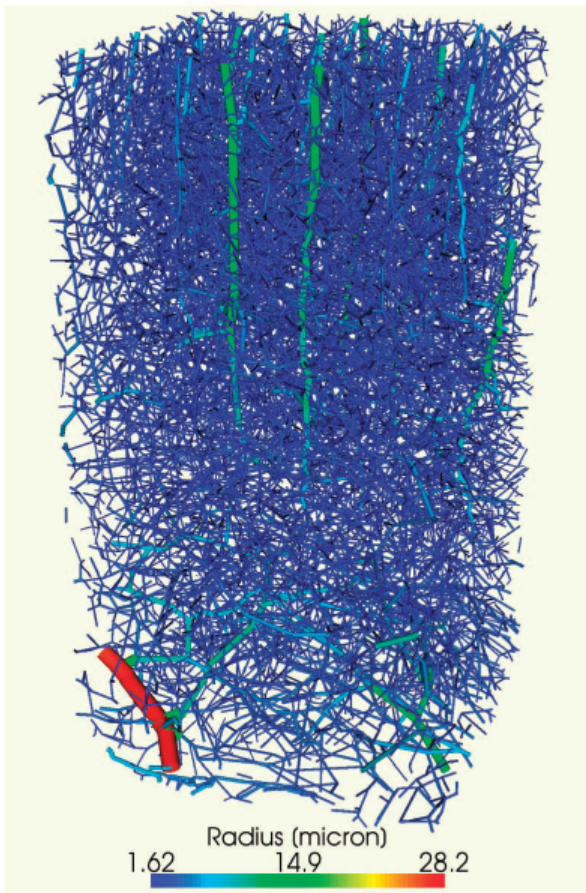
Short feeding artery dilated
near the cortical surface



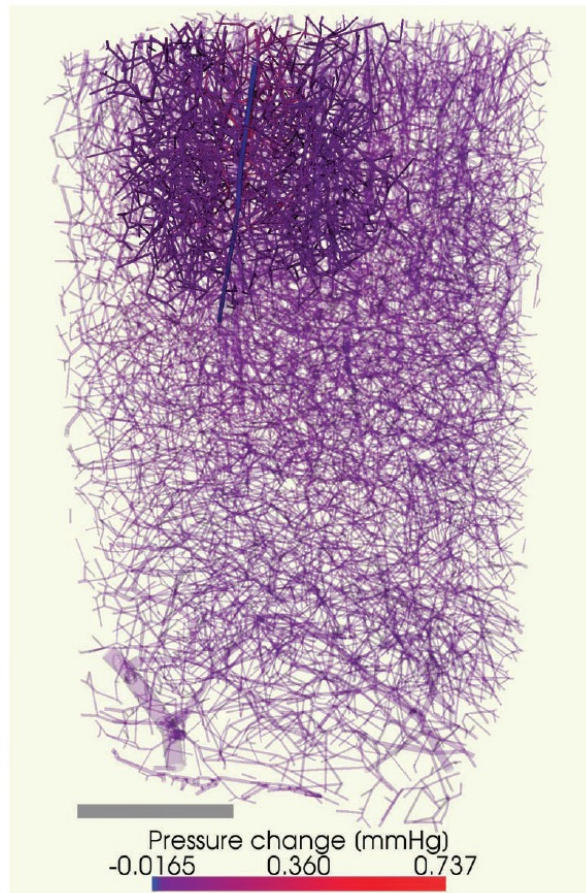
Long artery dilated just
upstream of the capillary bed

From Reichold et al., Journal of Cerebral Blood Flow and Metabolism, 29(8), 1429-1443 (2009)

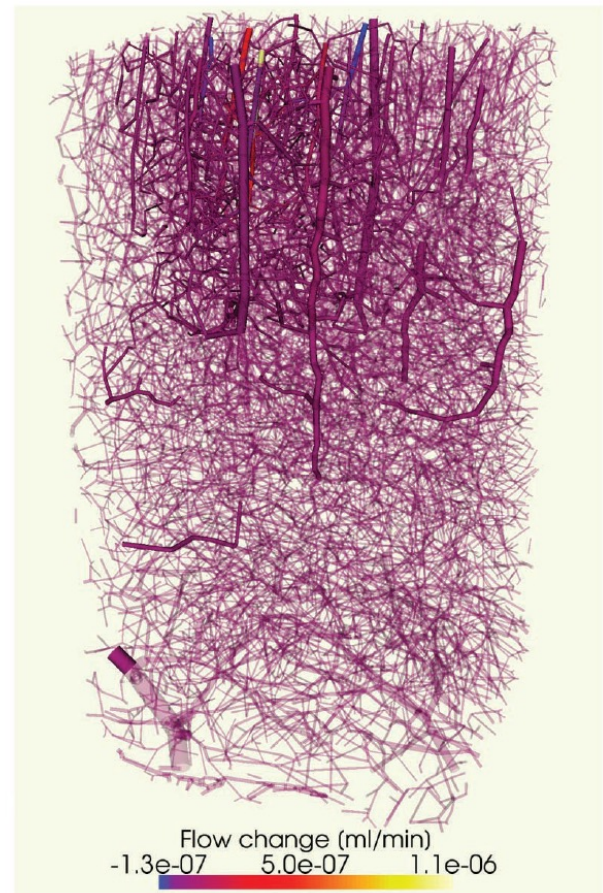
Modeling the Cerebral Blood Flow – Hyperemia



Short feeding artery dilated
near the cortical surface



Pressure Change

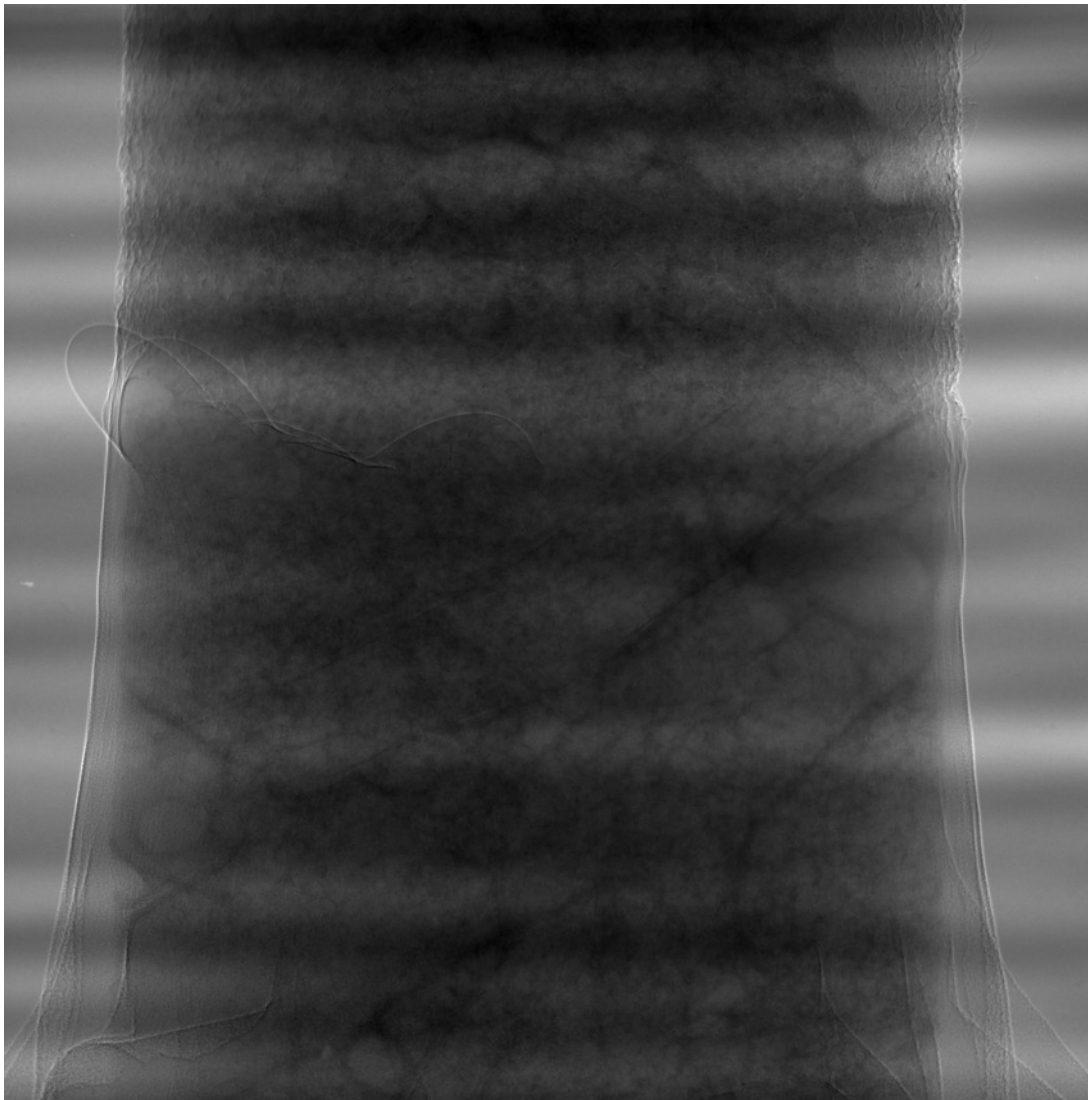


Flow Change

From Reichold et al., Journal of Cerebral Blood Flow and Metabolism, 29(8), 1429-1443 (2009)

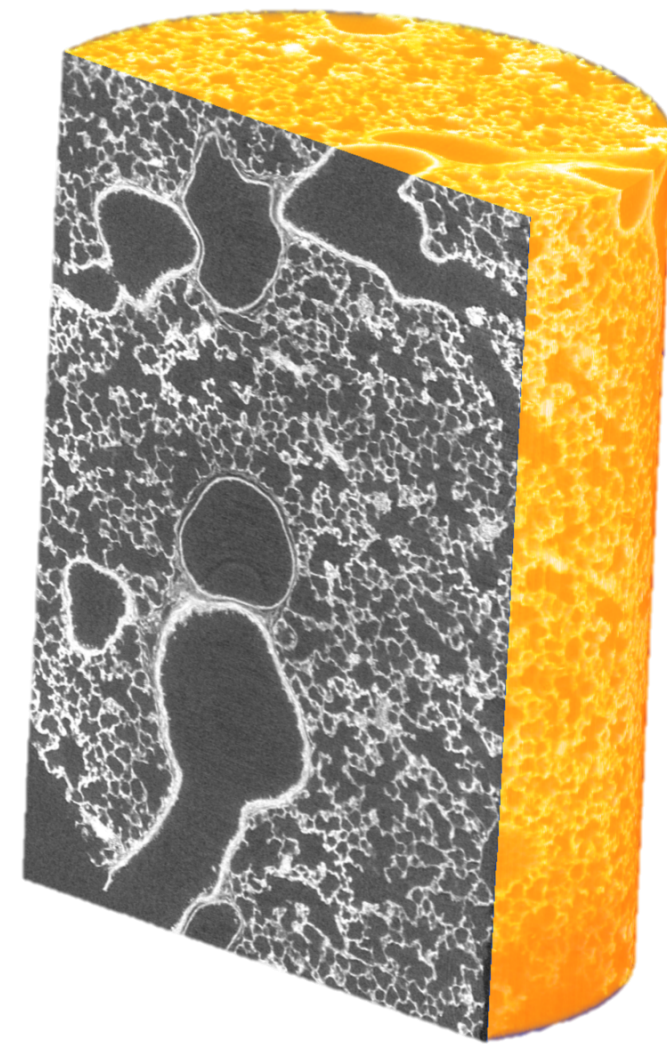
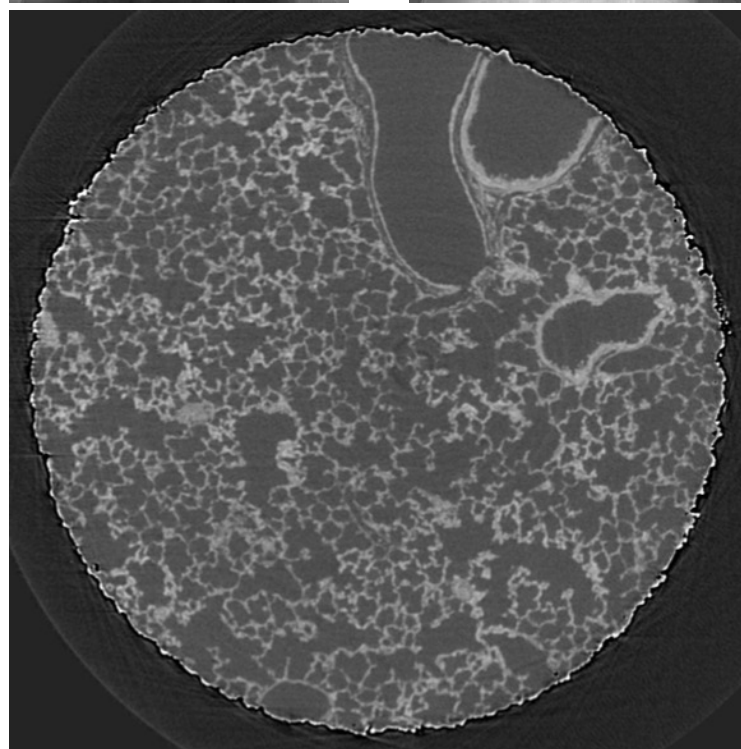
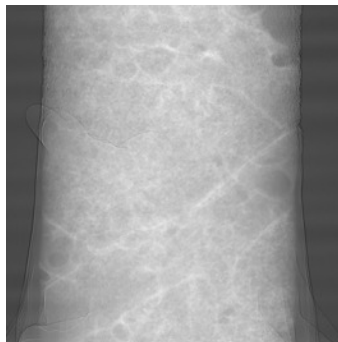
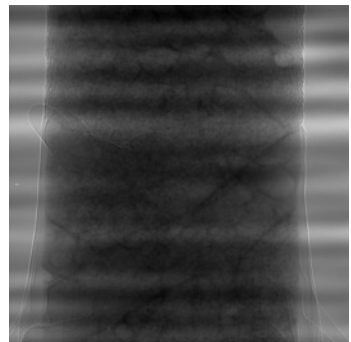
Imaging of lung alveolar structure

Energy 12 keV, Pixel size 0.7 microns

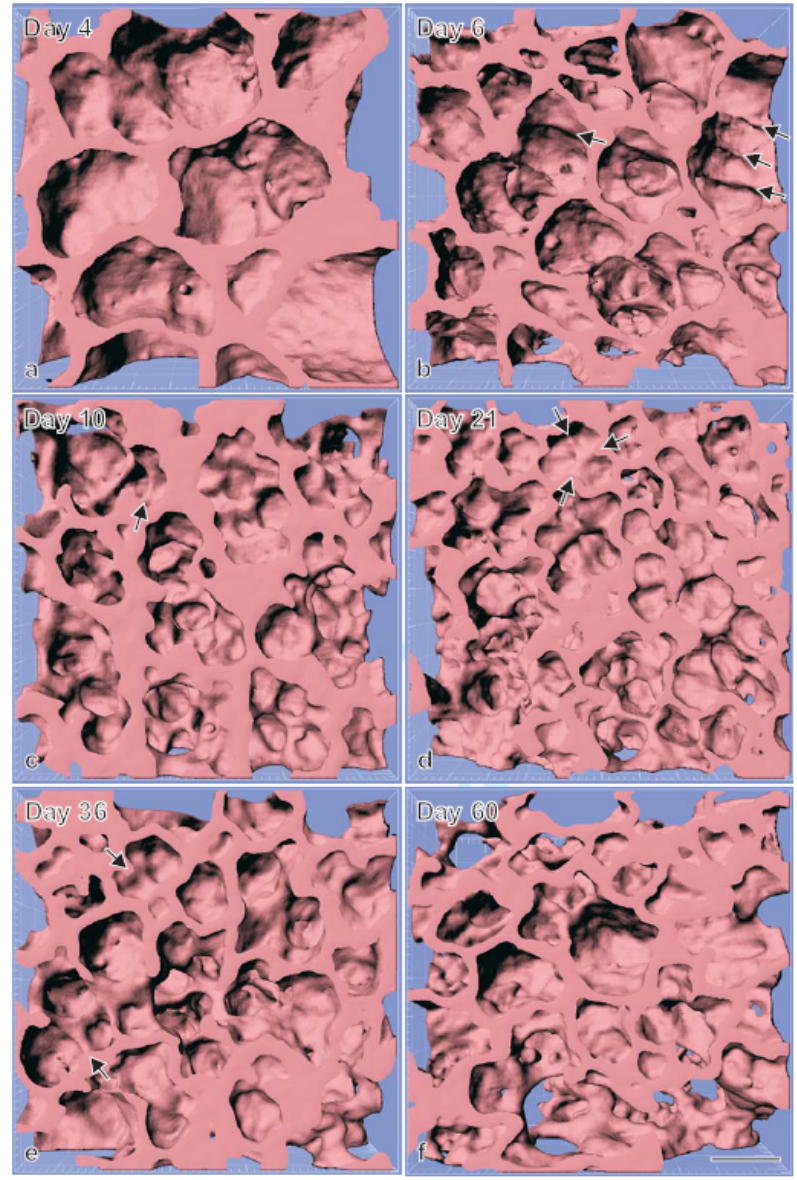
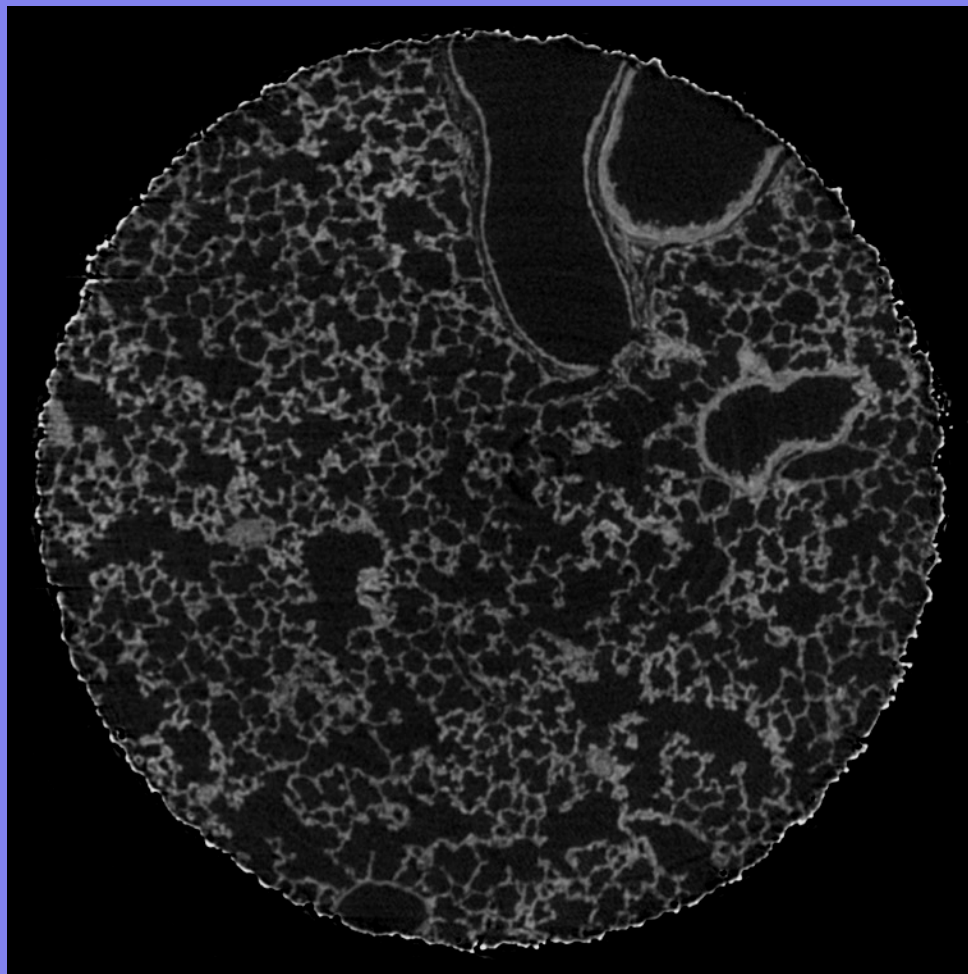


Imaging of lung alveolar structure

Energy 12 keV, Pixel size 0.7 microns



Quantitative visualization of lung alveolar structure



Schittny J.C., Mund S., and Stampanoni M., Evidence and structural mechanism for late lung alveolarization., Am J Physiol Lung Cell Mol Physiol 294: L246-L254, 2008

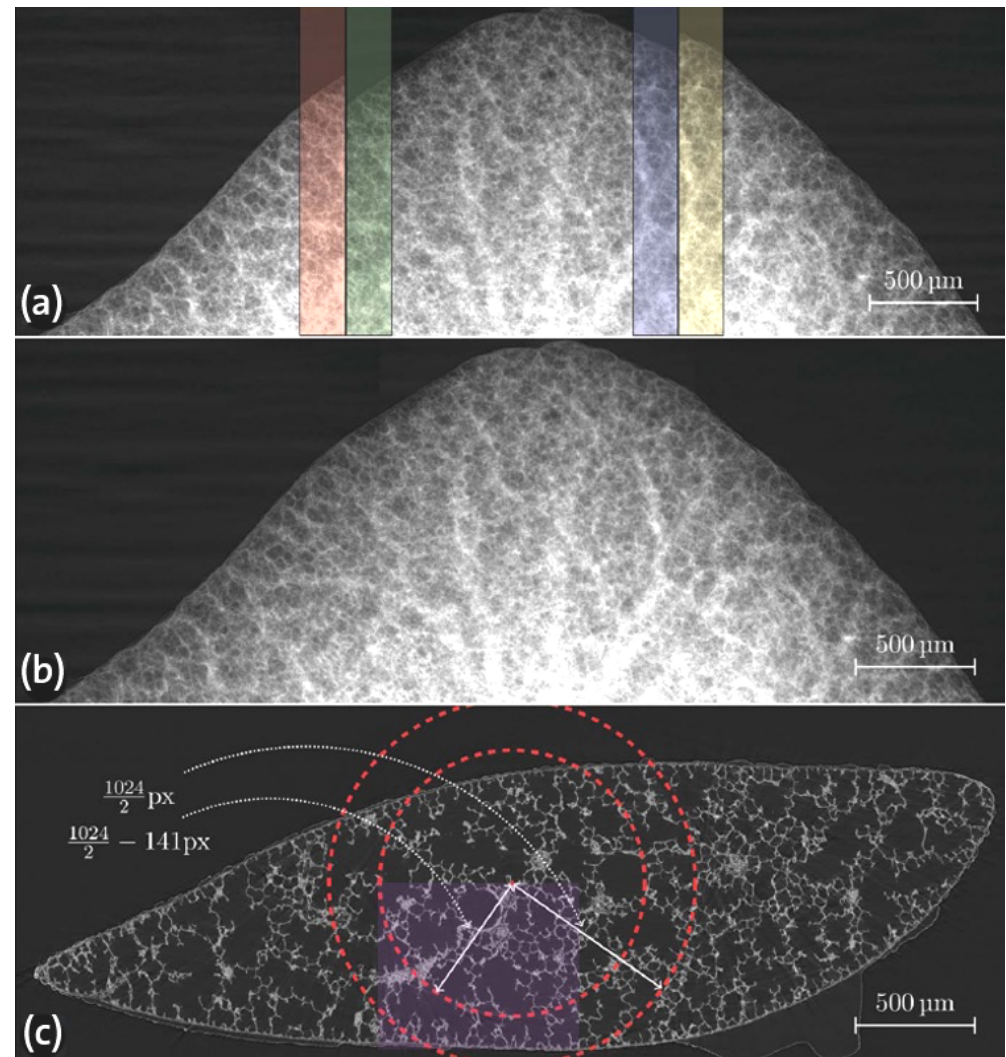
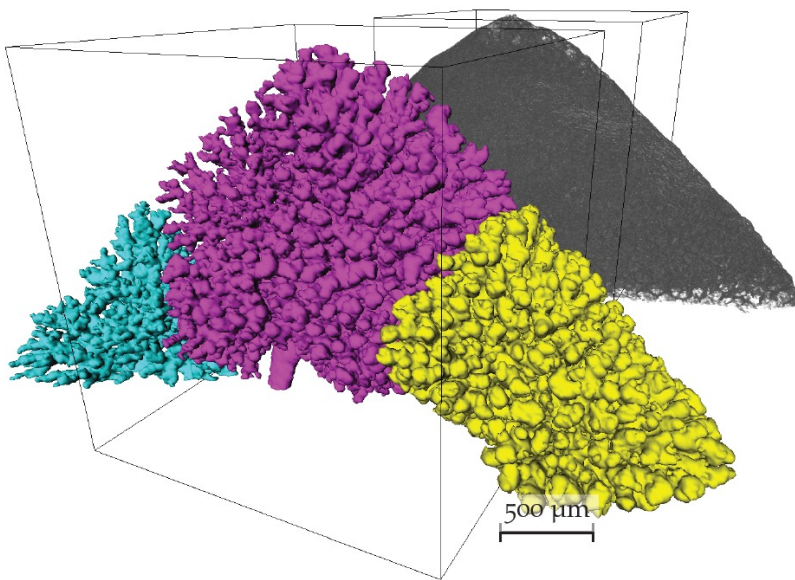
Modeling the rat pulmonary acinus – The data

Raw data

- 2.5% glutaraldehyde filling by 20 cm constant H₂O pressure
- Postfixation with 1% OsO₄ and paraffin embedding
- 12.398 keV, 1.48 microns pix. siz.

Scanning protocol

- Wide-field scanning with approx. 3000 pixel within 4.5 mm



From Haberthür et al., Journal of Synchrotron Radiation, 17(5), (2010)

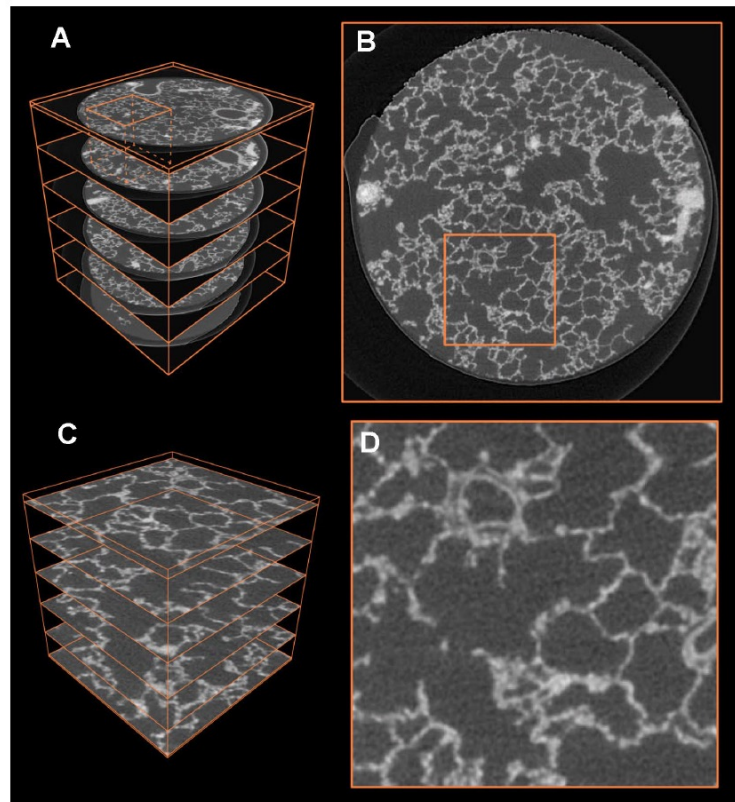
Modeling of the pulmonary acinus – The model

- Airflow into and out of the lung is driven by pressure differences between alveoli and the outside environment
- Pressure gradients are induced through the lung wall expansion and contraction motion during breathing
- Lung expansion approx. satisfies geometric self-similarity: geometrical lengths scale approximately with the $V^{1/3}$
- Sznitman model: alveolar airspaces expand and contract sinusoidally, with a breathing period T , according to:

$$L(t) = L_0 \left[1 + \frac{\beta}{2} + \frac{\beta}{2} \cdot \sin\left(2\pi \cdot f \cdot t - \frac{\pi}{2}\right) \right]$$

- Flow is incompressible (in terminal acinar airspaces). Fluid motion governed by unsteady, incompressible Navier-Stokes equations:

$$\nabla \cdot \underline{u} = 0 \quad \rho \left(\frac{\partial \underline{u}}{\partial t} + \underline{u} \cdot \nabla \underline{u} \right) = -\nabla p + \mu \nabla^2 \underline{u}$$



Selection of a Region Of Interest

Sznitman et al., Journal of Visualization, Online Version, June 2010

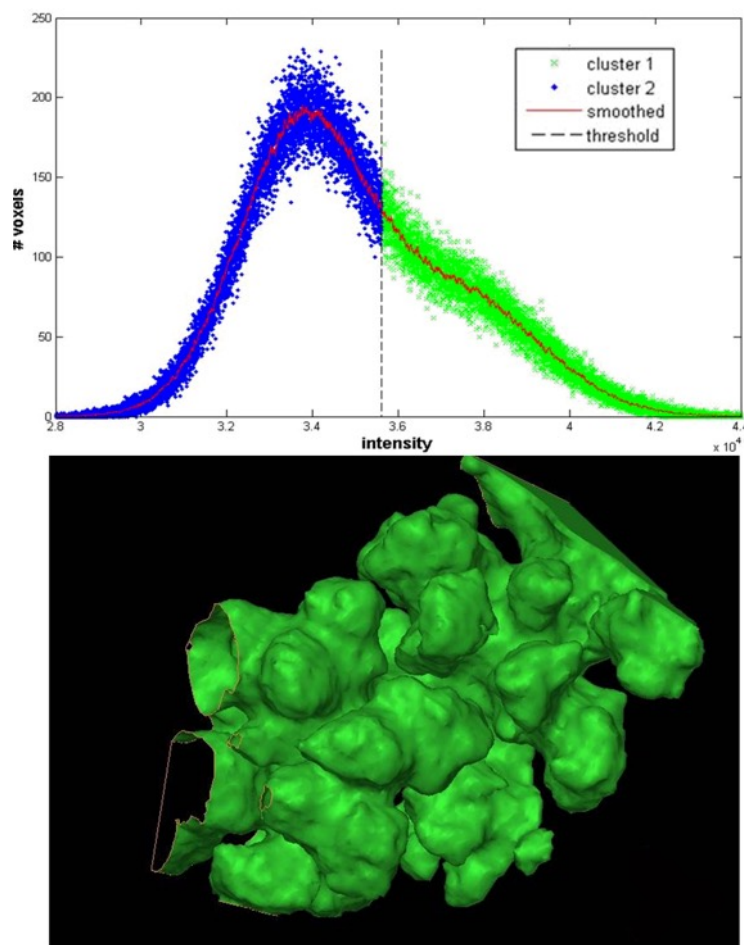
Modeling of the pulmonary acinus – The model

- Airflow into and out of the lung is driven by pressure differences between alveoli and the outside environment
- Pressure gradients are induced through the lung wall expansion and contraction motion during breathing
- Lung expansion approx. satisfies geometric self-similarity: geometrical lengths scale approximately with the $V^{1/3}$
- Sznitman model: alveolar airspaces expand and contract sinusoidally, with a breathing period T , according to:

$$L(t) = L_0 \left[1 + \frac{\beta}{2} + \frac{\beta}{2} \cdot \sin\left(2\pi \cdot f \cdot t - \frac{\pi}{2}\right) \right]$$

- Flow is incompressible (in terminal acinar airspaces). Fluid motion governed by unsteady, incompressible Navier-Stokes equations:

$$\nabla \cdot \underline{u} = 0 \quad \rho \left(\frac{\partial \underline{u}}{\partial t} + \underline{u} \cdot \nabla \underline{u} \right) = -\nabla p + \mu \nabla^2 \underline{u}$$



Segmentation via clustering algorithm

Sznitman et al., Journal of Visualization, Online Version, June 2010

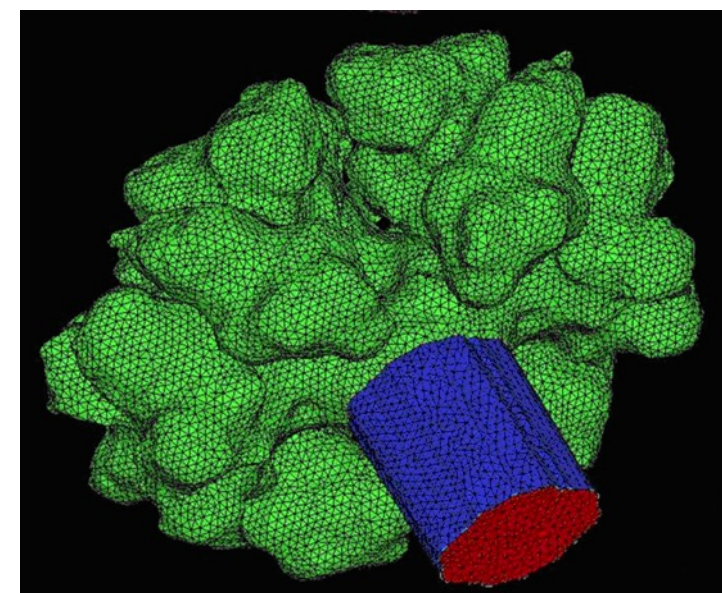
Modeling of the pulmonary acinus – The model

- Airflow into and out of the lung is driven by pressure differences between alveoli and the outside environment
- Pressure gradients are induced through the lung wall expansion and contraction motion during breathing
- Lung expansion approx. satisfies geometric self-similarity: geometrical lengths scale approximately with the $V^{1/3}$
- Sznitman model: alveolar airspaces expand and contract sinusoidally, with a breathing period T , according to:

$$L(t) = L_0 \left[1 + \frac{\beta}{2} + \frac{\beta}{2} \cdot \sin\left(2\pi \cdot f \cdot t - \frac{\pi}{2}\right) \right]$$

- Flow is incompressible (in terminal acinar airspaces). Fluid motion governed by unsteady, incompressible Navier-Stokes equations:

$$\nabla \cdot \underline{u} = 0 \quad \rho \left(\frac{\partial \underline{u}}{\partial t} + \underline{u} \cdot \nabla \underline{u} \right) = -\nabla p + \mu \nabla^2 \underline{u}$$

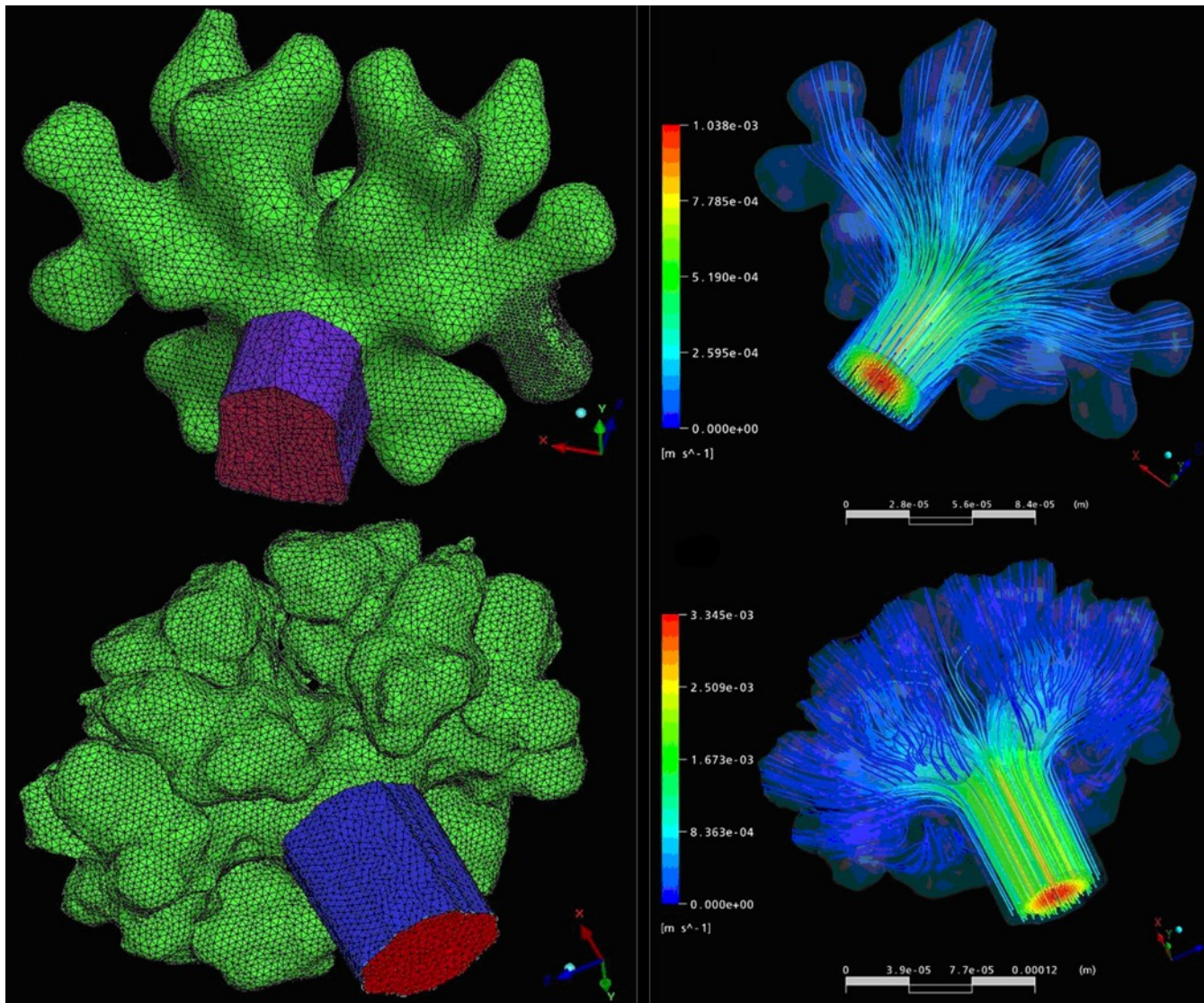


FE mesh, bounded flow domain

Segmentation via clustering algorithm

Sznitman et al., Journal of Visualization, Online Version, June 2010

Modeling of the pulmonary acinus – Streamlines



- Two geometries of different complexity (280000 and 600000 volume elements, corresponding to 0.8 nL and 2.3 nL)
- Flow streamlines at peak inspiration showing similar flow topology despite different size and complexity
- Flow topology does not change appreciably throughout the breathing period
- Flow in terminal sacculi is quasi-steady.

Key features of an imaging beamline

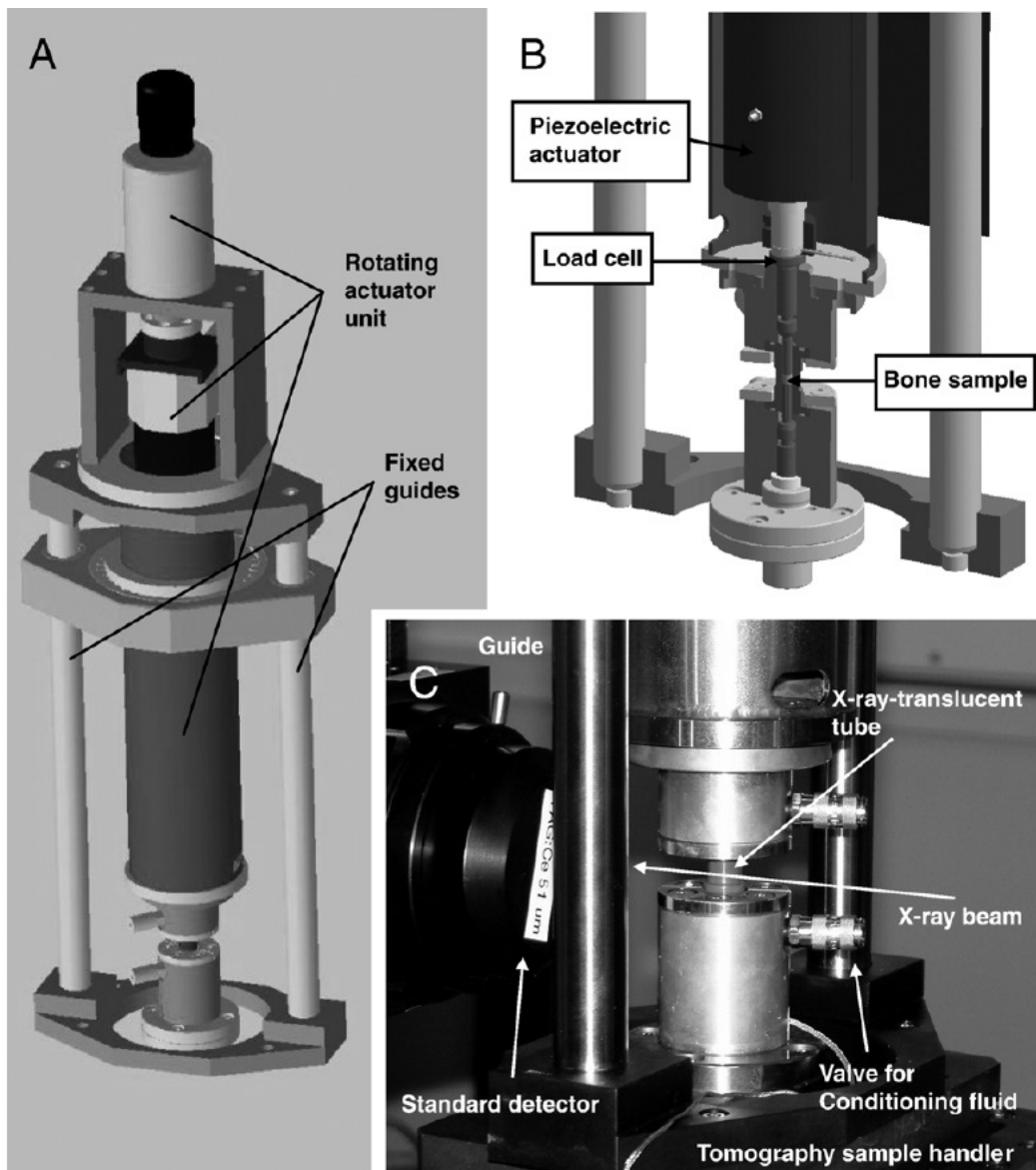
HIGH

WIDE

- Spatial resolution, field of view
 - **FAST and AUTOMATED**
- Data acquisition
 - **HIGH**
- Sensitivity (absorption / phase contrast)
- Energy range / Sample Flexibility
 - **BROAD**
 - **HIGH**
- Data post-processing
 - **FAST and ONLINE**
- In-situ experiments
 - **MULTIPLE**
- User friendliness
 - **EASY**



Sample environments: compression devices

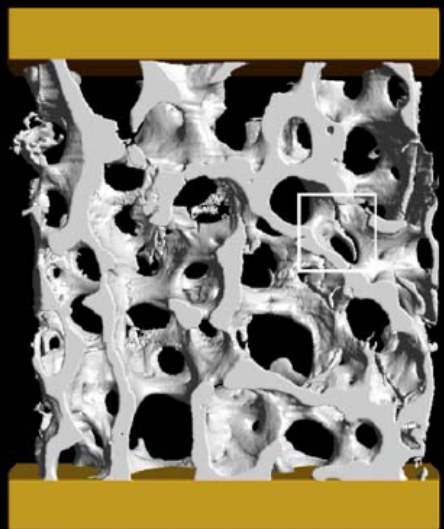
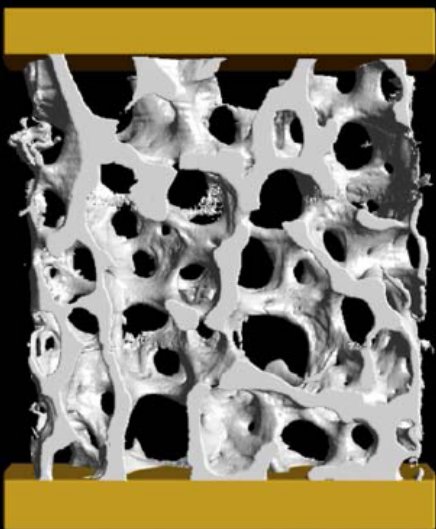


- **Goal: Image-guided failure assessment (IGFA)**
- In-situ mechanical compression device (IMCD)
- Technical data:
 - 300 μ m displacement @ 0.1 μ m accuracy
 - Load cells of 100 N and 500 N
 - Sample size : 3.5 mm
 - Wet environment

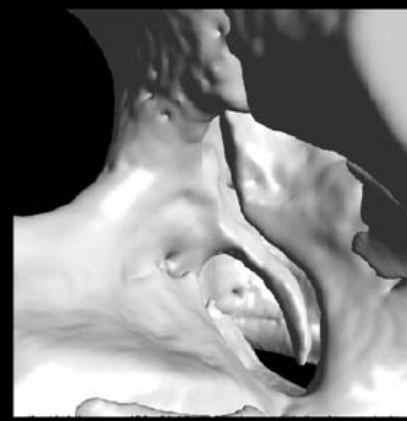
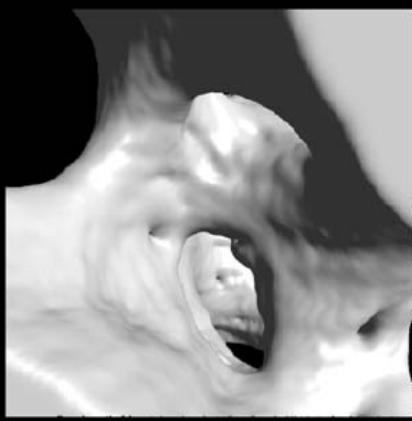
Image guided bone failure assessment

before failure

after failure



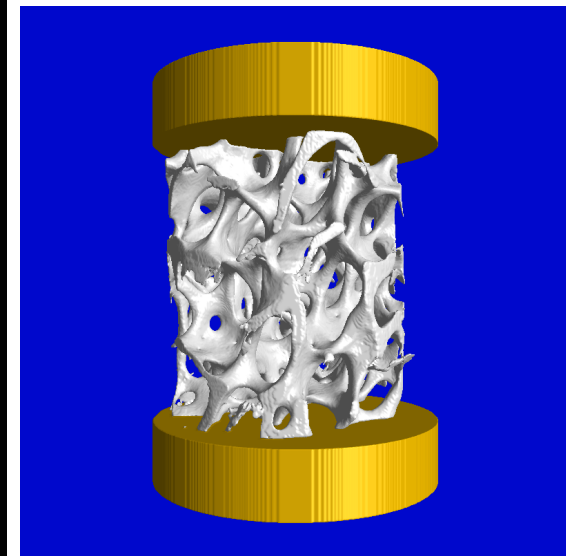
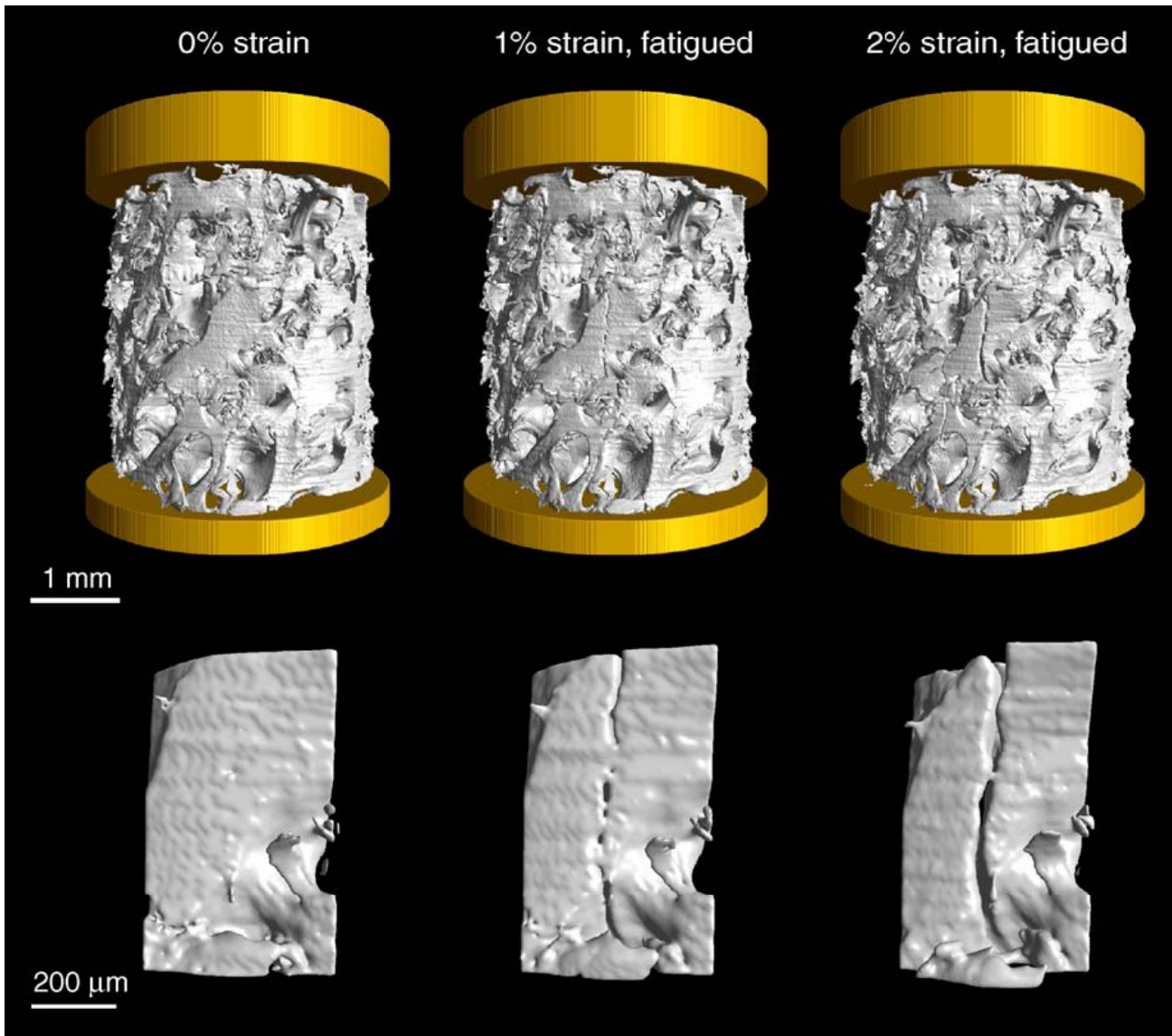
1 mm



200 µm

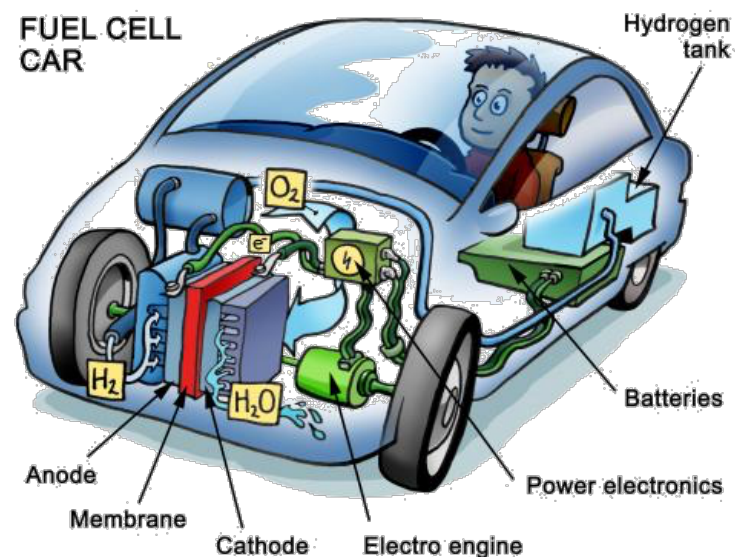
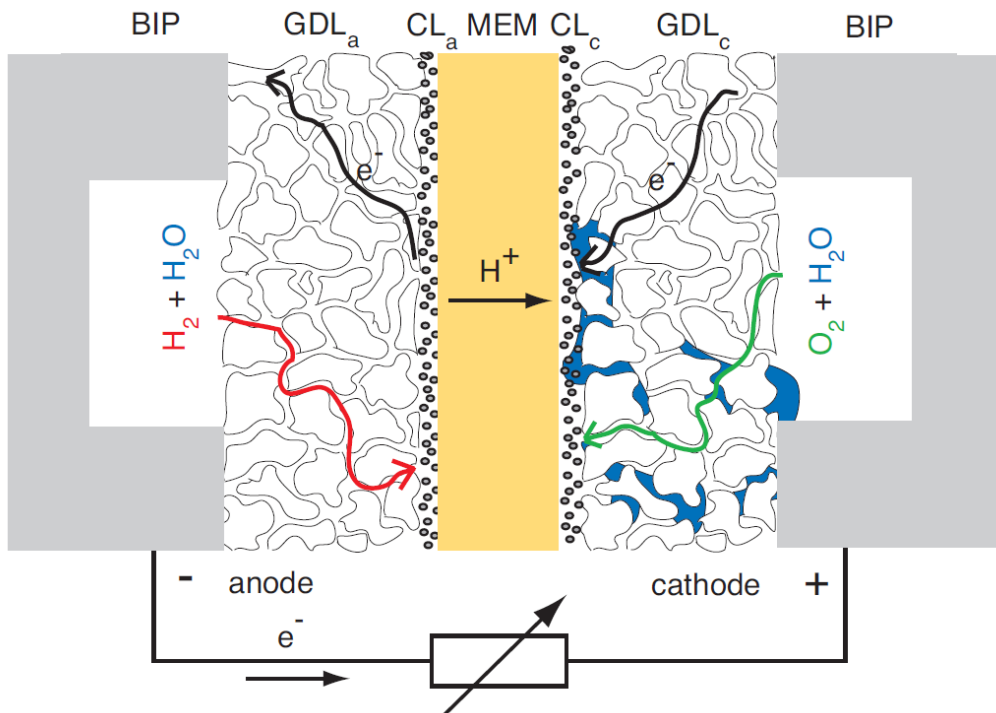
- 3D visualization of non-fatigued bone sample subjected to IGFA before and after obvious tissue failure.
- The image on the right side shows an oblique fracture band ranging from the upper left to the lower right of the sample.
- A detailed view shows micro-crack formation and crack opening in three dimensions.

Image guided bone failure assessment



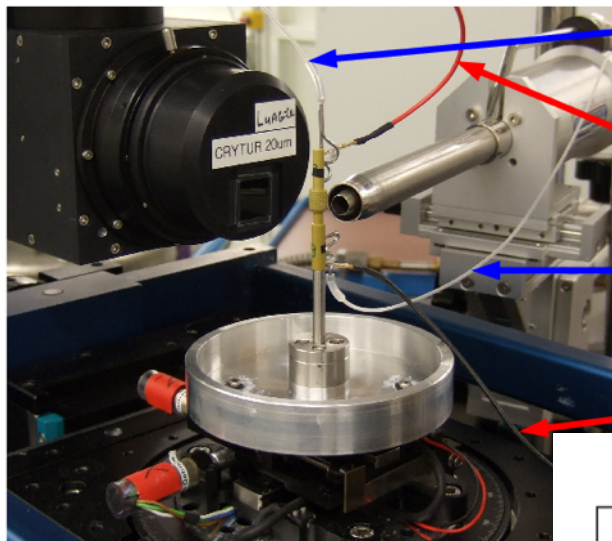
P. Thurner, Bone 39 (2006) 289–299

Modeling a polymer electrolyte membrane fuel cell (PEFC)

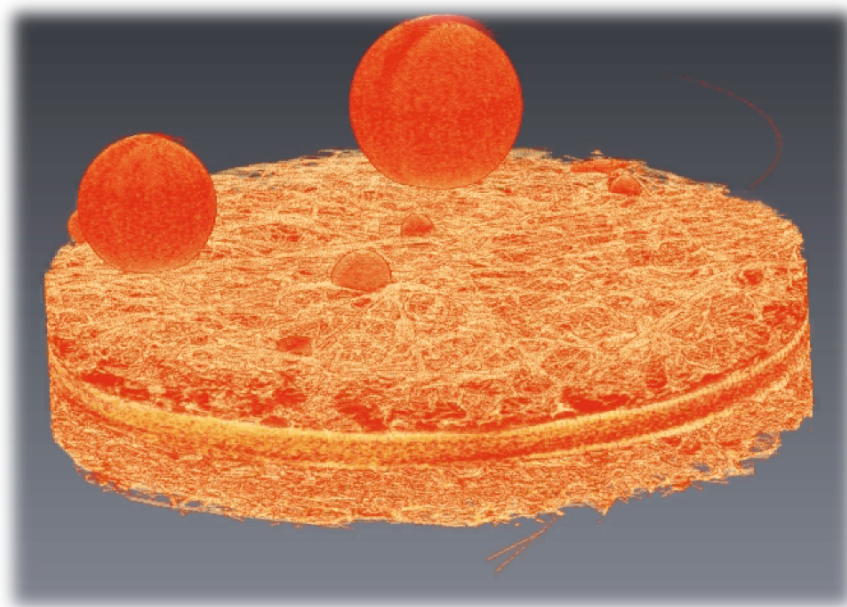
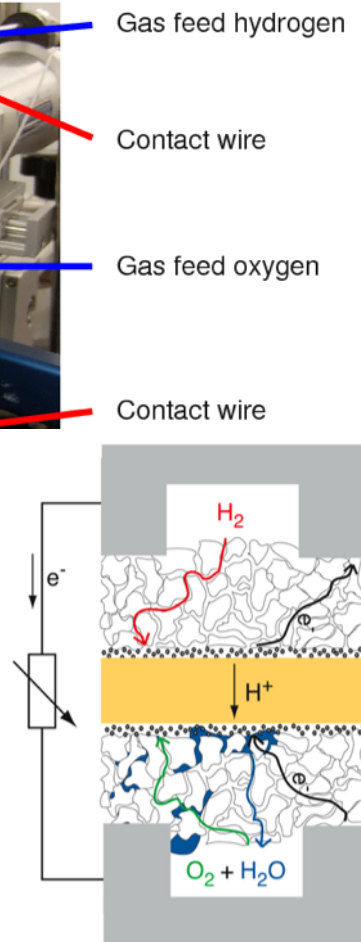


- Humidified reactant gases are feed through the channels of the bipolar plates (BIP) and diffuse through the gas diffusion layers to the reaction sites in the catalyst layers.
- Electrons freed in the CL_a pass over the external circuit and load to the cathode side where they recombine with protons that moved through the electrolyte and with oxygen to water.
- Product water has to pass mainly the GDL_c in liquid or gaseous form.

“In-situ” investigation of an active fuel cell



(Courtesy of J. Eller et al., PSI)



- 3D water distribution in the gas diffusion layer
- Acquisition of 3D data on gas diffusion layers
- Simulation of diffusion, permeability and conductivity

Key features of an imaging beamline

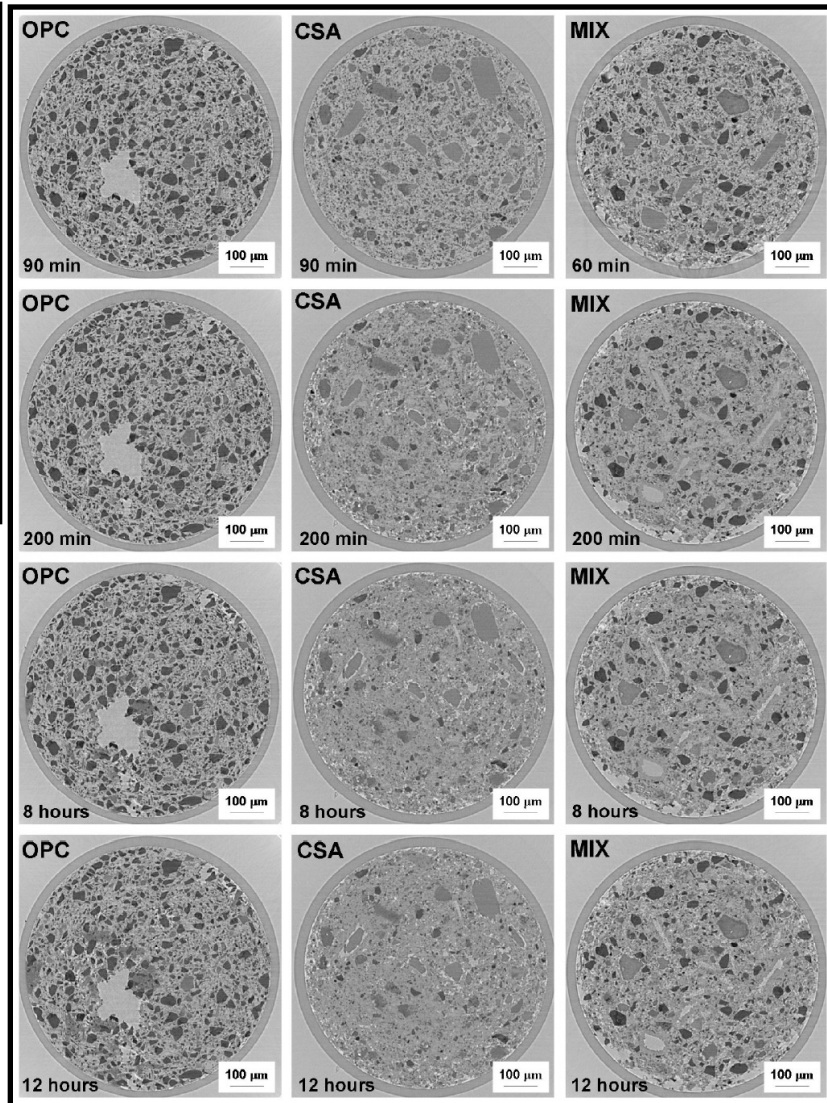
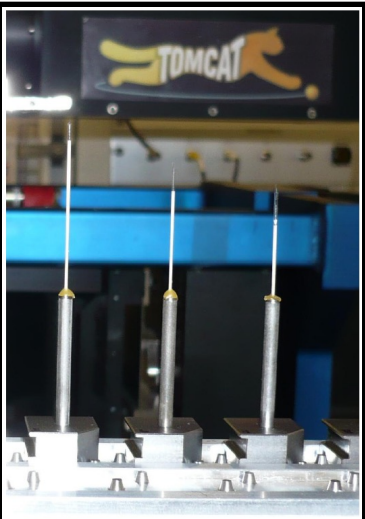
HIGH

WIDE

- Spatial resolution, field of view
- Data acquisition
 - **FAST and AUTOMATED**
- Sensitivity (absorption / phase contrast)
 - **HIGH**
- Energy range / Sample Flexibility
 - **BROAD**
 - **HIGH**
- Data post-processing
 - **FAST and ONLINE**
- In-situ experiments
 - **MULTIPLE**
- User friendliness
 - **EASY**

High-throughput: sample changing and sequencing

D. Attenborough's "First Life", BBC 2011

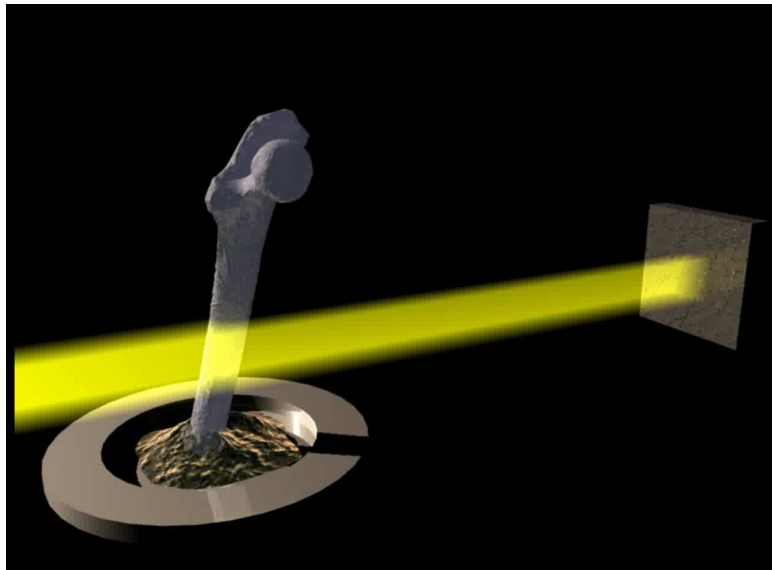


- Cement materials in capillaries of 600 microns diameter
- Study on different binders:
 - Ordinary Portland Cement (OPC)
 - Calcium Sulphoaluminate Cement (CSA)
 - Mixed sample(MIX)
- Sample mounting and sequencing fully automatic
- Unattended monitoring of hydration process over 12h

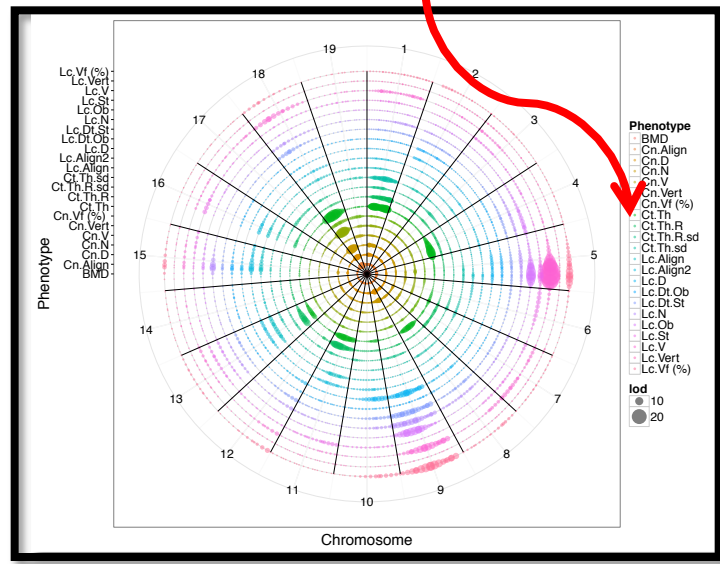
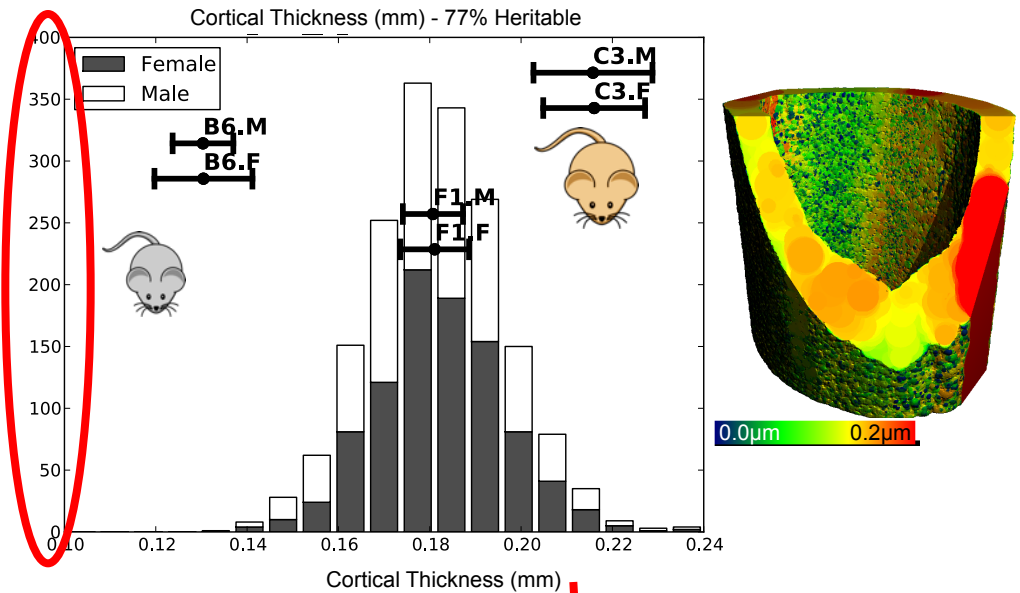
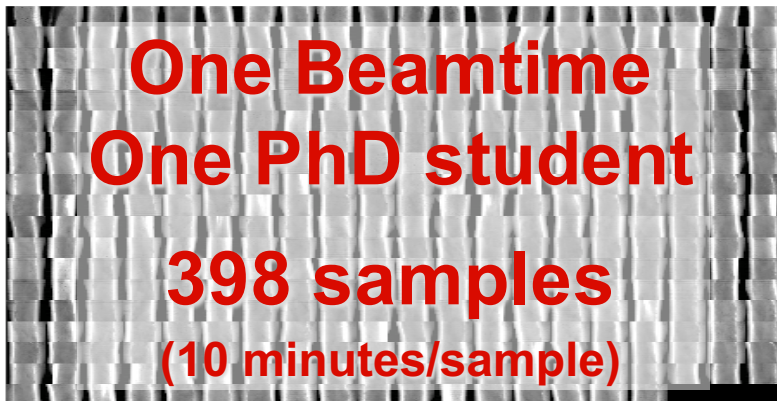
D. Gastaldi, Construction and Building Materials 29 (2012) 284–290

High-throughput imaging: from sample alignment to QTL analysis

High-throughput: ROI selection and alignment

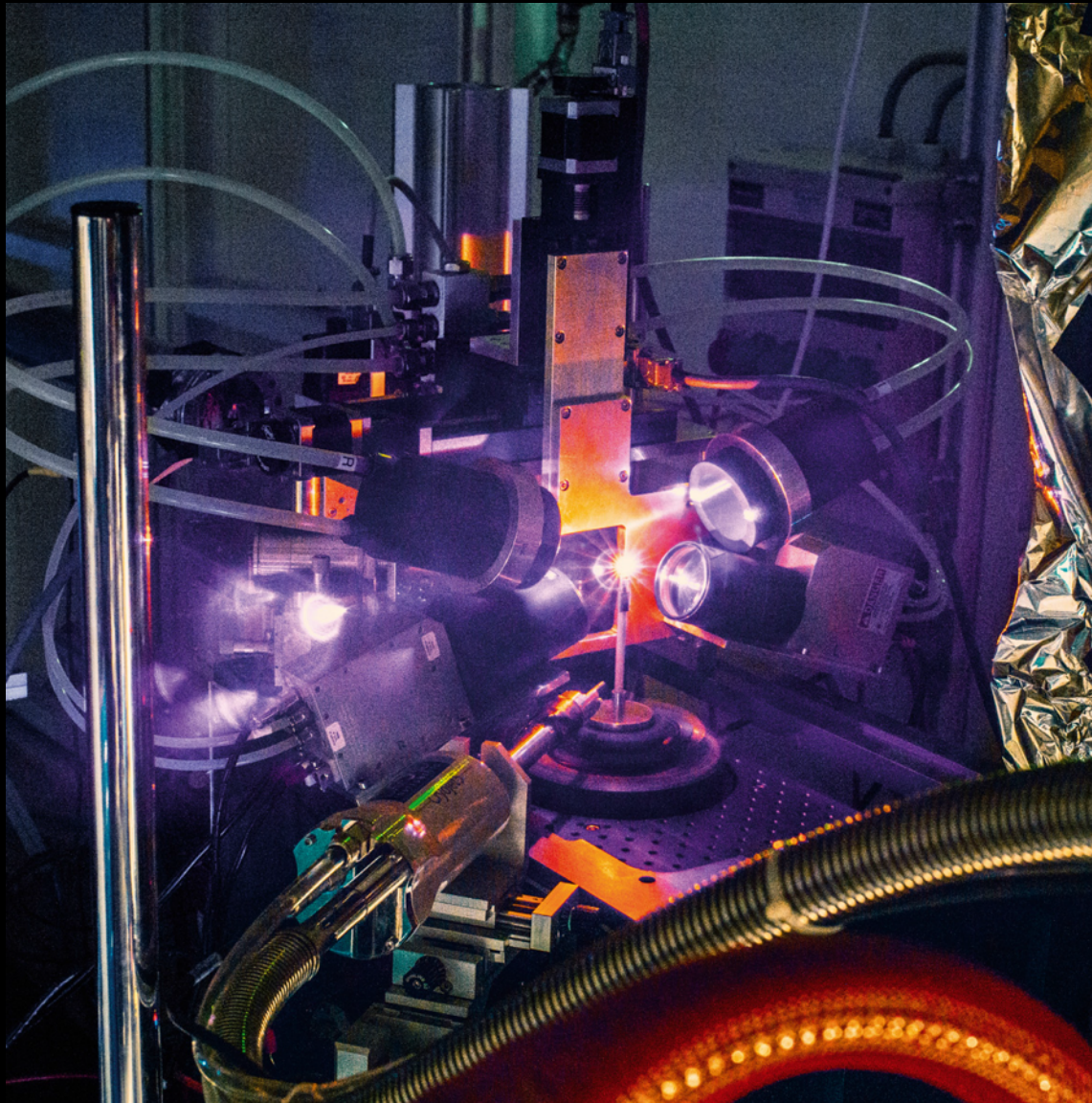


Femur samples automatically aligned using goniometer and moved to region of interest using projections and image processing scripts



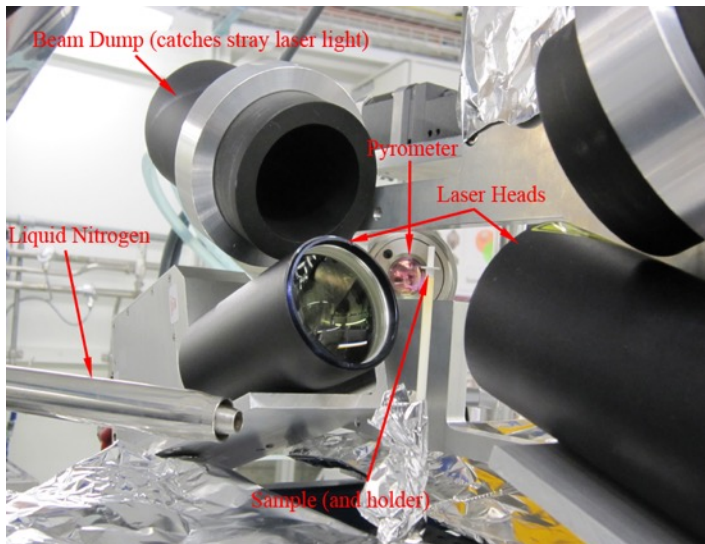
K. Mader, PhD Thesis 2013 and K. Mader et al., BMC Genomics 16:493 (03 Jul 2015)

Mimicking volcano eruptions

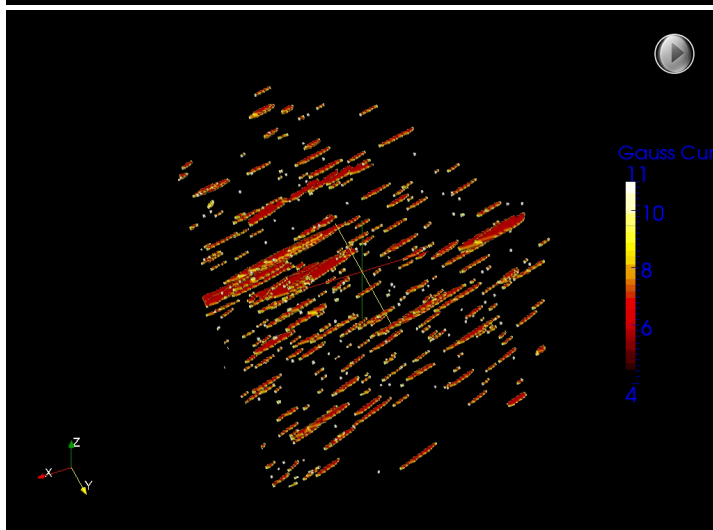


Mimicking volcano eruptions

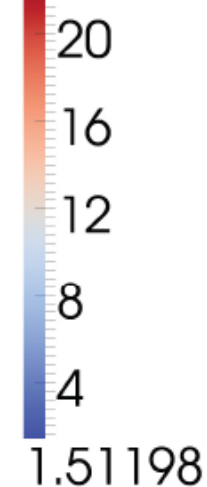
2 cross firing 150W, 980nm cw, class 4 lasers



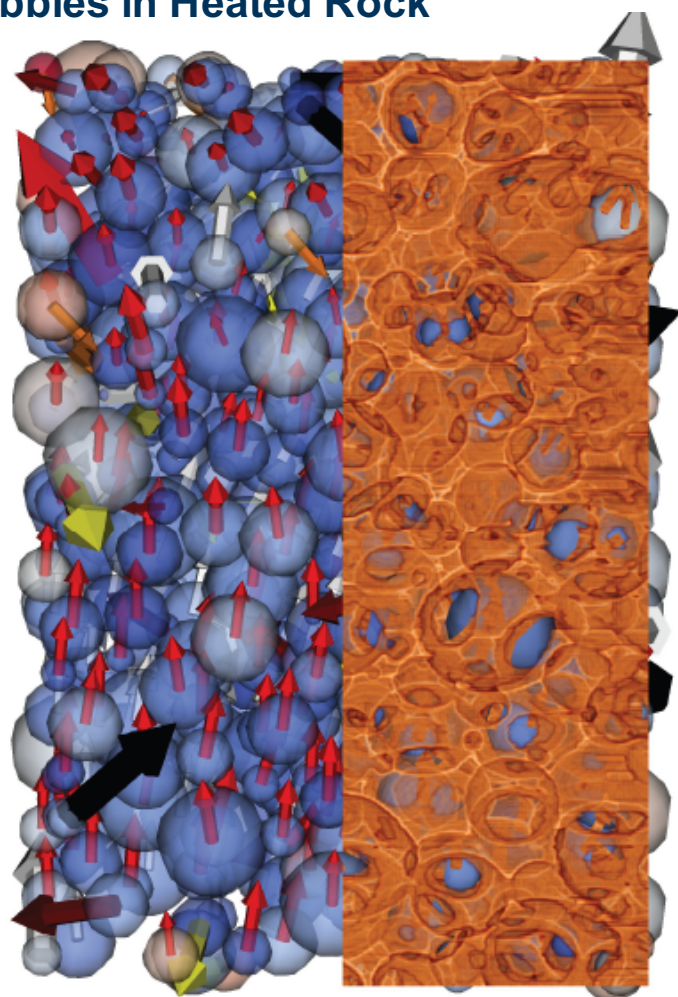
Gas Evolution in Heated Volcanic Rock



Anisotropy
21.6748



Tracking Bubbles in Heated Rock



Thanks to M. Pistone (ETHZ) and J. Fife (PSI)

Post-processing framework

Processing Plugins

Contouring	Thickness
Component Labeling	Voxel Functions
Morphology Operations	NVoxel Functions
Distance Map [2]	Connectivity
Curvature	W-Voronoi Tessellation [1]
Filtering [1]	Watershed

Analysis Plugins

2D Histogram
Histogram
Shape Analysis [1,2]
Two Point Correlation Function
Radial Distribution Function
Tracking

Database

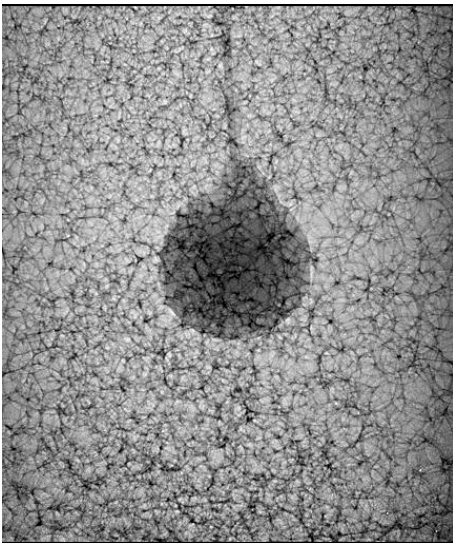
Metric Table <i>Stores custom ensemble sample metrics as double</i>
Cell Table <i>Stores fixed shape metrics for objects within a sample</i>
Link Table <i>Stores connections between cells</i>
BLOB Table <i>Stores any data about a sample, histogram, picture, etc</i>
Statistics - R/Python/Matlab..

[1] K. Mader *et al.*, "Quantitative 3D Characterization of Cellular Materials: Segmentation and Morphology of Foam", *Colloids and Surfaces A*, 2012;415:230–238

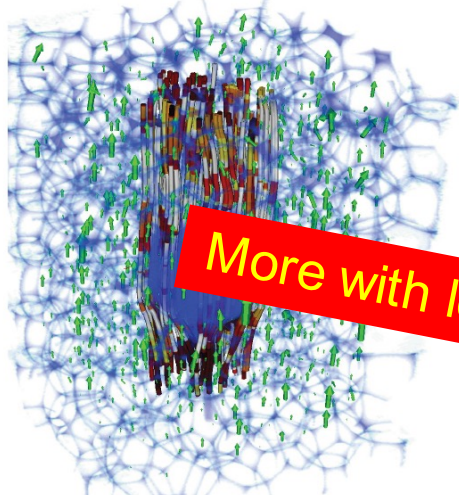
[2] K. Mader *et al.*, "Quantitative 3D Characterization of Cortical Microstructure", *Bone*, <http://dx.doi.org/10.1016/j.bone.2013.06.026>

Foam rheology in 3D: complex quantification

Wet, liquid foam



Flow around obstacle

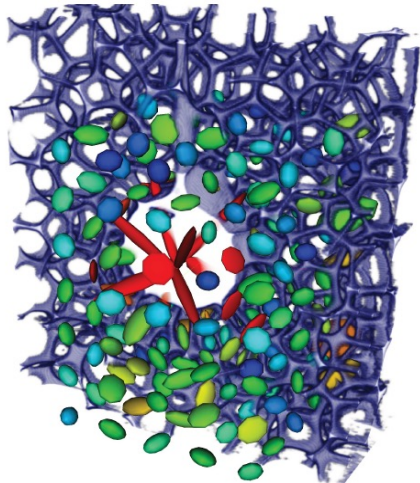


Flow through constriction

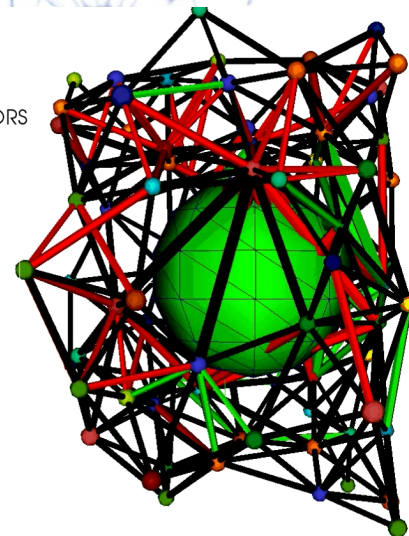
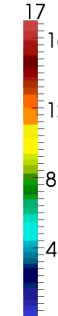


More with lectures of K. Mader

Strain tensor quantification

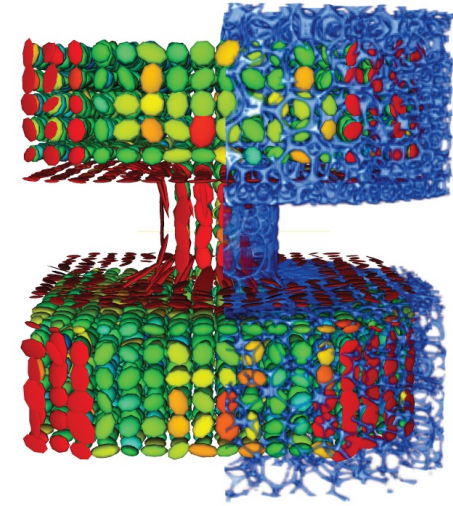


NEIGHBORS



K. Mader, PhD thesis, 2013

Strain tensor quantification



Key features of an imaging beamline

HIGH

WIDE

- Spatial resolution, field of view
- Data acquisition
 - **FAST and AUTOMATED**
- Sensitivity (absorption / phase contrast)
 - **HIGH**
- Energy range / Sample Flexibility
 - **BROAD**
 - **HIGH**
- Data post-processing
 - **FAST and ONLINE**
- In-situ experiments
 - **MULTIPLE**
- User friendliness
 - **EASY**

Get insights in insect flight control

Investigate the biomechanics underlying flight manoeuvres and gaze shifts

→ CT following the dynamics of 100+ Hz wing beat!



Need:

- single-shot propagation-based phase contrast
- high-speed X-ray tomographic microscopy

Requires: Coherence and Flux



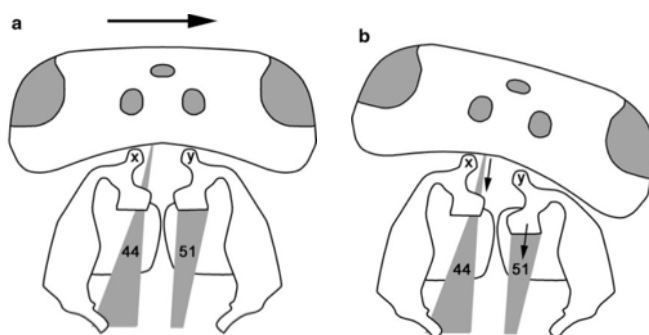
BRIGHTNESS



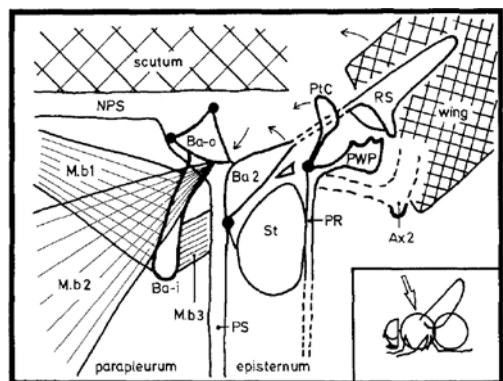
So, this is a perfect task for a synchrotron!

Anatomy and biomechanics of flight

Static anatomy and indirect evidence

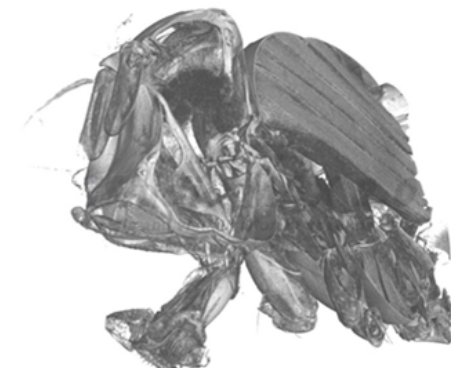


Bee head yaw, Hung 2011.

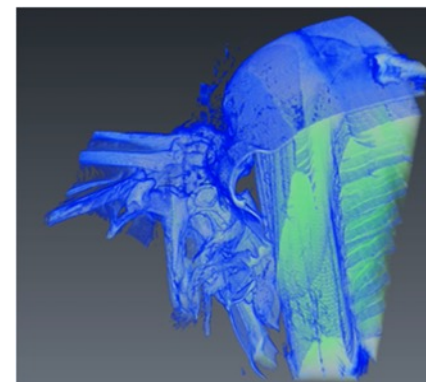


Gear change mechanism in Blowfly wing hinge, Nalbach 1989.

Dynamic, "functional" anatomy.

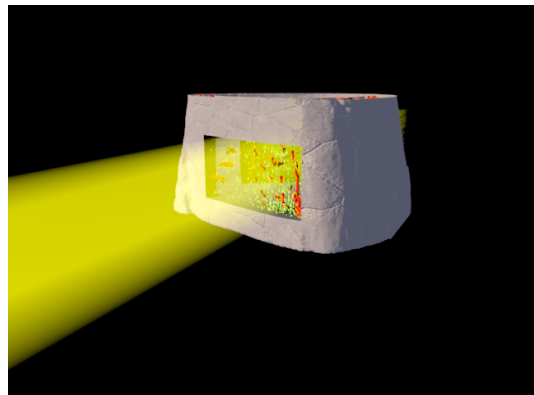


uCT of Blowfly head-neck system.

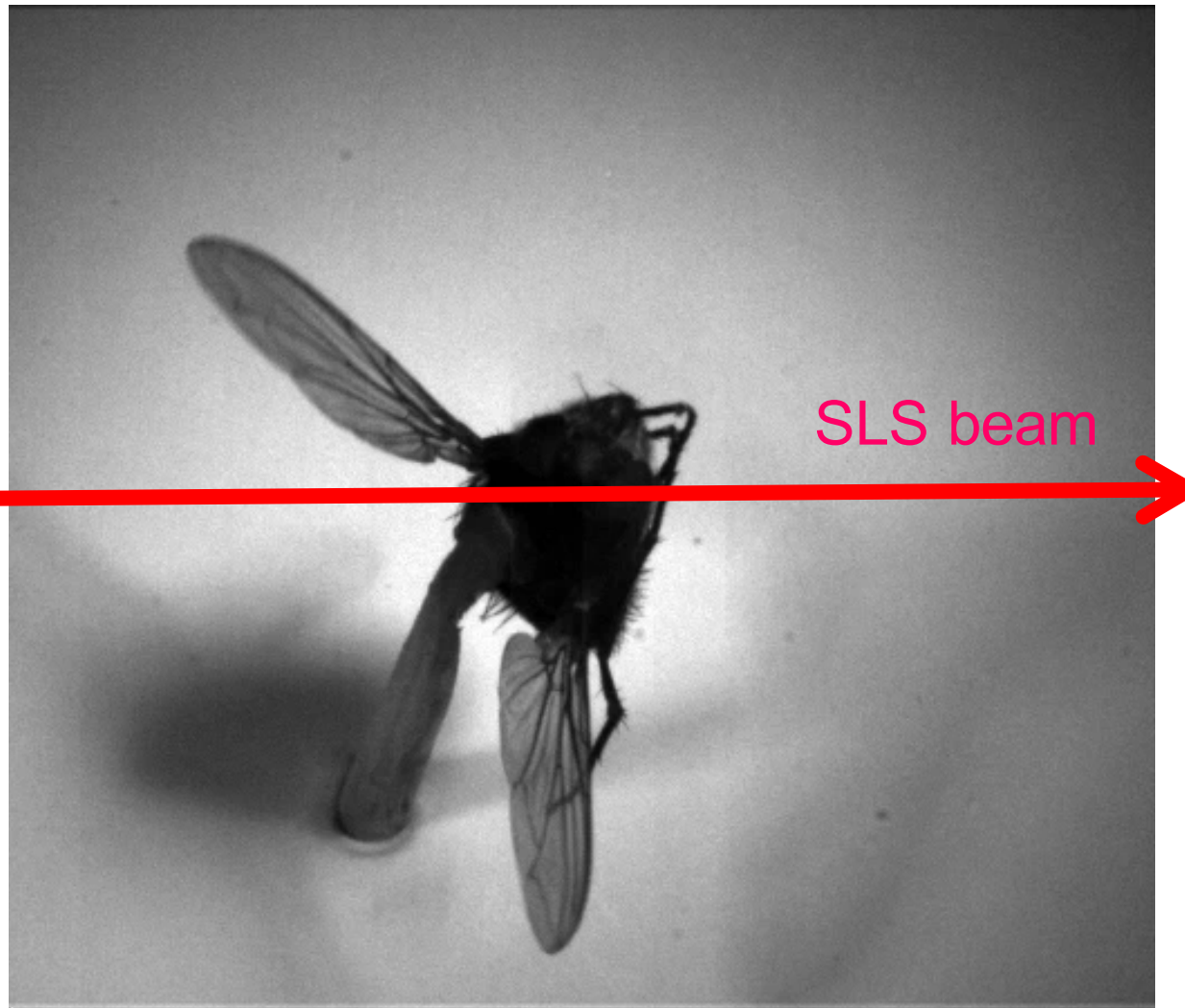


SR-CT of Hoverfly wing hinge.

Post-gated, stroboscopic X-ray imaging



Wings beat at 150 Hz !!



2500 Xray images per second...

The “fly” experiment

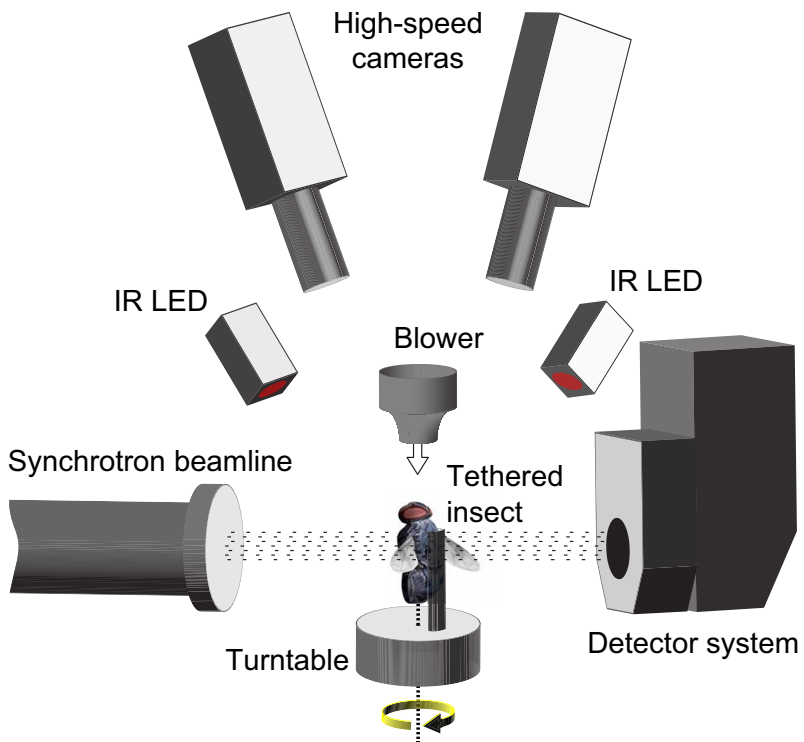


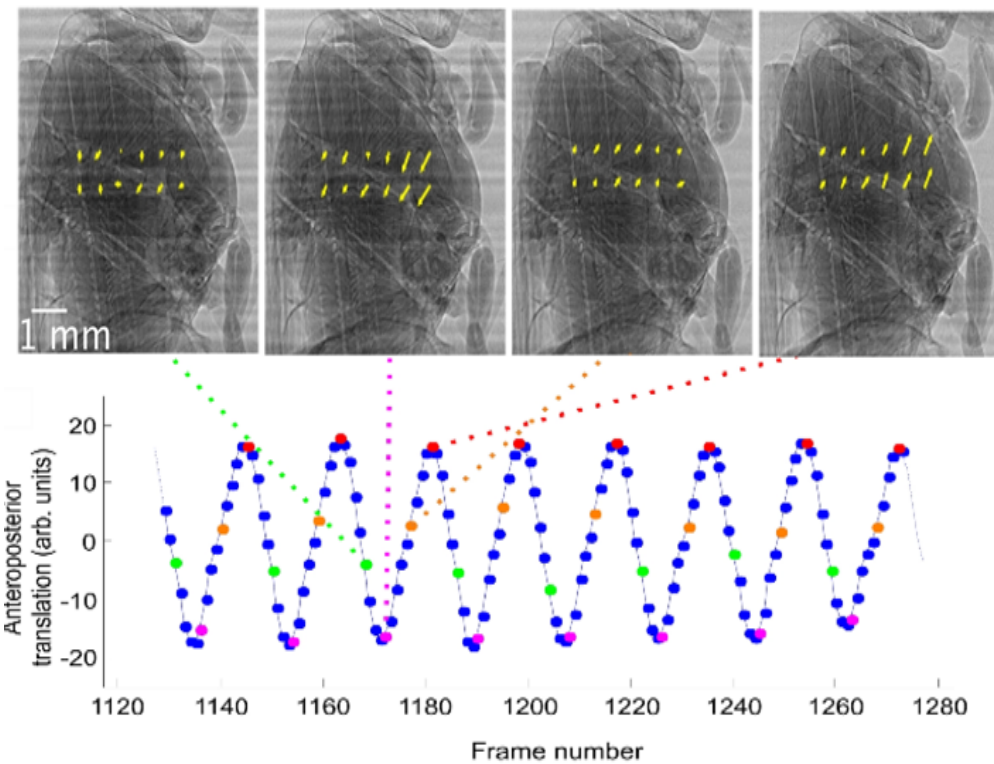
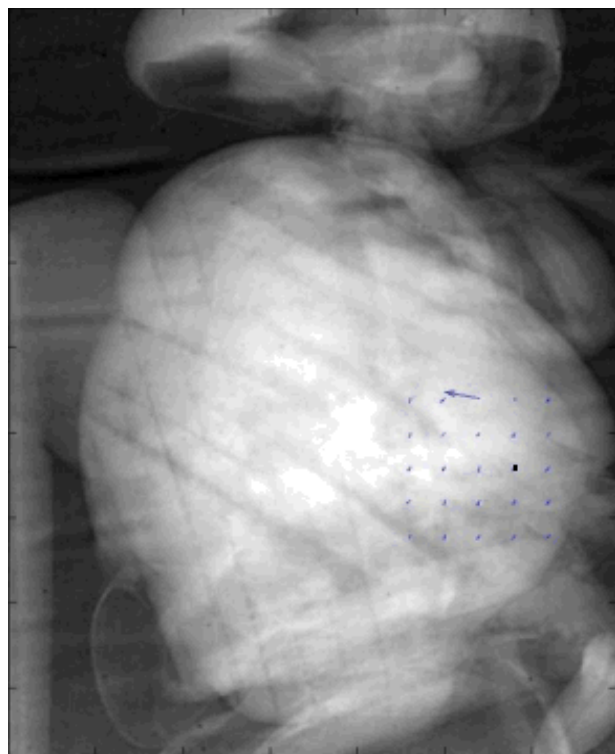
Figure 1. Schematic diagram of the experimental setup, showing the direction of the wind stimuli (white arrow) and rotational stimuli (yellow arrow).

doi:10.1371/journal.pbio.1001823.g001



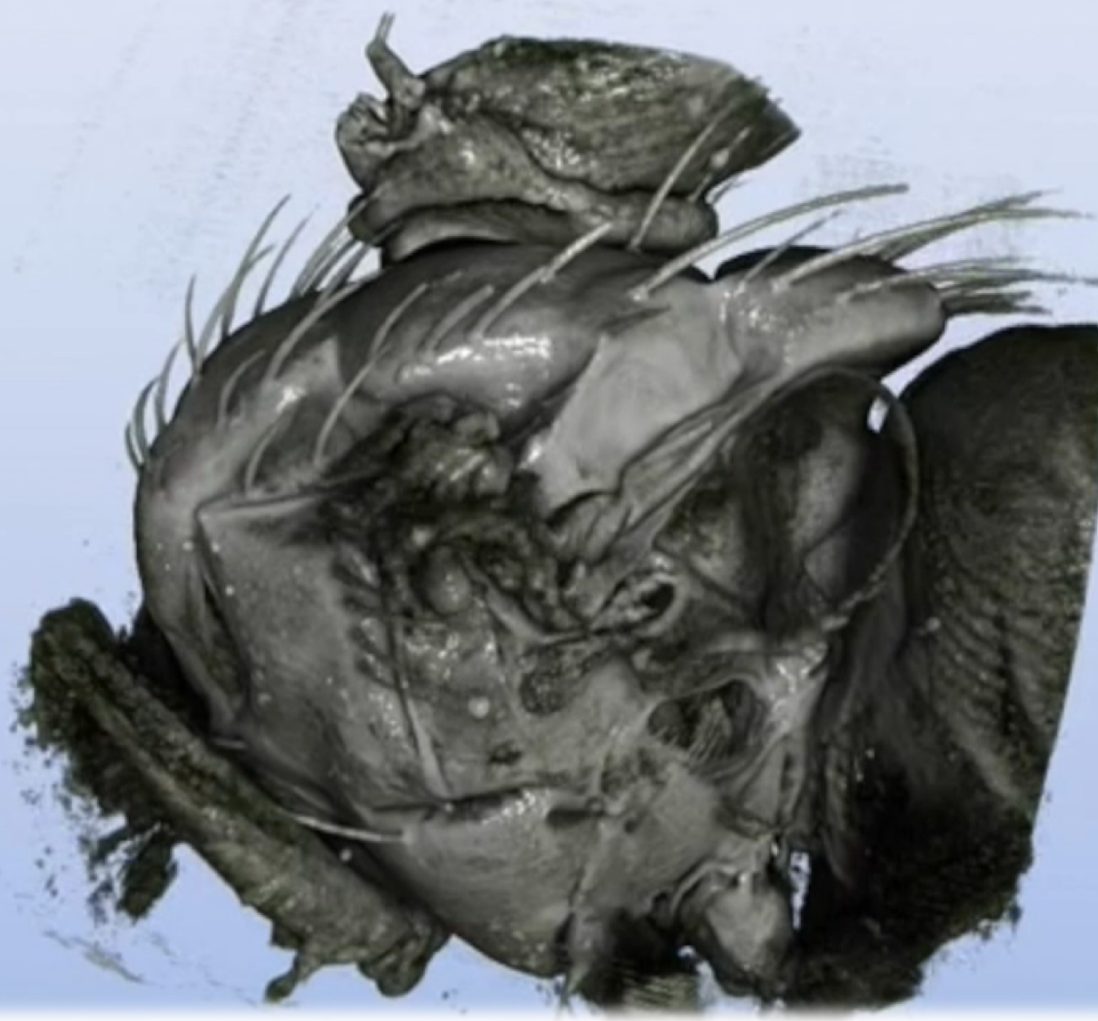
Retrospective gating

Mokso *et al.*, Sci Rep 2015



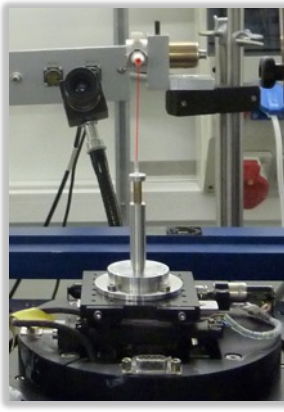
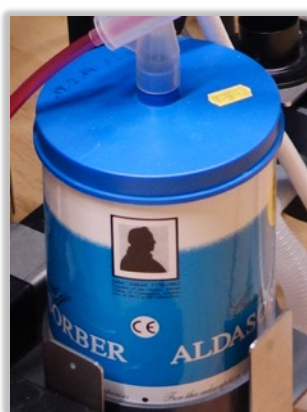
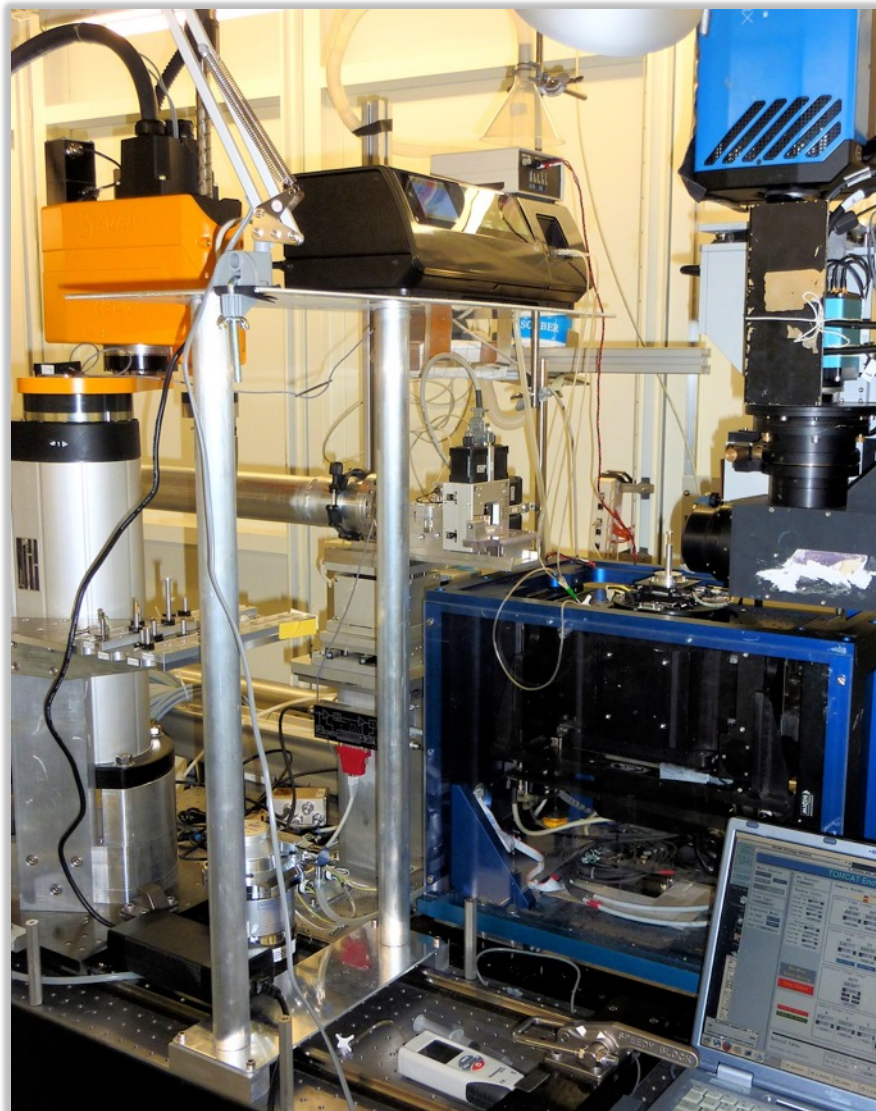
- Normalized projections at four stages of one wingbeat cycle, with local image motion vectors (yellow arrows).
- The translation vectors were found by spatial cross-correlation of consecutive projections tracking the movements of twelve evenly spaced regions each containing 24x24 pixels. Orientation: head-neck joint at the top, posterior end of the thorax at the lower end of the images. Sequence of wingbeat phases from left to right: dorsal stroke reversal, downstroke, ventral stroke reversal, upstroke.
- The gating signal (blue) derived from spatial cross-correlation of successive projections (after smoothing). The peaks of the signal (red points) identified the beginning of each new wing beat cycle, which was divided into uniformly spaced wingbeat phases

Muscles and tracheal network during flight



Walker et al., PloS Biology (2014) & Mokso et al., SciRep (2015)

Dynamic 3D imaging in-vivo: complex triggering

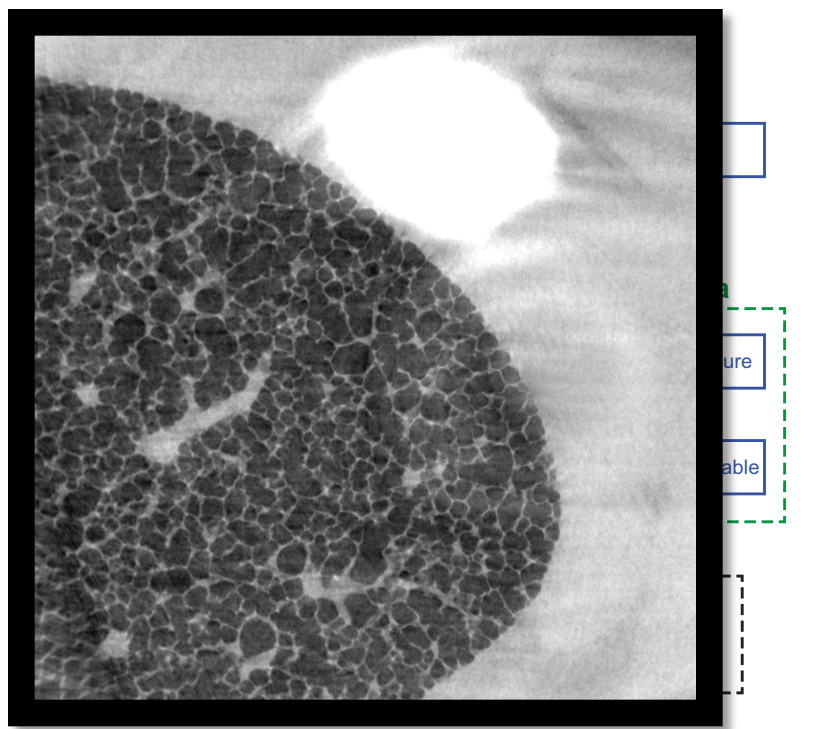
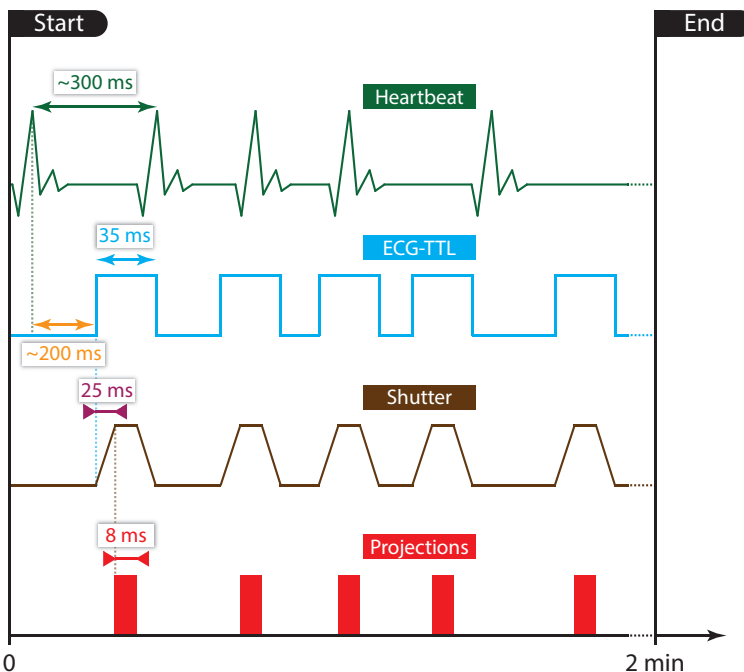


G. Lovric, ETH PhD thesis 2015 & this conference

Dynamic 3D imaging in-vivo: complex triggering



Image acquisition schematic



Key features of an imaging beamline

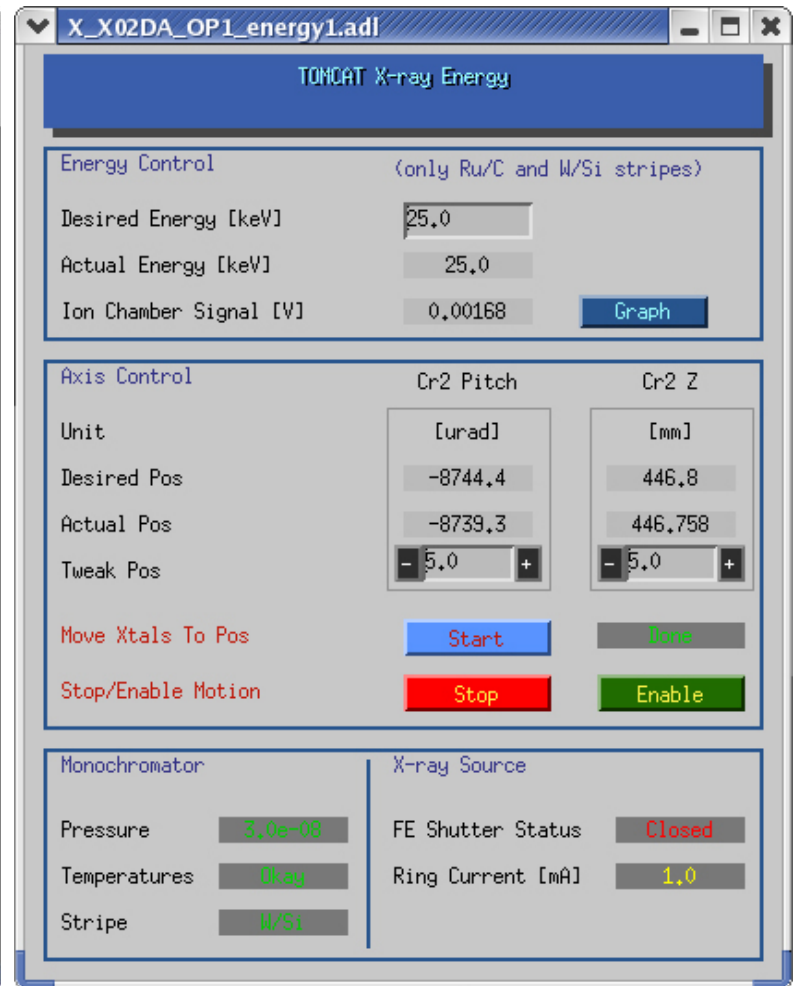
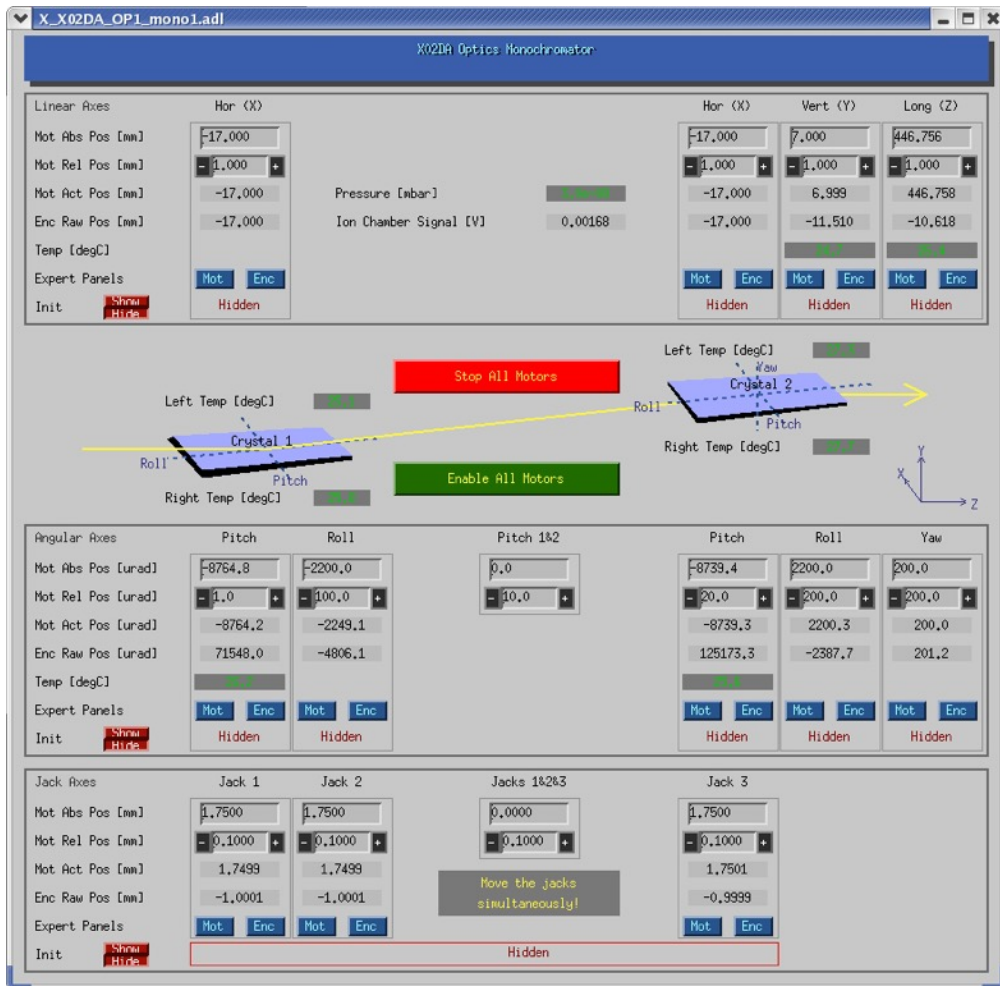
HIGH

WIDE

- Spatial resolution, field of view
 - **FAST and AUTOMATED**
- Data acquisition
 - **HIGH**
- Sensitivity (absorption / phase contrast)
- Energy range / Sample Flexibility
 - **BROAD**
 - **HIGH**
- Data post-processing
 - **FAST and ONLINE**
- In-situ experiments
 - **MULTIPLE**
- User friendliness
 - **EASY**



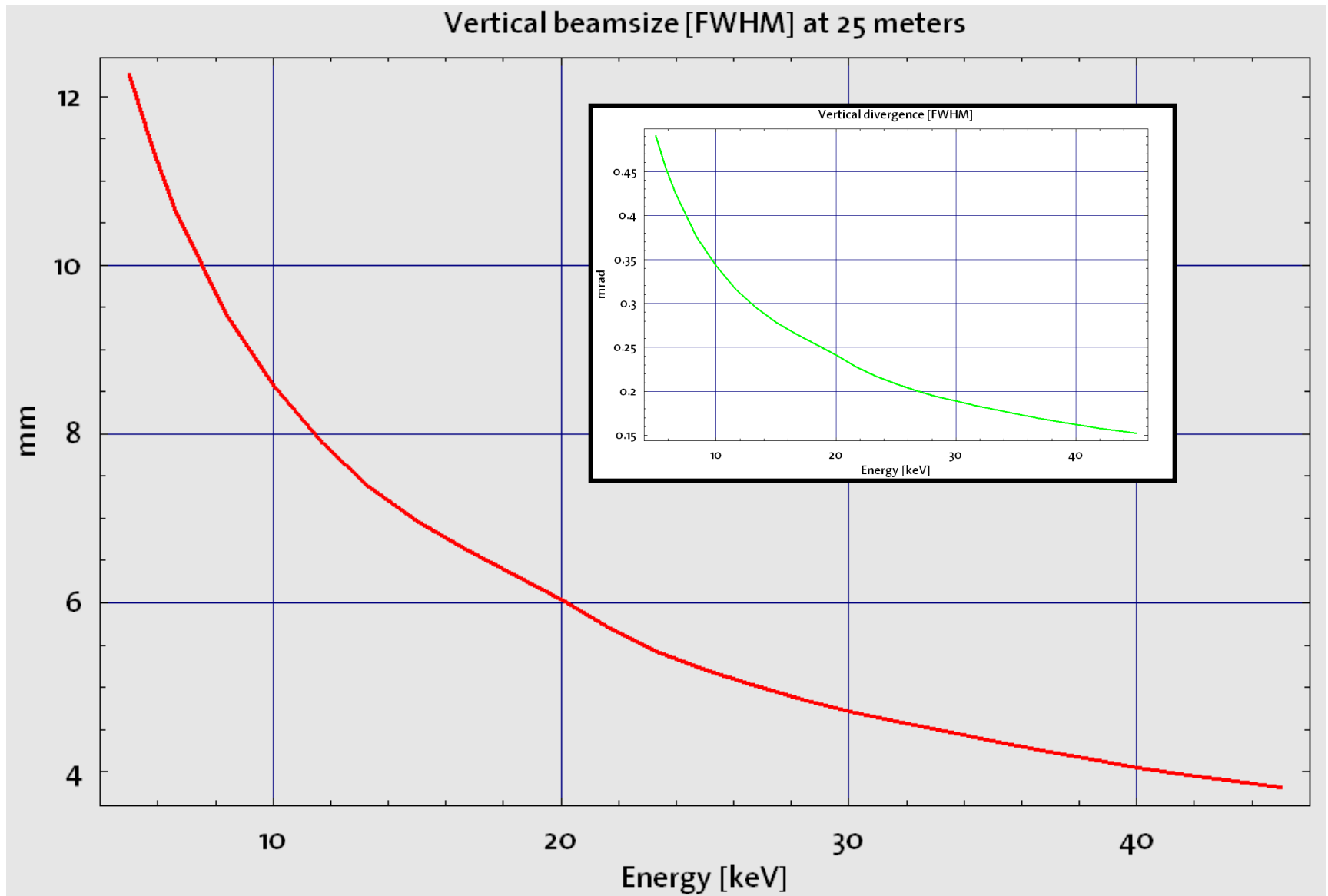
User friendliness (mono controls)



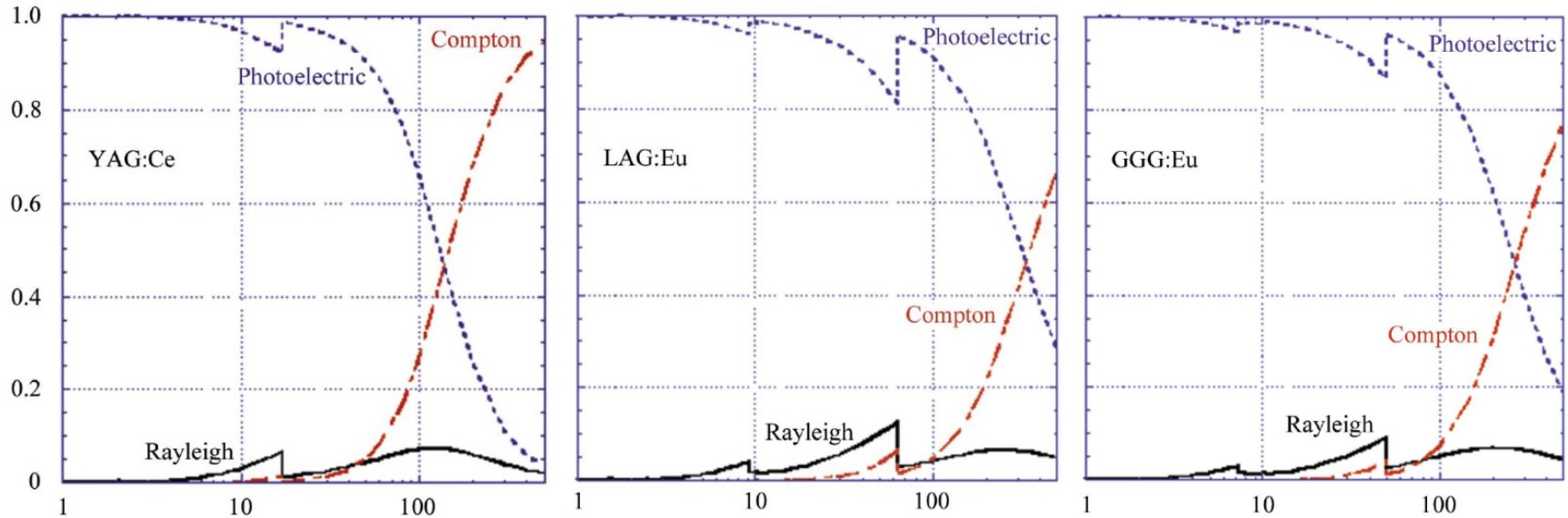
28 parameters
(expert user)

3 parameters
(standard user)

Appendix 1: Beamsize at TOMCAT superbend



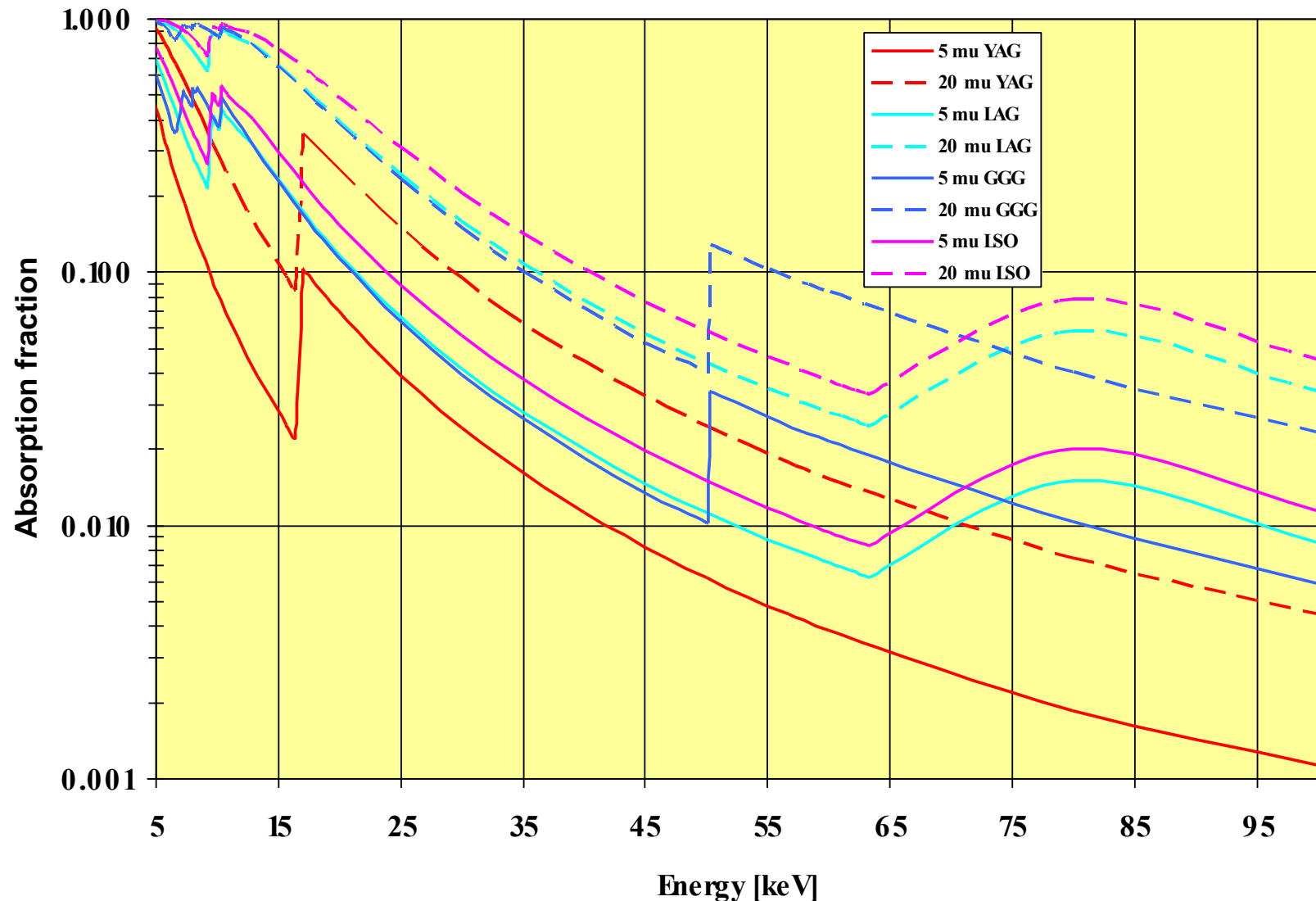
Appendix 2: Scintillator parameters



Scintillators	Name	Z_{eff}	ρ (g cm $^{-3}$)	$\rho Z_{\text{eff}}^4 (\times 10^6)$	$\eta_{x/\nu}$	Light yield	λ (nm)	n	Cleavage
Gd ₂ O ₂ S:Tb	P43	59.5	7.3	91	13	40000–50000	545	1.82	Powder
Y ₃ Al ₅ O ₁₂ :Ce	YAG	32	4.55	5	4.0	8200	550	2.15	None
Bi ₄ Ge ₃ O ₁₂	BGO	75	7.13	225		20000	480	1.85	None
Lu ₃ Al ₅ O ₁₂ :Ce	LAG	61	6.73	93		15000	535	1.85	None
Lu ₃ Al ₅ O ₁₂ :Eu	LAG	61	6.73	93			535	1.85	None
CdWO ₄		63	7.9	124		65000	470	2.2	Yes
Gd ₃ Ga ₅ O ₁₂ :Eu	GGG	52	7.1	80		25000	540	1.8	None
CsI:Tl		54.1	4.52	39	15	20000	611	1.88	None
Lu ₂ O ₃ :Eu		68.8	8.4	180		19000	611	1.82	None
Gd ₂ O ₃ :Eu		61	7.1	98		420	1.82		None
Lu ₂ SiO ₅ :Ce	LSO	65.2	7.4	136					
Lu ₃ Ga ₅ O ₁₂ :Eu	LGG	58.2	7.4	85					

T. Martin, A. Koch, J. Synchrotron Rad. (2006). 13, 180–194

Appendix 2: Scintillator absorption



YAG:Ce (Y₃Al₅O₁₂) LAG:(Eu,Tb) (Lu₃Al₅O₁₂) GGG:Eu (Gd₃Ga₅O₁₂) LSO:(Eu,Tb,Sm) (Lu₂SiO₅)

Appendix 3 : Optical Microscopy (I)

- Resolution:** The resolving power of a microscope is the most important feature of the optical system and influences the ability to distinguish between fine details of a particular specimen.

- Rayleigh Criterion:**
Resolving two adjacent objects (no noise):

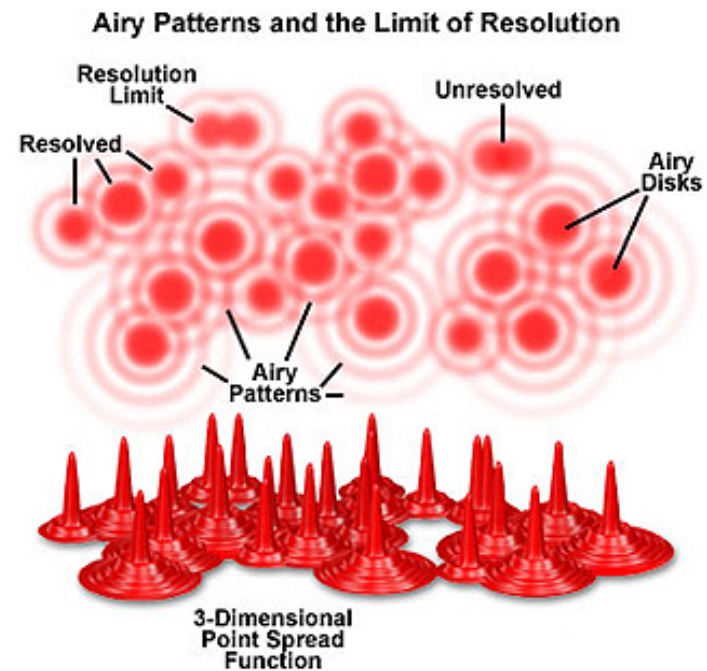
$$R_{\text{Rayleigh}} = c \lambda / NA$$

(high resolution at short wavelength)

- Rose Criterion:**
Influence of noise on spatial resolution
(photon stat. /dose limit resolution):

$$N_{\text{Phot}}^{\text{tot}} = \left(\frac{D}{R} \right)^4 \frac{\exp(\mu D)}{[\mu D(\sigma/\mu)]^2}$$

- With sample diameter D constant:
if R ↓ then N_{Phot} ↑ as (1/R)⁴



Pixel/Voxel size

Often stated as “resolution” in tomography...

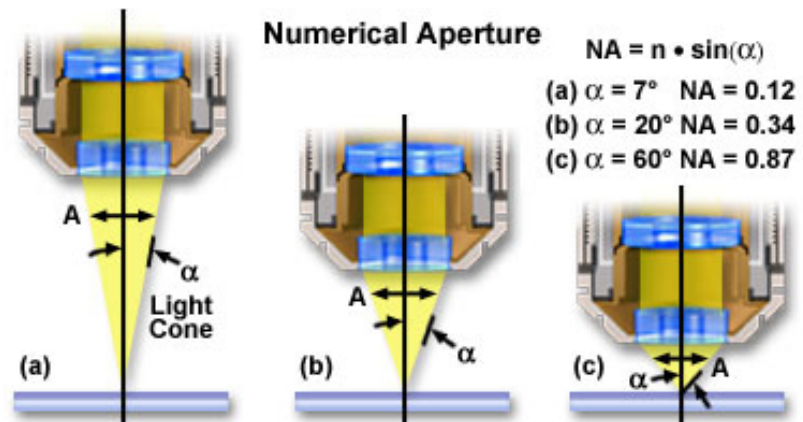
$$f_{\max} < f_{\text{Nyquist}} = \frac{1}{2 \cdot \text{pixelsize}}$$

Nikon: <http://www.microscopyu.com/>

Appendix 3 : Optical Microscopy (II)

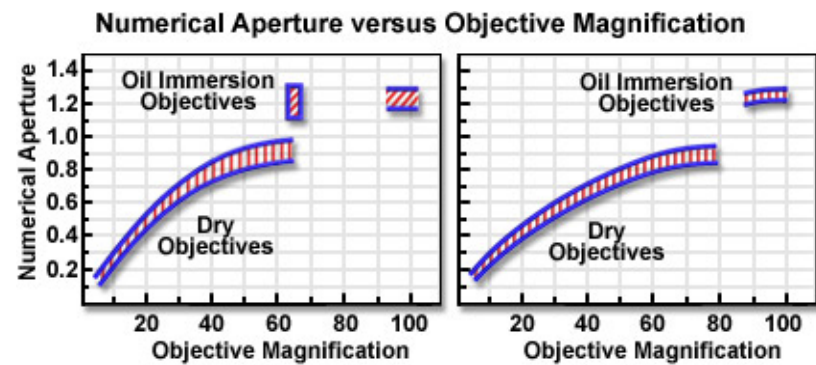
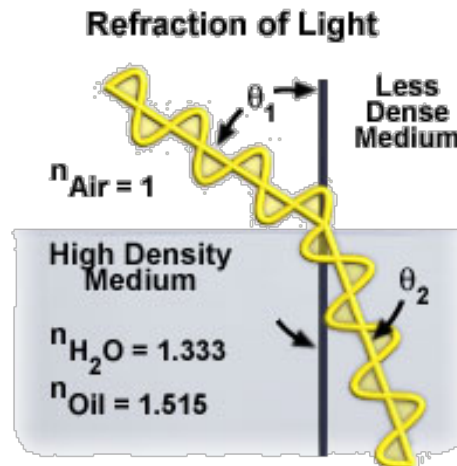
Numerical Aperture

The numerical aperture of a microscope objective is a measure of its ability to gather light and resolve fine specimen detail at a fixed object distance.



Def: $NA = n \cdot \sin(\alpha)$

Snell's law: $n_1 \cdot \sin(\theta_1) = n_2 \cdot \sin(\theta_2)$



Nikon: <http://www.microscopu.com/>

Appendix 3 : Optical Microscopy (III)

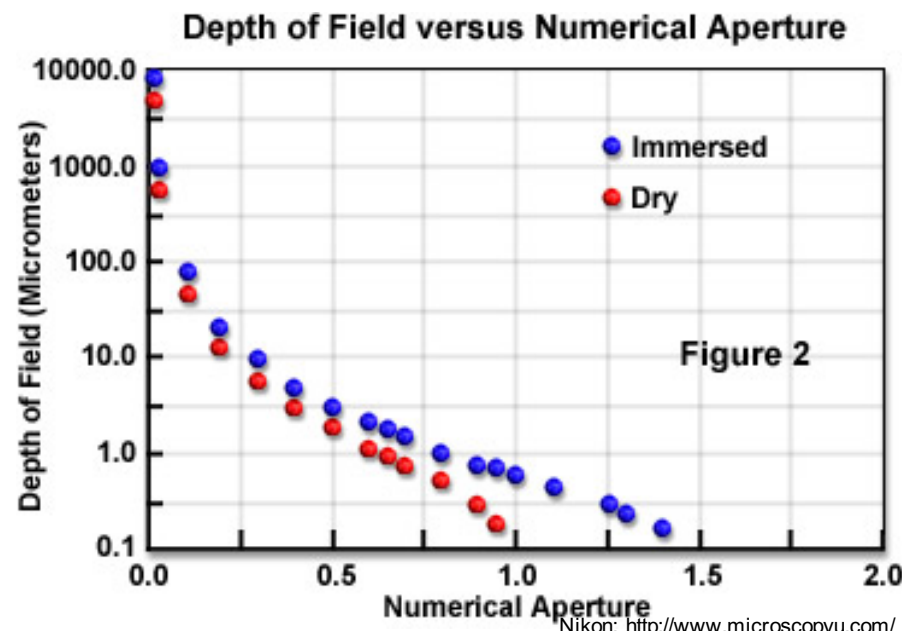
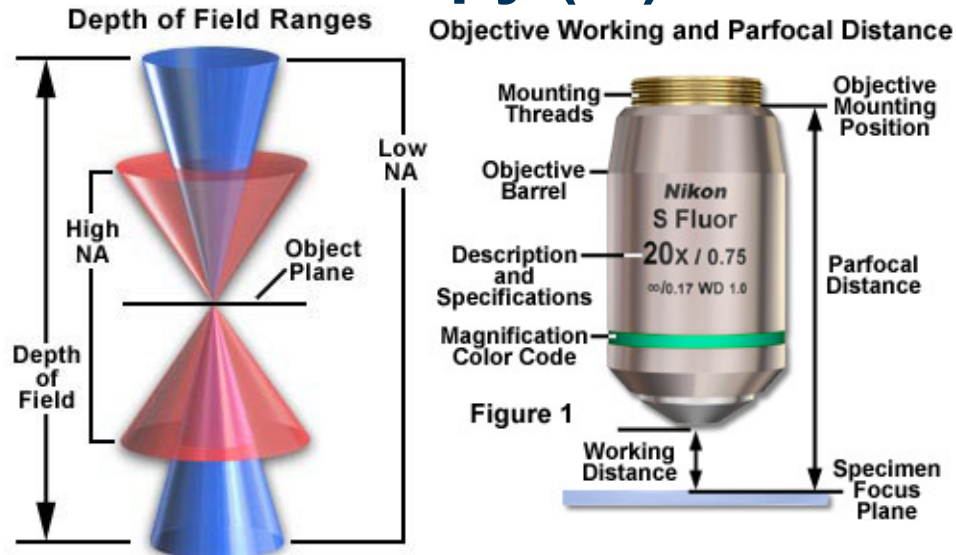
- **Depth of Field:** thickness of the specimen that is acceptably sharp at a given focus level.

$$d_{tot} = \frac{\lambda \cdot n}{NA^2} + \frac{n}{M \cdot NA} e$$

- **Depth of Focus:** range over which the image plane can be moved while an acceptable amount of sharpness is maintained.

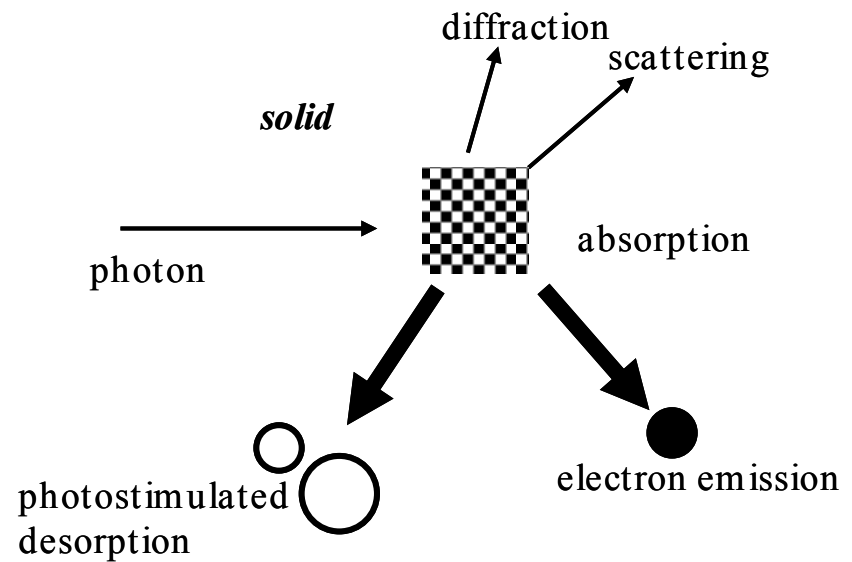
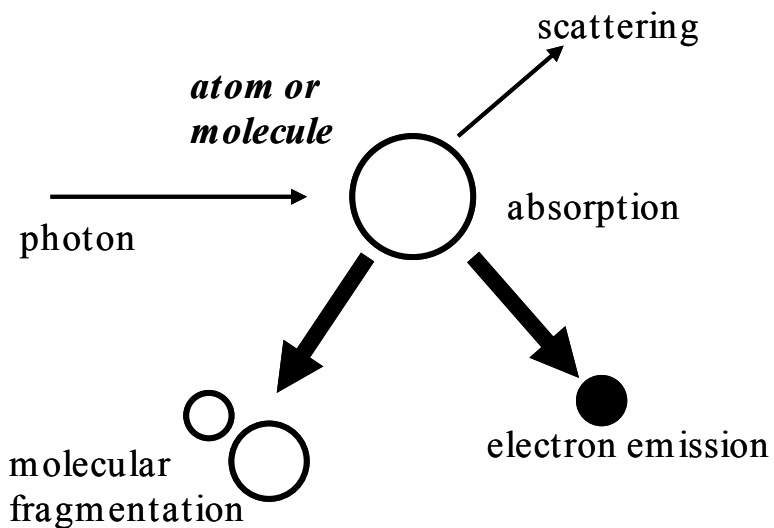
- **Working distance**

Microscope objectives are generally designed with a short free working distance, which is defined as the distance from the front lens element of the objective to the closest surface of the coverslip when the specimen is in sharp focus.



Applications of synchrotron light

- Photons interact with atoms, molecules, solids and complex biological systems in many different ways. Each of the interaction mechanisms constitutes the basis of several experimental techniques.



Synchrotron-based analysis techniques

Absorption/scattering by *atoms or molecules in gas*:

- Atom/molecule excitation or electrons extraction from the atom
Techniques: **absorption spectroscopy, molecular EXAFS** (extended molecular X-ray absorption fine structure)
gas-phase photoelectron spectroscopy and Auger-electron spectroscopy
- Molecule braking to produce smaller fragments
Techniques: **molecular fragmentation spectroscopy**
- Elastically (without energy loss) or in-elastically scattering
Techniques: **small angle X-ray scattering**

Absorption/scattering by *solid and complex biological systems*:

- **X-ray microscopy** and fluorescence analysis
- **Absorption spectroscopy, solid-state EXAFS**
- **(Protein) crystallography**
- **Powder and surface diffraction, topography and small angle scattering**
- **Solid-state photoelectron spectroscopy, photoelectron spectromicroscopy and Auger spectroscopy**